Point-by-point response to review comments on manuscript acp-2017-582 "Quantifying black carbon light absorption enhancement by a novel statistical approach"

By Cheng Wu et al.

We thank the two anonymous reviewers for their constructive comments to improve the manuscript. Our point-by-point responses to the review comments are listed below. Changes to the manuscript are marked in blue in the revised manuscript. The marked manuscript is submitted together with this response document.

Anonymous Referee #1

R1-Q1. This paper proposed a new approach to characterize the light absorption enhancement of BC and reported its application to the observed results based on an aethalometer and a thermo-optical carbon analyzer in Pearl River Delta area. This manuscript includes sufficient originality, and the topic seems to fit the journal. However, there are several concerns on the accuracy of the light absorption measurements, definition of E_{abs}, and discussions on the observed optical properties. I believe that the points below should be addressed before considering the publication in ACP.

Author's Response: Thanks for the very insightful and detailed comments. Please see below for point-by-point response to reviewers' comments.

General comments

R1-Q2. 1) Accuracy of the aethalometer measurements. Although the authors used the correction scheme reported by Weingartner et al. (2003) to correct the artifacts due to aerosol loading, filter matrix and scattering effect, it is not clear that the light absorption for "coated-BC" can be accurately measured (or corrected), especially under "high RH" conditions. For example, Arnott et al (2003) reported that a filter-based photometer has large potential artifacts above 80% RH. The authors need to give more detailed information on accuracy of aethalometer measurements.

Author's Response: We add the following content in section 2.1 to elaborate the factors that can affect the accuracy of Aethalometer in details.

> Besides these artifacts, RH is also a source of σ_{abs} measurement uncertainty. Elevated RH is not only a driving force of increased σ_{abs} due to the hygroscopic growth of particles, but also a factor affecting ambient σ_{abs} measurements. Previous studies found σ_{abs} by PAS exhibit a systematic decrease when RH>70% (Arnott et al., 2003;Kozlov et al., 2011). Water evaporation was found as the major cause for the biased PAS σ_{abs} measurements under high RH (Raspet et al., 2003;Lewis et al., 2009;Langridge et al., 2013). Filter-based measurements are also affected under high RH conditions. For example, Arnott et al. (2003) observed erratic responses by particle soot absorption photometer (PSAP) as RH changed. The main reason is traced to the hydrophilic cellulose membrane, which serves to reinforce the quartz filter used in PSAP. The fibers can swell and shrink as RH changes, causing unwanted light attenuation signal. The PTFE-coated glass-fiber tape has become available since 2012 for the recent model of Aethalometer to minimize the RH interference (Magee-Scientific, 2017). A study by Schmid et al. (2006) reported dependency of PSAP σ_{abs} on RH, but found negligible effect of RH on Aethalometer performance. It is also worth noting that RH in the Aethalometer optical chamber may be lower than the ambient RH due to the

slightly elevated temperature inside the instrument. The magnitude of RH difference was found similar between different instruments: 20% for the Aethalometer (Schmid et al., 2006) and 15% for the nephelometer (Guyon et al., 2004). The RH in the Aethalometer optical chamber was not measured in this study. We expected its level to be slightly lower than the ambient RH. Cappa et al. (2008) found σ_{abs} measurements by PSAP and PAS maintained a high linearity even under high RH conditions (65-91%). Inter-comparison studies demonstrated that with proper corrections, Aethalometer σ_{abs} measurements agree well with those by PAS (Ajtai et al., 2011). During the inter-comparison study of an Aethalometer (AE-16) and a PAS in Guangzhou (Wu et al., 2009), good correlation was found (R^2=0.96) as shown in Figure S1. These comparison results imply that the Aethalometer results are linearly correlated with PAS measurements and RH has a limited interference on Aethalometer measurements.

The Aethalometer measurements correlated well with the PAS results during a field campaign in Guangzhou as evidenced by the high R^2 (0.96) shown in Figure R-1. The ambient RH during the comparison period ranged from 20% to 95%. Since the PAS inlet was equipped with a dryer while Aethalometer was sampling without a dryer, the high R^2 proved that RH did not affect the correlation between Aethalometer and PAS. The results proved that Aethalometer can achieve comparable precision of PAS for hourly resolution data. We add tests in section 4.1 to evaluate the robustness of MRS against systematic biases. The results show that MRS is insensitive to systematic biases and details can be found in the response to R2-Q5.

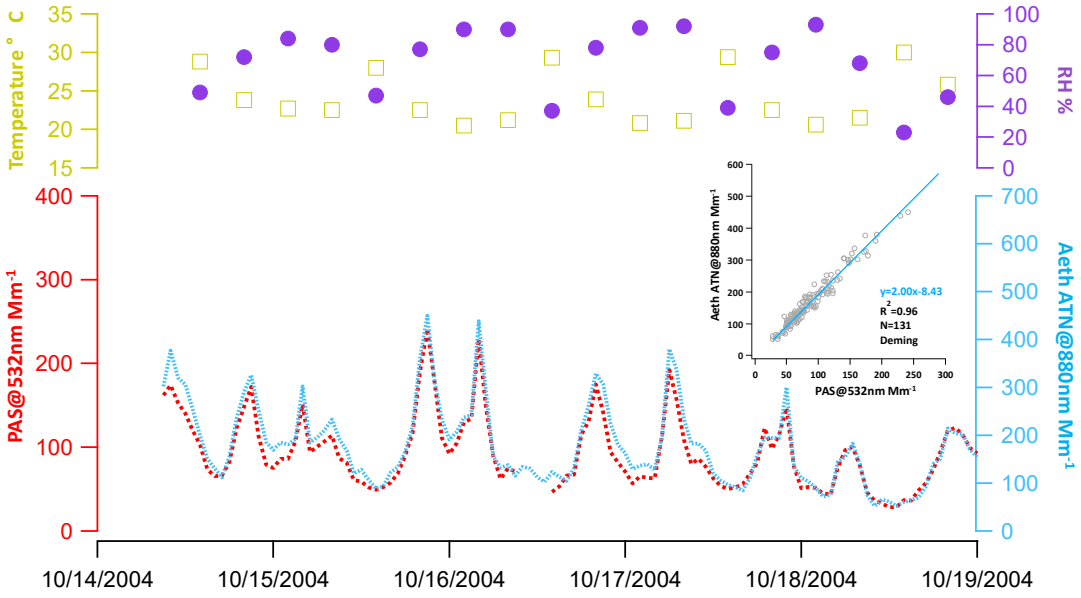

Figure R-1. Comparison of collocated Aethalometer and PAS at Guangzhou (Oct 2004). Both PAS and Aethalometer (AE-16) were equipped with $PM_{2.5}$ inlets. RH of the sampled air was controlled to be <45% for PAS. Aethalometer sampling was conducted without RH control.

R1-Q3. 2) Definitions of the MAE_p and E_{abs} The MAE_p obtained by the method in this study is MAE value for primary emission source. I think that the MAE_p, which was obtained in this study, includes the effects of "lensing effect" due to co-emitted OC. Therefore, the definition of E_{abs} values should be

different with the E_{abs} in the previous studies, at least, using TD technique. Detailed explanation on this point should be added.

Author's Response: Thanks for raising this point, which we did not make it clear in our manuscript. Yes, we agree with the reviewer that the nature of $MAE_{p,TD}$ is different from MAE_p at emission source. The following contents are added to clarify this point.

In introduction:

> It's also worth noting that MAE_p by the TD approach is different from the MAE_p at the emission source. First, the morphology of thermally denuded BC particles (compact aggregates) is different from that of freshly emitted BC particles (chain-like aggregates). Second, most of the coatings is removed with the TD denuded soot particles, but freshly emitted soot particles usually come with a thin coating of OC formed from condensation of OC vapors as the temperature drops from engine to the ambient air. As a result, the MAE_p by TD approach is expected to be lower than the MAE_p of emission source. In this sense, the TD approach may not be a prefect "time machine" to reverse the aging process for E_{abs} determination.

In section 4.1:

> As mentioned in section 1, the definition of MAE_p by the TD approach is different from the MAE_p of emission source. The TD MAE_p is expected to be slightly lower than the MAE_p of emission source. Therefore, the corresponding E_{abs} are slightly different and it should be cautioned when comparing MRS-derived E_{abs} with E_{abs} by the TD approach and Mie simulations.

R1-Q4. 3) The effect of biomass burning

3-1) Lines 371-374: "During the rainy season when oceanic prevailing wind dominates, BC from BB emission in Southeast Asia can reach PRD through long range transport (LRT), resulting in an elevated K^+/EC ratio and MAE_{550}, which might be a combination of a thicker coating when freshly emitted from BB sources and enhanced coating during LRT."

=> If so, I think the MAE_p values should be higher in summer (rainy season). Please consider about this point.

Author's Response: BB is one aerosol source affecting $MAE_{p,550}$ but not the dominating source. As shown in Figure 8 in the revised manuscript, the data points are scattered and the R^2 (0.33) is relatively low. The intercept in Figure 8 represents the part of MAE that are not explained by K^+/EC ratio. To further clarify this point, we calculate K^+/EC ratio and MAE_{550} - K^+/EC regression intercept of each month, then we compare the correlation of $MAE_{p,550}$ vs. K^+/EC ratio and $MAE_{p,550}$ vs. K^+/EC intercept. As shown in Figure R-2, $MAE_{p,550}$ has higher correlation with K^+/EC intercept (R^2=0.58) than with K^+/EC ratio (R^2=0.23). These results imply that BB is one of the contributors to the $MAE_{p,550}$ variations, but unlikely to be the dominating one. As a result, in some summer months, the $MAE_{p,550}$ is higher than the winter months but some months are not. Other BC sources and BB combustion conditions may affect the overall $MAE_{p,550}$. The relevant content is revised as follow:

> During the rainy season when oceanic wind prevails, BC from BB emission in Southeast Asia can reach PRD through long range transport (LRT), resulting in an elevated K^+/EC ratio and MAE_{550}. The Deming regression intercept (11.89) in Figure 8 represents the MAE without the BB effect. This non-BB MAE_{550} (11.89 $m^2\ g^{-1}$) is only slightly lower than $MAE_{p,550}$ (13 $m^2\ g^{-1}$) obtained in section 4.3, implying that a large fraction of

$MAE_{p,550}$ could not be explained by the BB source. Additional evidence was obtained through examining regression relationships of $MAE_{p,550}$ with K^+/EC month-by-month (Figure S17b). Correlation of monthly $MAE_{p,550}$ vs. K^+/EC ratio yield a R^2 of 0.23 (Figure S17c). In contrast, a much higher correlation (R^2=0.58) was observed (Figure S17d) between $MAE_{p,550}$ and non-BB MAE_{550} (i.e., K^+/EC intercepts from Figure S17b). These results imply that BB is one of the contributors to the $MAE_{p,550}$ variations, but unlikely to be the dominating one.

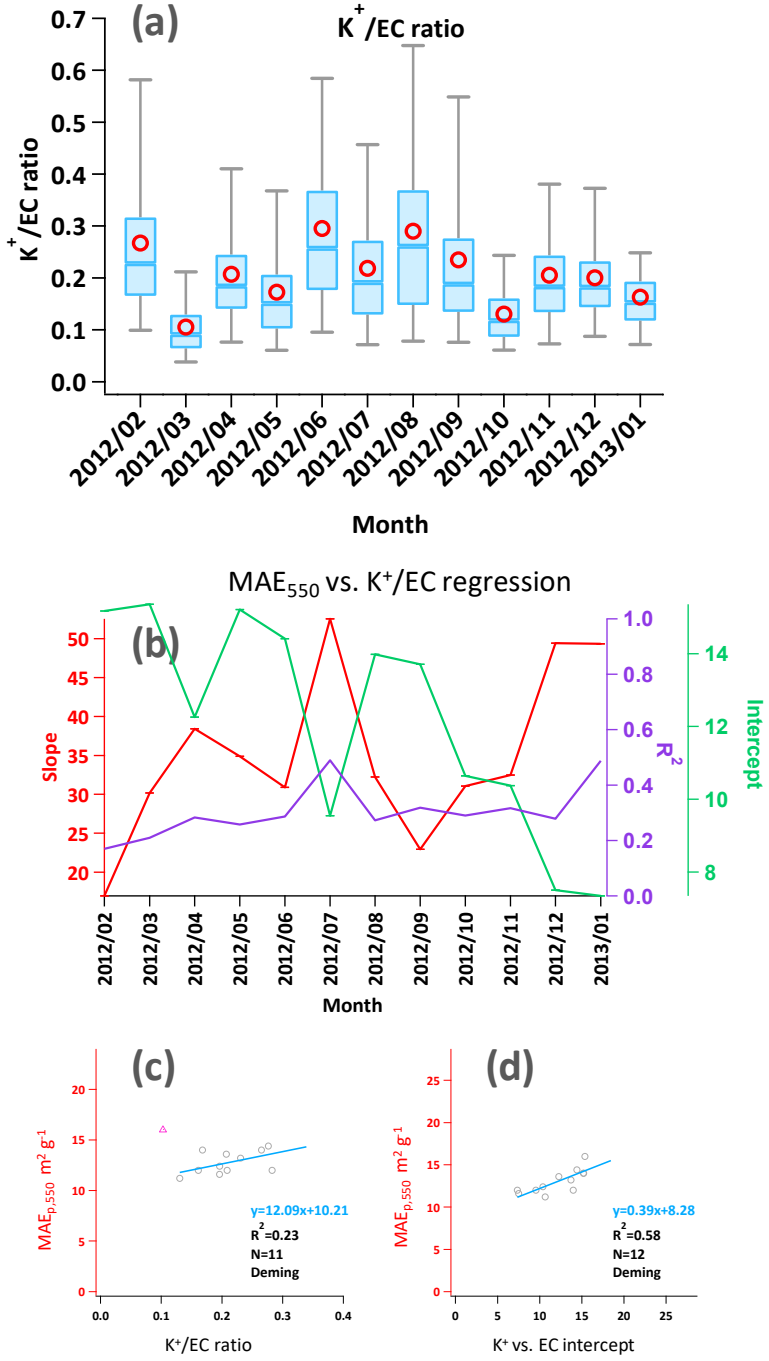

Figure R-2. (a) Monthly variations of K^+/EC ratio from 2012 Feb to 2013 Jan at NC site. (b) Monthly regressions between MAE_{550} and K^+/EC with slope in red, intercept in green and R^2 in purple. (c) regressions between monthly $MAE_{p,550}$ and K^+/EC. (d) regression between monthly $MAE_{p,550}$ and intercepts from (b).

R1-Q5. 3-2) Lines 384-388: "Since the monthly average AAE in wintertime didn't exceed 1.2 (Table S3), the variations of AAE in the PRD are likely more associated with thicker coatings rather than the contribution of BrC. The results also imply that attempts on BrC absorption attribution for the PRD dataset presented in this study could be risky, considering that elevation of AAE is actually dominated by coating (Lack and Langridge, 2013)."

=> Because higher E_{abs} values were observe in summer, the coating would be thicker in summer. The suggestion that "the higher AAE in winter are likely more associated with thicker coatings" is not reasonable. Please consider about this point.

Author's Response: The point we intend to make here is that since the seasonal variations of $AAE_{470-660}$ is small, such variations are likely induced by the coating effect as shown in the Mie simulation rather than the presence of BrC. The corresponding text is rephrased as below to improve the clarity.

> Since the monthly average $AAE_{470-660}$ in wintertime did not exceed 1.2 (Table S3), the variations of $AAE_{470-660}$ in the PRD are more likely associated with coatings rather than the contribution of BrC.

R1-Q6. 4) The effect of relative humidity (RH) on optical properties As mentioned above, the authors need to show some evidences suggesting that the obtained positive correlation between f(RH) (i.e., MAE) and RH is not due to the artifact of RH on aethalometer measurements. If the measurements are assumed to be accurate, the observed higher E_{abs} (and MAE) and lower AAE values in summer may be explained only by RH, considering that the RH may be higher in summer and RH for air masses from Southeast Asia. Which one of higher OC/EC ratio and higher RH do you suggest as a main contributor for observed higher E_{abs} in summer?

Author's Response: The study by Schmid et al. (2006) found PSAP σ_{abs} shows dependency on RH, but the effect of RH on Aethalometer performance is neglectable. See our response to R1-Q2 for more detailed discussion on RH effect.

The contribution of elevated OC/EC ratio to the increase of E_{abs} might not be as important as RH in the summer time. First, the OC/EC ratios in summer is only slightly higher than other seasons (Figure R-3a). Second, as shown by the $f(OC/EC)_{MAE}$ plot (Figure R-3b), OC/EC induced MAE enchantment only occurred when OC/EC>4, which corresponded to the data with the highest 20% OC/EC ratio. As a result, the OC/EC induced MAE enhancement was only important for episodes of high OC/EC hours, which have a limited temporal coverage.

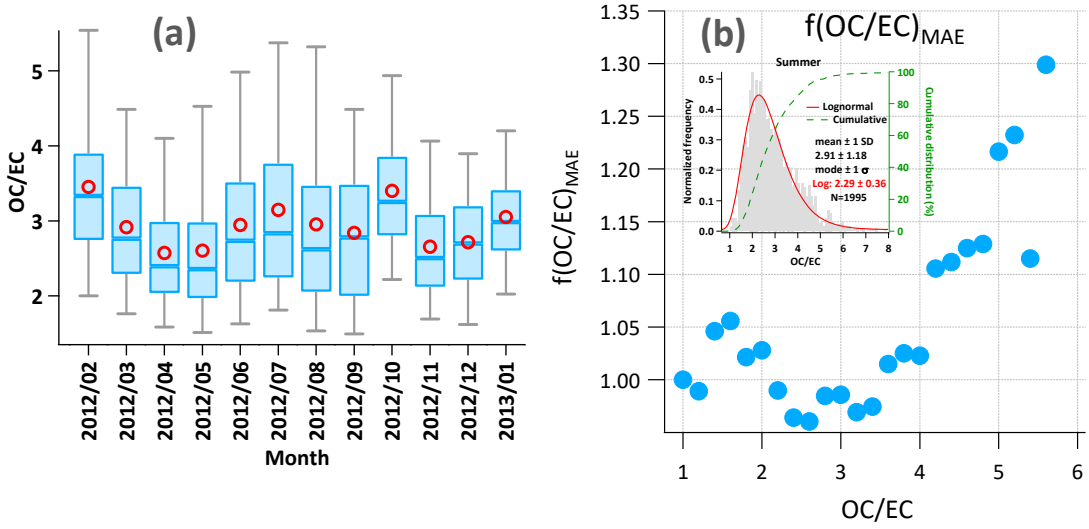

Figure R-3. (a) Monthly variations of OC/EC (b) MAE_{550} enhancement as a function of OC/EC.

Specific comments

R1-Q7. 1) Line 235-236 "Thus, a BrC coating (brown shell) scenario is also considered in Mie simulation following the wavelength dependent RI suggested by Lack and Cappa (2010)." => Because the results of Mie simulation should be varied depending on the RI values given here, I recommend adding the range of RI values.

Author's Response: Suggestion taken. The corresponding content is revised as follows:

> Thus, a BrC coating (brown shell) scenario is also considered in Mie simulation following the wavelength-dependent RI suggested by Lack and Cappa (2010), which ranges from 1.55-0.059i (370 nm) to 1.55-0.0005i (950 nm).

R1-Q8. 2) Section 3.2.4, 1st paragraph. For the brown shell scenario, I think that both of lensing effect and light absorption by BrC contribute to the E_{abs} values. I recommend adding the fraction of each contribution.

Author's Response: We agree with the reviewer on this point. Fractional contribution from BrC is discussed as shown below. The following figure is added in SI (Figure S7).

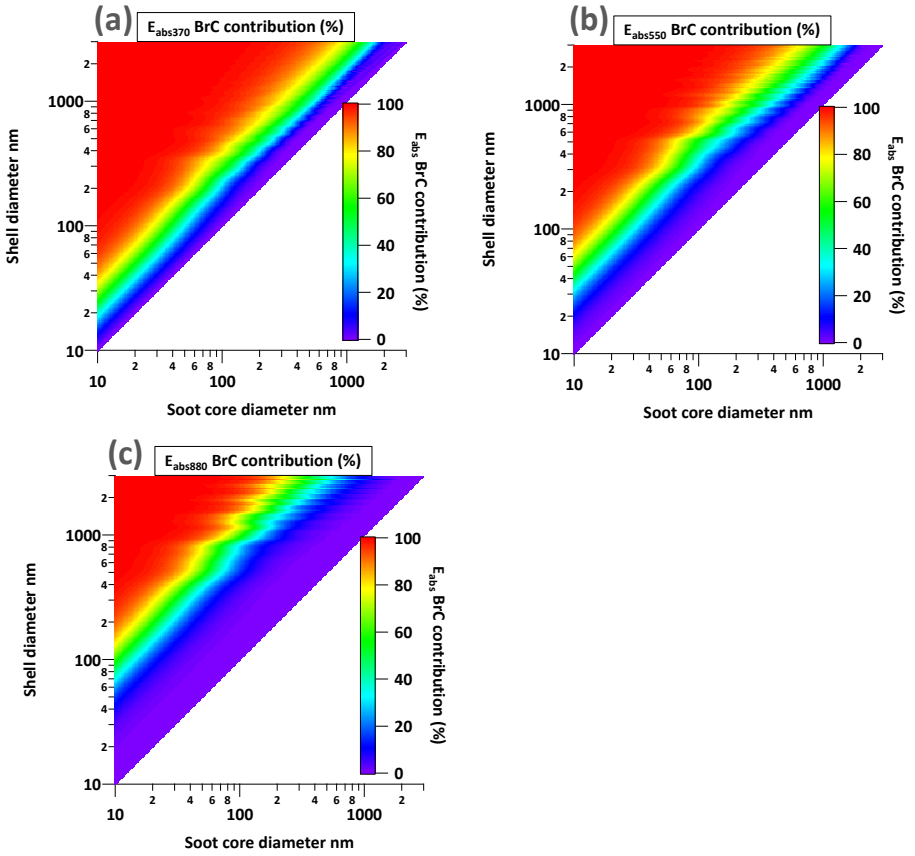

Figure R-4. Mie simulated BrC absorption contribution to total E_{abs} (lensing effect + BrC absorption) in the brown shell scenario. (a) 370 nm (b) 550 nm (c) 880 nm.

The following text is added in the revised manuscript (section 3.2.4):

> The main reason behind is that in the brown shell scenario, both lensing effect and BrC absorption contribute to E_{abs}. As shown in Figure S7, the BrC absorption contribution to total E_{abs} strongly depends on coating thickness and is insensitive to soot core diameters. When the coating is relatively thin (<5 nm for λ@370 nm, <15 nm for λ@550 nm and

<40 nm for λ@880 nm), BrC absorption contribution to the total E_{abs} is less than 20%. As the coating increases to a certain level (~15 nm for λ@370 nm, ~35 nm for λ@550 nm and ~90 nm for λ@880 nm), BrC absorption contribution is comparable to the lensing effect contribution, each contributing ~50% to the total E_{abs}. When the BrC coating is sufficiently thick (>30 nm for λ@370 nm, >90 nm for λ@550 nm and >110 nm for λ@880 nm), BrC absorption dominates the E_{abs} contribution. As a result, if BrC coating is indeed present in ambient samples, a strong wavelength dependent E_{abs} could be observed, since a BrC coating of 30 nm would be enough to induce a large amount of detectable E_{abs} in the UV range.

R1-Q9. 3) Section 4.1, 2nd paragraph The annual average MAE_p value (13 m^2/g) is larger than those estimated for bare BC. It may indicate that the obtained MAEp values include the effects of "lensing effect" due to co-emitted OC, as mentioned above. If so, caution on the definition of MAEp in each study should be taken during comparison with other studies. Also, it is better to add information on the wavelength used in each study.

Author's Response: The authors fully agree with the reviewer that the difference in MAE_p definition should be emphasized. Following contents are added in section 4.1 to clarify this point.

MAE_p by MRS represents the MAE_p at the emission source, which is different from the MAE_p by the TD approach for two reasons. First, the morphology of thermally denuded BC particles (compact aggregates) is different from that of freshly emitted BC particles (chain-like aggregates). Second, most of the coatings are removed for TD denuded soot particles, but freshly emitted soot particles usually come with a thin coating of OC formed from condensation of OC vapors as the temperature drops from the flame to the ambient air. As a result, the MRS-derived MAE_p is expected to be higher than the MAE_p by the TD approach.

The MAE mentioned from literature was scaled to 550 nm for comparison. The following text is added to improve the clarity.

For comparison purpose, MAE measured at original wavelength and MAE scaled to 550 nm following the λ^{-1} assumption are both shown in Table S1. The MAE comparisons discussed below are MAE at 550 nm.

R1-Q10. 4) Section 4.5 How did the absorption coefficients for dry conditions determine to obtained f(RH)?

Author's Response: The sampled air into the Aethalometer was not dried in this study. As the sampling covered a whole year, the RH also spanned a range sufficiently large to study the RH effect. The MAE data obtained at RH=30% (as shown in Figure 9a of the revised manuscript, the starting point of the f(RH) curve) are used as the dry condition to calculate f(RH).

R1-Q11. 5) Figure 9 What do to want to suggest from 30:1 line in Fig. 9?

Author's Response: The 30:1 line is to serve as a reference line with an integer slope that is close to the regressed slope through the origin.

References

Arnott, W. P., Moosmuller, H., Sheridan, P. J., Ogren, J. A., Raspet, R.Slaton, W. V. 2003. Photoacoustic and Filter-Based Ambient Aerosol Light Absorption Measurements: Instrument Comparisons and the Role of Relative Humidity. J.Geophys. Res.-Atmos., 108: 4034–4045.

Quantifying black carbon light absorption enhancement by a novel statistical approach

Cheng Wu[1,2], Dui Wu[1,2,3], Jian Zhen Yu[4,5,6]

[1]Institute of Mass Spectrometer and Atmospheric Environment, Jinan University, Guangzhou 510632, China

[2]Guangdong Provincial Engineering Research Center for on-line source apportionment system of air pollution, Guangzhou 510632, China

[3]Institute of Tropical and Marine Meteorology, China Meteorological Administration, Guangzhou 510080, China

[4]Division of Environment, Hong Kong University of Science and Technology, Clear Water Bay, Hong Kong, China

[5]Atmospheric Research Centre, Fok Ying Tung Graduate School, Hong Kong University of Science and Technology, Nansha, China

[6]Department of Chemistry, Hong Kong University of Science and Technology, Clear Water Bay, Hong Kong, China

Corresponding to: Cheng Wu (wucheng.vip@foxmail.com) and Jian Zhen Yu (jian.yu@ust.hk)

Abstract

Black carbon (BC) particles in the atmosphere can absorb more light when coated by non-absorbing or weakly absorbing materials during atmospheric aging, due to the lensing effect. In this study, the light absorption enhancement factor, E_{abs}, was quantified using one year's measurement of mass absorption efficiency (MAE) in the Pearl River Delta region (PRD). A new approach for calculating primary MAE (MAE_p), the key for E_{abs} estimation, is demonstrated using the Minimum R Squared (MRS) method, exploring the inherent source independency between BC and its coating materials. A unique feature of E_{abs} estimation by the MRS approach is its insensitivity to systematic biases in EC and σ_{abs} measurements. The annual average E_{abs550} is found to be 1.50±0.48 (±1 S.D.), exhibiting a clear seasonal pattern with higher values in summer and lower in the winter. Elevated E_{abs} in the rainy summer season is likely associated with aged air masses dominating from marine origin, along with long-range transport of biomass burning influenced air masses from Southeast Asia. E_{abs}

induced by hygroscopic growth at elevated RH could be as high as 1.3. Core-shell Mie simulations along with measured E_{abs} and Angstrom absorption exponent (AAE) constraints suggest that in the PRD, the coating materials are unlikely to be dominated by brown carbon and the coating thickness is higher in the rainy season than the dry season. A negative correlation is found between $AAE_{470\text{-}660}$ and RH, suggesting a dominant particle size of D_{core} = 130 nm and D_{shell}/D_{core} range of 2 to 4.

1 Introduction

Originating from incomplete combustion, black carbon (BC) is a crucial constituent of atmospheric aerosols, and is an air pollutant itself, having an adverse health impacts on humans (Suglia et al., 2008). BC has also been recognized as the third most important climate forcer due to its broad light absorbing capability across the UV-Vis-IR spectrum (IPCC, 2013). BC can alter the climate in a variety of ways, including by direct forcing (Bond et al., 2011), affecting cloud cover (Koch and Del Genio, 2010) and precipitation (Tao et al., 2012), reducing the albedo of snow and ice (Hansen and Nazarenko, 2004) and causing surface dimming (Wild, 2011). The climate effects of BC can be global or regional (Ramanathan and Carmichael, 2008). A recent study found BC can modify planetary boundary layer meteorology, and thus enhance local pollution indirectly (Ding et al., 2016). However, due to its variable optical characteristics induced during atmospheric aging, large uncertainties still exist in estimating the radiative forcing from BC. Optical properties of BC can be predicted by knowing the mass concentration, mixing state and size distribution, which collectively serve as the cornerstone for modeling the climate effect of BC. In 3D modeling studies, to conserve computational resources, the mass absorption efficiency (MAE) or mass absorption cross-section (MAC) is widely used to convert black carbon mass concentration to light absorption coefficient (σ_{abs}). MAE is a quantity to describe the light absorption ability per unit EC mass:

$$\text{MAE}\ (m^2\ g^{-1}) = \frac{absorption\ coefficient\ \sigma_{abs}\ (Mm^{-1})}{EC\ mass\ concentration\ (\mu g\ m^{-3})} \quad (1)$$

As a fundamental input parameter, MAE has a critical impact on BC's radiative forcing estimation in climate modeling studies. Mixing state is one of the governing factors affecting MAE.

Light absorption of soot particles is enhanced when coated with non-absorbing materials (Fuller et al., 1999) or weakly absorbing materials (Lack and Cappa, 2010) during atmospheric aging. The coating materials can focus more light onto the soot core through the lensing effect, resulting in elevated MAE (Wang et al., 2017). Strong correlations between MAE and the number/volume fraction of coated particles have been reported in urban areas like Tokyo (Naoe et al., 2009), Shenzhen (Lan et al., 2013) and Xi'an (Wang et al., 2014), implying that the elevated MAE observed at these locations was mainly due to the elevated fraction of coated of soot particles. Total absorption ($\sigma_{abs,t}$) of coated particles can be separated into two parts: primary absorption ($\sigma_{abs,p}$) due to the uncoated soot core alone, and extra absorption ($\sigma_{abs,c}$) due to lensing effect of the coating (Bond et al., 2006; Jacobson, 2006; Liu et al., 2016a) and the presence of secondarily formed brown carbon (BrC) (Lack and Cappa, 2010; Liu et al., 2016b).

$$\sigma_{abs,t} = \sigma_{abs,p} + \sigma_{abs,c} \quad (2)$$

The absorption enhancement factor (E_{abs}) then can be defined as ratio of the total absorption and primary absorption coefficients or the corresponding MAE values:

$$E_{abs} = \frac{\sigma_{abs,t}}{\sigma_{abs,p}} = \frac{MAE_t}{MAE_p} \quad (3)$$

Where MAE_p represents the ratio of $\sigma_{abs,p}/EC$ for uncoated soot particles, similar to the concept of the primary OC/EC ratio in the EC tracer method:

$$MAE_p = \frac{\sigma_{abs,p}}{EC} \quad (4)$$

And the MAE of coated BC can be defined as:

$$MAE_t = \frac{\sigma_{abs,t}}{EC} \quad (5)$$

Thus, elevated MAE induced by coating during atmospheric aging results in an E_{abs} larger than 1.

Previous model studies suggest that absorption by aged soot particles can be 1.5 times greater than fresh soot (Fuller et al., 1999; Bond et al., 2006). Laboratory studies have demonstrated that soot particles coated with SOA (Saathoff et al., 2003; Schnaiter et al., 2005) and sulfuric acid (Zhang et al., 2008; Khalizov et al., 2009) can increase E_{abs}. An artificial coating experiment by Shiraiwa et al. (2010)

found an E_{abs} of 2 for graphite particles growing in diameter from 185 to 370 nm. A laboratory study by McMeeking et al. (2014) found that in the presence of BrC, light absorption enhancement is more pronounced at the shorter wavelength. A recent chamber study coupling actual ambient air with seed BC particles implies that the timescale for E_{abs} reaching 2.4 is only 5 hours in Beijing but 18 hours in Houston (Peng et al., 2016). Field studies conducted in recent years have also substantiated enhanced light absorption in Canada (Knox et al., 2009; Chan et al., 2011), US (Lack et al., 2012b), UK (Liu et al., 2015) and Japan (Nakayama et al., 2014; Ueda et al., 2016). In contrast, field studies in California, US (Cappa et al., 2012) found a weaker light absorption enhancement (6% on average). A recent study suggests the mass ratio of non-BC content to BC particles determines the occurrence of the absorption enhancement of black-carbon particles (Liu et al., 2017).

Two approaches are widely used to determine E_{abs} from ambient measurements. The first approach removes the coating materials on particles physically using a thermal denuder (TD) (Lack et al., 2012a) or by aerosol filter filtration-dissolution (AFD) (Cui et al., 2016b). The TD approach is briefly discussed here. Coating materials can be removed by TD at a working temperature around 200 to 300 °C (depending on the charring characteristics of aerosols at the sampling site) to measure $\sigma_{abs,p}$, which are cycled with measurements of $\sigma_{abs,t}$ (without passing through TD), allowing E_{abs} to be obtained from the ratio of $\sigma_{abs,t}/\sigma_{abs,p}$ following Eq.3. The major advantage of the TD approach is its ability to provide highly time resolved measurements (minutes). A photo-acoustic spectrometer (PAS) is commonly used with TD for detection to satisfy its high time resolution demands. As an in-situ technique, PAS eliminates the artifacts associated with filter-based methods (Weingartner et al., 2003; Coen et al., 2010) and is often considered as the reference instrument for light absorption coefficient determination (Arnott et al., 2003; Arnott et al., 2005). One limitation of the TD approach is that a universal optimal operation temperature does not exist. If the temperature is too low, the coating cannot be fully removed, and charring can occur if the TD temperature is too high, leading to biased results. Another issue is particle loss due to TD, which can be ~ 20% and needs to be taken into account (Ueda et al., 2016). It's also worth noting that MAE_p by the TD approach is different from the MAE_p at the emission source. First, the morphology of thermally denuded BC particles (compact aggregates) is different from that of freshly emitted BC particles (chain-like aggregates). Second, most of the

coatings is removed with the TD denuded soot particles, but freshly emitted soot particles usually come with a thin coating of OC formed from condensation of OC vapors as the temperature drops from engine to the ambient air. As a result, the MAE_p by TD approach is expected to be lower than the MAE_p of emission source. In this sense, the TD approach may not be a prefect "time machine" to reverse the aging process for E_{abs} determination.

The second approach is the MAE ratio method, which is also stated in Eq. 3. The key to this method is determining an appropriate MAE_p that can represent the MAE from primary emissions. One approach is to adopt the reference MAE_p from the literature but it may fail to represent the actual MAE_p at a specific sampling site, since MAE_p varies temporally and spatially. For example, MAE_p of diesel soot was found to be 7.1 m^2g^{-1} at 532 nm (Adler et al., 2010). A much higher MAE_p (16 m^2g^{-1} at 530 nm) was observed from natural gas flaring (Weyant et al., 2016). MAE_p of biomass burning (BB) samples is highly varied due to a wide range of fuel types and combustion conditions (Reid et al., 2005; Roden et al., 2006). A range from 6.1 to 80.8 m^2g^{-1} was reported for BB MAE_p at 550 nm (Pandey et al., 2016). Without the knowledge of source contributions, it is not feasible to derive a representative MAE_p for E_{abs} estimation. The other commonly used approach is to determine MAE_p from the dependency of MAE on the number fraction of coated soot particles measured by SP2 (Lan et al., 2013). Since MAE (y axis) is positively correlated with the number fraction of coated soot particles (x axis), MAE_p can be determined by extending the regression line to x=0. It is worth noting that this approach provides only a rough approximation of E_{abs} since the parameter used here (coated soot particles number fraction) ignores other main drivers of light absorption enhancement (e.g. coating thickness). As a result, this approach is only valid for a period of measurements, for which coating thickness is relatively constant and the MAE variations are dominated by coated soot particles number fraction.

However, the high cost of the TD-PAS system and SP2 limit the field measurement of E_{abs} around the world. In addition, long-term E_{abs} measurements by a TD-PAS system and SP2 are not easily achieved and rarely reported. On the other hand, an Aethalometer and RT-ECOC analyzer can be effectively deployed for long term measurements and E_{abs} estimation, at a relatively lower cost. In this study, based on one year of hourly MAE measurements (with the field carbon analyzer and

Aethalometer) at a suburban site in the Pearl River Delta (PRD) region of China, quantification of MAE_p is demonstrated by a novel statistical approach, the Minimum R squared method (MRS) (Wu and Yu, 2016). The aim of this study is to demonstrate the capability of E_{abs} estimation using a year-long dataset from cost-effective instrumentation. The seasonal variability of MAE, AAE and E_{abs} in the PRD region are characterized and their dependency on air mass origin, biomass burning and RH are discussed. Abbreviations used in this study are summarized in Table 1 for a quick lookup.

2 Ambient measurements

Sampling was conducted from Feb 2012 to Jan 2013 at the suburban Nancun (NC) site (23° 0'11.82"N, 113°21'18.04"E). NC, situated on the top of the highest peak (141 m ASL) in Guangzhou's Panyu district, is located at the geographic center of the PRD region, making it a representative location for average atmospheric mixing characteristics of city clusters in the PRD region. Light absorption measurements were performed by a 7-λ Aethalometer (AE-31, Magee Scientific Company, Berkeley, CA, USA). The Aethalometer was equipped with a 2.5 μm cyclone with a sampling flow rate of 4 L min^{-1}. Weingartner's algorithm (Weingartner et al., 2003) was adopted to correct the sampling artifacts (aerosol loading, filter matrix and scattering effect) rooted in filter based method. A customized Aethalometer data processing program (Wu, 2017a) with graphical user interface was developed to perform data correction and detailed descriptions can be found in the SI (The program is available from https://sites.google.com/site/wuchengust). Details of the Aethalometer setup and data correction can be found in our previous paper (Wu et al., 2013).

EC mass concentrations were determined by a real time ECOC analyzer (Model RT-4, Sunset Laboratory Inc., Tigard, Oregon, USA). The sunset carbon analyzer was sampling on hourly cycles at a flow rate of 8 $Lmin^{-1}$ with a $PM_{2.5}$ sharp-cut cyclone inlet. For each measurement hour, the first 45min were for sample collection and the remaining 15 min for thermal-optical analysis. OC is volatized first by step-wise temperature ramping in an oxygen-free atmosphere while in the second stage EC is combusted in the presence of oxygen. Laser transmittance is applied to correct the charring artifact during the OC stage.

Considering a measurement precision of 5% for the Aethalometer (Hansen, 2005) and 24% for the RT-ECOC analyzer (Bauer et al., 2009), the propagated relative precision of E_{abs} ($E_{abs,Unc}$) is 35% following Eq. S1&S2 in the SI. It should be noted that $E_{abs,Unc}$ is mainly attributed to the measurement precision of EC by the RT-ECOC analyzer. Since the measurement precision of the RT-ECOC analyzer estimated by Bauer et al. (2009) is obtained from field measurement at an environment (EC below 1 μg m^{-3}) where EC is much lower than the present study (annual average EC 2.63 μg m^{-3}), the $E_{abs,Unc}$ of 35% should be considered as an upper limit for the present study.

Light scattering was measured by an integrating nephlometer (Aurora-1000, Ecotech, Melbourne, Australia). Water soluble ions were measured by MARGA (The instrument for Measuring AeRosols and GAses)(ten Brink et al., 2007). Both instruments are equipped with a $PM_{2.5}$ inlet to remove the coarse particles.

2.1 Uncertainties of MAE determination

Two major uncertainties associated with the σ_{abs} and EC determination techniques should be taken into account when comparing MAE across different studies. For the σ_{abs} determination technique, photo-acoustic spectroscopy (PAS) is an in-situ technique free from filter based artifacts, but its application is limited by its high cost. The filter based optical transmittance method (e.g., Aethalometer and Multi Angle Absorption Photometer, MAAP) is the most widely used technique around the world, but data correction is needed to minimize the bias from artifacts due to the loading effect, matrix effect and scattering effect (Weingartner et al., 2003; Arnott et al., 2005; Schmid et al., 2006; Virkkula et al., 2007; Coen et al., 2010; Drinovec et al., 2017; Saturno et al., 2017). Besides these artifacts, RH is also a source of σ_{abs} measurement uncertainty. Elevated RH is not only a driving force of increased σ_{abs} due to the hygroscopic growth of particles, but also a factor affecting ambient σ_{abs} measurements. Previous studies found σ_{abs} by PAS exhibit a systematic decrease when RH>70% (Arnott et al., 2003; Kozlov et al., 2011). Water evaporation was found as the major cause for the biased PAS σ_{abs} measurements under high RH (Raspet et al., 2003; Lewis et al., 2009b; Langridge et al., 2013). Filter-based measurements are also affected under high RH conditions. For example, Arnott et al. (2003) observed erratic responses by particle soot absorption photometer (PSAP) as RH changed. The main reason is traced to the hydrophilic cellulose membrane, which serves to reinforce the quartz filter used in PSAP. The fibers can swell and shrink as RH changes, causing unwanted light attenuation signal. The PTFE-coated glass-fiber tape has become available since 2012 for the recent model of

Aethalometer to minimize the RH interference (Magee-Scientific, 2017). A study by Schmid et al. (2006) reported dependency of PSAP σ_{abs} on RH, but found negligible effect of RH on Aethalometer performance. It is also worth noting that RH in the Aethalometer optical chamber may be lower than the ambient RH due to the slightly elevated temperature inside the instrument. The magnitude of RH difference was found similar between different instruments: 20% for the Aethalometer (Schmid et al., 2006) and 15% for the nephelometer (Guyon et al., 2004). The RH in the Aethalometer optical chamber was not measured in this study. We expected its level to be slightly lower than the ambient RH. Cappa et al. (2008) found σ_{abs} measurements by PSAP and PAS maintained a high linearity even under high RH conditions (65-91%). Inter-comparison studies demonstrated that with proper corrections, Aethalometer σ_{abs} measurements agree well with those by PAS (Ajtai et al., 2011). During the inter-comparison study of an Aethalometer (AE-16) and a PAS in Guangzhou (Wu et al., 2009), good correlation was found (R^2=0.96) as shown in Figure S1. These comparison results imply that the Aethalometer results are linearly correlated with PAS measurements and RH has a limited interference on Aethalometer measurements. In our study, careful corrective measures (Wu et al., 2013) are conducted for the Aethalometer σ_{abs} data treatment to minimize these artifacts. But such artifacts still cannot be fully eliminated.

For the EC determination, different thermal optical analysis (TOA) protocols can impact the measurement variability and thus MAE. As shown in Table S1, MAE for the same samples at Fresno varied from 6.1 to 9.3 $m^2\ g^{-1}$, depending on which EC analysis protocol was applied (Chow et al., 2009). Studies in the PRD found that discrepancies in measured EC by different analysis protocols could be as large as a factor of 5 (Wu et al., 2012; Wu et al., 2016a), which adds to the uncertainty for the MAE estimation. In addition, EC by TOA is also different from refractory BC (rBC) reported by the laser induced incandescence (LII) technique (e.g. single particle soot photometer, SP2). For example, two studies in Toronto (Knox et al., 2009; Chan et al., 2011) both used the PAS for σ_{abs} measurement but different techniques for EC mass determination, resulting in very different MAE results. LII instruments are usually calibrated with a commercially available surrogate (e.g. fullerene) since direct calibration with ambient soot is not easy to achieve. Laborde et al. (2012) indicates that the incandescence response of SP2 exhibits a dependency on soot type (15% between fullerene and denuded diesel soot particles; 14% between biomass burning and denuded diesel soot particles). Due to the absence of widely accepted reference materials for EC, the uncertainties in EC determination

will exist in the foreseeable future. All these uncertainties, including the uncertainty of rBC mass determination by SP2, uncertainty of EC in TOA, the discrepancy between SP2 rBC and TOA EC and the discrepancy of σ_{abs} between filter transmission and photo-acoustic methods, can contribute to the differences in MAE listed in Table S1.

Systematic bias in MAE (e.g. overestimation of σ_{abs} and variability of EC mass by different TOA protocols) discussed above have little effect on E_{abs} estimation by MRS. As shown in Eq. 3, E_{abs} is the ratio of MAE_t to MAE_p or $\sigma_{abs,t}$ to $\sigma_{abs,p}$, thus most of the bias in EC mass or σ_{abs} is cancelled out during the E_{abs} calculation. More details are discussed in section 4.1.

3 Methodology

3.1 MAE_p estimation by MRS from the ambient data

In this section, a new approach for MAE_p estimation is introduced for E_{abs} determination, which requires the knowledge of differentiating $\sigma_{abs,p}$ and $\sigma_{abs,c}$ portions in $\sigma_{abs,t}$. The idea of decoupling $\sigma_{abs,t}$ into $\sigma_{abs,p}$ and $\sigma_{abs,c}$ is conceptually similar to decoupling OC into primary OC (POC) and secondary OC (SOC) in the EC tracer method as shown in Table 2. In the EC tracer method, if $(OC/EC)_p$ is known, POC can be determined from OC (Turpin and Huntzicker, 1991). The role of MAE_p here is similar to the role of $(OC/EC)_p$, the primary OC/EC ratio in the EC tracer method (a comparison is given in Table 2). If MAE_p (average MAE from primary emission sources) is known, E_{abs} can be obtained from the ratio of MAE_t/MAE_p (Eq. 3). Therefore, the key for E_{abs} estimation is to derive an appropriate MAE_p. It is worth noting that MAE_p here does not represent MAE from a single or specific primary emission source, instead it reflects an average and effective MAE that has taken consideration of various primary emission sources. Thus, the MAE_p is conceptually analogous to $(OC/EC)_p$ in the EC tracer method, in which the primary ratio reflects an overall ratio from primary emission sources rather than from a single primary source.

The Minimum R squared method (MRS) explores the inherent independency between pollutants from primary emissions (e.g., EC) and products associated with secondary formation processes (e.g., SOC, $\sigma_{abs,c}$) to derive the primary ratios (e.g., $(OC/EC)_p$, MAE_p) in the EC tracer

method (Wu and Yu, 2016). When applying MRS for light absorption enhancement estimation, MRS is used to explore the inherent independency between EC and $\sigma_{abs,c}$, which is gained during atmospheric aging after emission. An example of MAE_p estimation by MRS is shown in Figure 1. Firstly, the assumed MAE_p value is varied continuously in a reasonable range (0.01 to 50 $m^2\ g^{-1}$ as shown in Figure 1). Then at each hypothetical MAE_p, $\sigma_{abs,c}$ can be calculated by Eq. 6 (a combination of Eq. 2&4) using EC and $\sigma_{abs,t}$ from ambient measurements.

$$\sigma_{abs,c} = \sigma_{abs,t} - MAE_p \times EC \quad (6)$$

Accordingly, for each hypothetical MAE_p, a correlation coefficient value (R^2) of $\sigma_{abs,c}$ vs. EC (i.e., $R^2(\sigma_{abs,c}, EC)$) can be obtained. The series of $R^2(\sigma_{abs,c}, EC)$ values (y axis) are then plotted against the assumed MAE_p values (x axis) as shown by the red curve in Figure 1. The physical meaning of this plot can be interpreted as follows. The $\sigma_{abs,p}$ is the fraction of light absorption owing to primary emitted soot particles. As a result, $\sigma_{abs,p}$ is well correlated with EC mass. In contrast, the $\sigma_{abs,c}$ is the fraction of light absorption gained by the lensing effect of the coating on particles after emission. The variability of $\sigma_{abs,c}$ mainly depends on the coating thickness of the soot particles. Consequently, $\sigma_{abs,c}$ is independent of EC mass. Since variations of EC and $\sigma_{abs,c}$ are independent, the assumed MAE_p corresponding to the minimum $R^2(EC, \sigma_{abs,c})$ would then represent the most statistically probable MAE_p of the tested dataset.

A computer program (Wu, 2017b) in Igor Pro (WaveMetrics, Inc. Lake Oswego, OR, USA) was developed to facilitate MRS calculation with a user friendly graphical user interface. Another two Igor Pro based computer programs Histbox (Wu, 2017c) and Scatter Plot (Wu, 2017d) are used for generating histograms, box plots and scatter plots (with Deming regressions) presented in this study. Detailed descriptions of these computer programs can be found in the SI and the computer programs are available from https://sites.google.com/site/wuchengust.

3.2 Mie simulation

It can be informative to model a single soot particle using Mie theory (Bohren and Huffman, 1983) and understand the theoretical range and variability of the soot particle's optical properties.

Three types of mixing state are widely employed for parameterization: internal mixing, external mixing and core-shell. To better represent the real situation (coating due to the aging process), a core-shell model is considered in the Mie calculation (Figure S2), which is more realistic than a volume mixture model (Bond et al., 2006). An aerosol optical closure study in the North China Plain (NCP) found that the core-shell model can provide better performance than assuming purely internal mixing and external mixing (Ma et al., 2012). A morphology study using Scanning Transmission X-ray Microscopy found that core-shell is the dominating mixing state in ambient samples (Moffet et al., 2016). It should be noted that the core-shell model assumption still has its own limitations. A single particle soot photometer (SP2) study by Sedlacek et al. (2012) reported a negative lag time between the scattering and incandescence signals in samples influenced by biomass burning, implying a near surface location of soot relative to non-absorbing materials. Near surface type mixing of soot has also been observed in Tokyo, but accounted for only 10% of total mixed soot containing particles (Moteki et al., 2014). Considering the domination of core-shell type particles in the ambient environment, the core-shell assumption in our optical model is sufficient to approximate the real situation.

As shown in Figure S2, fresh emitted soot particles are chain-like aggregates of small spheres (30~50 nm). After the aging process, soot particles are coated with organic and inorganic materials. Sufficient evidence has shown that the coating not only results in particle size growth, but also makes the soot core become more compact due to its collapse (Alexander et al., 2008; Zhang et al., 2008; Lewis et al., 2009a), especially under high RH conditions (Leung et al., 2017). Since the spherical like core and shell favor Mie simulation, both core and shell are considered as spheres in the Mie calculation.

To investigate the spectrum properties of soot particles, 11 wavelengths (370, 405, 470, 520, 532, 550, 590, 660, 781, 880 and 950 nm) are considered in calculations to cover wavelengths in the most frequently used absorption measurement instruments. A refractive index (RI) of 1.85 – 0.71i is adopted for soot core (Bond and Bergstrom, 2006) and 1.55 for non-absorbing coating (clear shell) in the Mie calculation for all wavelengths. Studies suggest a group of organic matter (OM), known as Brown Carbon (BrC), can absorb solar radiation at UV wavelengths (Kirchstetter et al., 2004). Thus, a BrC coating (brown shell) scenario is also considered in Mie simulation following the wavelength-

dependent RI suggested by Lack and Cappa (2010), which ranges from 1.55-0.059i (370 nm) to 1.55-0.0005i (950 nm). A modeling study by Bond et al. (2006) indicates that absorption amplification is not sensitive to the RI, thus the result below is not expected to be sensitive to the RI variability. Due to the spherical assumption of the BC core, a constant particle density is adopted for simplicity instead of size dependent particle density. But it is worth noting that in reality, the effective density of soot varies with particle size due to the morphology change during particle aging (Tavakoli and Olfert, 2014; Dastanpour et al., 2017). Both core diameters (D_{core}) and shell diameters (D_{shell}) are constrained in the range of 10 ~ 3000 nm in the model simulations. The Mie calculations are implemented with a customized program (Wu, 2017e) written in Igro Pro (WaveMetrics, Inc. Lake Oswego, OR, USA) and it is available from https://sites.google.com/site/wuchengust. It should be noted that the core-shell type mixing state of particles is still rare in 3D atmospheric models like WRF-Chem (Matsui et al., 2013; Nordmann et al., 2014) due to computational cost limitation.

3.2.1 Mie modeled absorption angstrom exponent (AAE)

Absorption Angstrom Exponent (AAE) is a widely used parameter that describes the wavelength dependence of aerosol light absorption (Moosmuller et al., 2011), which can be written explicitly as

$$AAE(\lambda_1, \lambda_2) = -\frac{\ln(\sigma_{abs,\lambda 1}) - \ln(\sigma_{abs,\lambda 2})}{\ln(\lambda_1) - \ln(\lambda_2)} \quad (7)$$

It is well known that ambient soot particles exhibit an AAE close to unity (Bond, 2001). Modeled variability in $AAE_{470\text{-}660}$ of bare soot particles is shown in Figure S3. For soot particles with D_{core} <200 nm, $AAE_{470\text{-}660}$ is very close to 1 and decreases significantly for particles with D_{core} >200 nm. Considering a typical D_{core} of fresh emitted soot particles smaller than 200 nm (Rose et al., 2006; China et al., 2013), the model results confirm the frequently observed AAE close to 1 from ambient measurements (Kirchstetter et al., 2004). Modeled variability in $AAE_{470\text{-}660}$ of soot particles coated by non-absorbing substances (clear shell) and weakly absorbing materials (brown shell) is shown in Figure 2. Elevated AAE to ~2 is observed in the clear shell scenario (Figure 2a and 3b) for the most probable soot core particle sizes (<200 nm), which agrees well with a previous model study (Lack and

Cappa, 2010), implying that elevated AAE cannot be exclusively attributed to mixing with BrC. AAE elevation is more pronounced in the brown shell scenario. For soot particles with D_{core} <200 nm, brown shell $AAE_{470\text{-}660}$ can easily reach 3 for a coating of D_{shell}/D_{core}=3 (Figure 2c and 2d). These high AAE results are consistent with the previous model study (Lack and Cappa, 2010) and could partially explain the high AAE observed in measurement studies (Kirchstetter et al., 2004; Hoffer et al., 2006), since the presence of externally mixed BrC particles also contribute to the wavelength dependent light absorption.

3.2.2 Mie modeled single scattering albedo (SSA)

Variability in modeled SSA of soot particles coated by non-absorbing substances and weakly absorbing materials (e.g. BrC) is shown in Figure S4. For particles with D_{core}<200 nm and D_{shell}/D_{core} <3, the SSA increases gradually (up to ~0.9) with a thicker coating and behaves similarly between clear shell and brown shell scenarios.

3.2.3 Mie modeled mass absorption efficiency (MAE)

MAE is a useful indicator for soot mixing state. Variability in MAE of bare soot particles as a function of particle size at a wavelength of 550 nm is illustrated in Figure S5. The magnitude of MAE is sensitive to the soot density assumption, especially for particles <200 nm (Figure S5), but the overall trend of particle size dependency is similar between different density scenarios. MAE peaks at a particle size of 200 nm and decreases dramatically for larger particles. In our MAE calculation, a soot density of 1.9 g cm^{-3} is adopted, as suggested by Bond and Bergstrom (2006). The purpose of adopting constant density is to simplify the MAE calculation. It should be noted that the effective density of soot core is highly variable in ambient environments. For example, a study in Beijing (Zhang et al., 2016b) found a value of 1.2 g cm^{-3}. A recent chamber study found the effective density of soot can evolve from 0.43 to 1.45 g cm^{-3} during aging as coated by m-Xylene oxidation products (Guo et al., 2016). A study by a single-particle aerosol mass spectrometer in Guangzhou found the effective density of soot increased with particle size in the range of 400 to 1600 nm (Zhang et al., 2016a). The MAE of coated particles from different core/shell diameter combinations are shown in Figure S6. For

thickly coated particles, the MAE in the clear shell scenario varied as D_{shell}/D_{core} increased, but the MAE of brown shell scenario increased quasi-monotonously with D_{shell}/D_{core}.

3.2.4 Mie modeled light absorption enhancement factor (E_{abs})

E_{abs} is a better indicator for soot mixing state than MAE since it does not rely on the soot density assumption and is more suitable for comparing Mie simulations with ambient measurements. Modeled variability in E_{abs} of soot particles coated by non-absorbing substances and weakly absorbing materials (e.g. BrC) is shown in Figure 3a and 3c respectively. E_{abs} is not only sensitive to the core/shell diameter combination, but also behaves very differently on the clear and brown shell assumptions. For the clear shell scenario, when D_{coat}/D_{core} <2, E_{abs} does not exceed 2 for particles with different soot core sizes, but for the same D_{coat}/D_{core}, a larger soot core size yields a higher E_{abs} (Figure 3b, cross-sections of Figure 3a). If D_{coat}/D_{core} >2, E_{abs} could be 3 to 5 for particles with a soot core smaller than 200 nm, but for particles with a soot core larger than 200 nm, the E_{abs} is limited to ~2 as shown in Figure 3b. For the brown shell scenario, E_{abs} increased quasi-monotonically with D_{coat}/D_{core}, and this trend is similar for different soot core sizes (Figure 3d). The main reason behind is that in the brown shell scenario, both lensing effect and BrC absorption contribute to E_{abs}. As shown in Figure S7, the BrC absorption contribution to total E_{abs} strongly depends on coating thickness and is insensitive to soot core diameters. When the coating is relatively thin (<5 nm for λ@370 nm, <15 nm for λ@550 nm and <40 nm for λ@880 nm), BrC absorption contribution to the total E_{abs} is less than 20%. As the coating increases to a certain level (~15 nm for λ@370 nm, ~35 nm for λ@550 nm and ~90 nm for λ@880 nm), BrC absorption contribution is comparable to the lensing effect contribution, each contributing ~50% to the total E_{abs}. When the BrC coating is sufficiently thick (>30 nm for λ@370 nm, >90 nm for λ@550 nm and >110 nm for λ@880 nm), BrC absorption dominates the E_{abs} contribution. As a result, if BrC coating is indeed present in ambient samples, a strong wavelength dependent E_{abs} could be observed, since a BrC coating of 30 nm would be enough to induce a large amount of detectable E_{abs} in the UV range. Another major difference between the clear and brown shell scenarios is that, for thickly coated particles (e.g. D_{coat}/D_{core} >2), the brown shell can yield a much higher E_{abs} than the clear shell.

Both primary soot size distribution and coating thickness can affect the absorption enhancement of ambient BC particles. Ambient measurements by LII found soot particle number and mass modes peaking at 110 nm and 220 nm, respectively, in the PRD (Huang et al., 2011b). A study in Shanghai found similar results (70 nm for number concentrations and 200 nm for mass concentrations)(Gong et al., 2016). Considering that the LII technique is specific for BC mass determination which is independent of BC mixing state, the size distribution reported by LII can represent the size distribution of the BC core. A study using a Micro Orifice Uniform Deposit Impactor (MOUDI) found a EC mass size distribution in the PRD exhibiting three modes peaking at ~300, ~900 and ~5000 nm (Yu et al., 2010), implying a substantial coating of BC particles, and a diameter amplification of 3. BC sizing by LII is based on volume equivalent diameter (VED), while MOUDI is based on aerodynamic diameter. As a result, these two techniques do not necessarily yield similar sizes, even for the bare soot particles. The conversion between these two types of diameters involves the knowledge of particle density and morphology (drag force). A recent closure study on BC mixing state in the PRD region suggests σ_{abs} is dominated by coated soot particles in the range of 300~400 nm (Tan et al., 2016). Considering the dominant BC core distribution measured by SP2 (110 nm), the upper limit of E_{abs} in the PRD is roughly estimated as ~2 for the clear shell scenario (Figure 3b).

4 Results and discussions

4.1 Annual measurement statistics

The frequency distribution (log-normal) of σ_{abs550} is shown in Figure 4a, with an annual average (±1 S.D.) of 42.65±30.78 Mm^{-1}. A log-normal distribution is also found in the EC mass concentration (Figure 4b), with an annual average of 2.66±2.27 μg m^{-3}. Figure 4c demonstrates the yearlong frequency distribution of MAE_{550} at the NC site. The annual average MAE_{550} is 18.75±6.16 $m^2\ g^{-1}$ and the peak (±1 S.D.) of the lognormal fit is 15.70±0.22 $m^2\ g^{-1}$. A good correlation is observed between σ_{abs} and EC mass (R^2=0.92) as shown in Figure 4d, and the color coding indicates a MAE dependency on RH (the RH effect will be discussed in section 4.5). Annual average $AAE_{470\text{-}660}$ is 1.09±0.13 (Figure S8a), indicating that soot is the dominant absorbing substance in the PRD and the brown shell scenario

shown in the Mie simulation is unlikely to be important. Annual mean SSA_{525} is 0.86±0.05 (Figure S8c), similar to previous studies in the PRD (Jung et al., 2009; Wu et al., 2009). For comparison purpose, MAE measured at original wavelength and MAE scaled to 550 nm following the λ^{-1} assumption are both shown in Table S1. The MAE comparisons discussed below are MAE at 550 nm. MAE_{550} by previous studies at various locations was found to cover a wide range, from 5.9 to 61.6 m^2 g^{-1}. Annual average observed MAE_{550} at NC (18.75 m^2 g^{-1}) is higher than many studies shown in Figure 5, e.g., Shenzhen (Lan et al., 2013), Beijing (Yang et al., 2009), Mexico city (Doran et al., 2007) and Fresno (Chow et al., 2009).

As shown in Figure 1, the annual average $MAE_{p,550}$ estimated by MRS is 13 m^2 g^{-1}. MAE_p by MRS represents the MAE_p at the emission source, which is different from the MAE_p by the TD approach for two reasons. First, the morphology of thermally denuded BC particles (compact aggregates) is different from that of freshly emitted BC particles (chain-like aggregates). Second, most of the coatings are removed for TD denuded soot particles, but freshly emitted soot particles usually come with a thin coating of OC formed from condensation of OC vapors as the temperature drops from the flame to the ambient air. As a result, the MRS-derived MAE_p is expected to be higher than the MAE_p by the TD approach. The estimated $MAE_{p,550}$ is higher than a previous study in Guangzhou (7.44 m^2 g^{-1}) (Andreae et al., 2008), but comparable to Xi'an (11.34 m^2 g^{-1}) (Wang et al., 2014) and Toronto (9.53~12.57 m^2 g^{-1}) (Knox et al., 2009). The annual average E_{abs550} by MRS following Eq. 3 is estimated to be 1.50±0.48 (mean ± 1 S.D.).

It should be noted that the E_{abs} estimation approach demonstrated here is insensitive to the MAE bias (e.g. overestimation of σ_{abs} and variability of EC mass by different TOA protocols) discussed in section 2.1, because bias in EC mass or σ_{abs} is cancelled out in the E_{abs} calculation (Eq. 3), since E_{abs} is the ratio of $\sigma_{abs,t}$ to $\sigma_{abs,p}$. To investigate the performance of the MRS approach in response to systematic bias in EC and σ_{abs}, two simple tests are conducted as shown in Figures S9 and S10 by adding systematic biases to σ_{abs550} and EC. Test A represents a situation when σ_{abs} is overestimated and EC is underestimated. The biased data are marked as σ'_{abs550} and EC' respectively, as shown below:

$$\sigma'_{abs550} = \sigma_{abs550} \times 2 \quad (8)$$

$$EC' = EC \times 0.7 \quad (9)$$

As a result, the average MAE_{550} changed from 18.75 to 53.58 $m^2\ g^{-1}$ and MAE_p changed from 13 to 37 $m^2\ g^{-1}$ (Figure S9). However, E_{abs} by ratio of averages remain the same (1.44).

In Test B, EC by different TOA protocols are compared to investigate the effect of different EC determination approaches while σ_{abs550} remains unchanged. EC by IMPROVE TOR protocol is calculated from NIOSH TOT EC following an empirical formula for suburban sites derived from a 3-year OCEC dataset in PRD (Wu et al., 2016a):

$$EC_{IMP\_TOR} = 2.63 \times EC_{NSH\_TOT} + 0.05 \quad (10)$$

As shown in Figure S10, MAE_{550} changed from 18.75 to 7.02 $m^2\ g^{-1}$ and MAE_p changed from 13 to 5 $m^2\ g^{-1}$, but E_{abs} remain almost the same (1.40). Result of Test B implies that although EC is operationally defined, the discrepancy of EC between TOA protocols did not weaken the role of EC serving as a tracer for primary emissions in MRS application. These examples demonstrate that systematic biases in σ_{abs550} and EC have no effects on E_{abs} estimation by the MRS approach.

As mentioned in section 1, the definition of MAE_p by the TD approach is different from the MAE_p of emission source. The TD MAE_p is expected to be slightly lower than the MAE_p of emission source. Therefore, the corresponding E_{abs} are slightly different and it should be cautioned when comparing MRS-derived E_{abs} with E_{abs} by the TD approach and Mie simulations. The E_{abs} could vary by location, depending on the coating thickness and size distribution of the primary aerosols. After undergoing atmospheric aging, the E_{abs} can be increased during transport from emission source to rural areas. The magnitude of the E_{abs} found at the NC site is comparable to other locations such as Boulder (Lack et al., 2012a) (1.38), London (Liu et al., 2015) (1.4), Shenzhen (Lan et al., 2013) (1.3), Yuncheng (Cui et al., 2016b) (2.25), Jinan (Chen et al., 2017) (2.07) and Nanjing (Cui et al., 2016a) (1.6) and is higher than studies in California (Cappa et al., 2012) (1.06), as listed in Table 3. Spectrum E_{abs} are calculated from 370 to 950 nm as shown in Figure S11. E_{abs} in the PRD exhibits a weak wavelength dependence, with slightly higher E_{abs} at the shorter wavelength (e.g. E_{abs370} = 1.55) and is relatively lower in the IR range (e.g. E_{abs950} = 1.49).

4.2 Monthly characteristics of MAE, AAE and SSA

Monthly variations of MAE_{550} at the NC site are shown in Figure 6a and Table S2, revealing distinct patterns of higher MAE_{550} in summer and lower in winter. On the other hand, $AAE_{470\text{-}660}$ is lower in summer and higher in winter (Figure 6b and Table S3). Monthly SSA_{525} varied from 0.83 to 0.90 without a clear seasonal pattern, as shown in Figure S12 and Table S4. $MAE_{p,550}$ estimation for individual months is shown in Figure 6a (the purple line) and monthly E_{abs550} is calculated accordingly following Eq. 3 (Figure 6c). E_{abs550} shows clear seasonal variations, with higher values from April to August (1.52~1.97 as shown in Table S5) and relatively lower values from September to March (1.24~1.49). The highest enhancement is found in August (1.97). Factors affecting variation of E_{abs550} are discussed in the following sections, including air mass origin, biomass burning and RH.

4.3 The effect of air mass origin

It's of interest to understand the seasonal variations of optical properties in the PRD. Hourly backward trajectories for the past 72 hours were calculated using NOAA's HYSPLIT (Hybrid Single Particle Lagrangian Integrated Trajectory, version 4) model (Draxier and Hess, 1998) from Feb 2012 to Jan 2013 as shown in Figure S13. Cluster analysis was conducted using MeteoInfo (Wang, 2014). By examining the total spatial variance (TSV), the number of clusters was determined to be four as shown in Figure S14. Cluster 1 (C1) represents continental air masses from the north, accounting for 44.4% of total trajectories. C2 (22.8%) represents marine air masses coming from the South China Sea. C3 represents air masses from the east (Taiwan island). C4 (15.8%) represents transitional air masses coming from the east coastline of China. As shown in Figure 7, E_{abs550} from C2 (1.78) is higher than other clusters (1.30 – 1.42). Further Wilcoxon-Mann-Whitney tests show that E_{abs550} from C2 is significantly higher than E_{abs550} from C1, C3 and C4 (Figure S15), implying that particles from the South China Sea cluster is likely more aged than other clusters. Air mass origin in the PRD is dominated by C2 from Apr to Aug (Figure S16a) as a result of the South China Sea monsoon in the rainy season. In contrast, the dry season is ruled by continental air masses from the north (C1) due to the influence of the northeast monsoon. E_{abs550} from C2 varied from 1.67 to 2.19, but was always

higher than E_{abs550} from C1 and C3 during the rainy season (Figure S16b). As a result, the domination of aged air mass from the vast ocean is one of the reasons for the much higher E_{abs550} found in the rainy season.

4.4 The effect of biomass burning

Biomass burning (BB) and vehicular emission are the two major sources of soot particles. BC from biomass burning emission, depending on the fuel type and burning condition, may have a higher OC/EC ratio and a thicker coating, resulting in a higher MAE than vehicular emission (Shen et al., 2013; Cheng et al., 2016) . In this study, the influence of BB on optical properties is investigated using the K^+/EC ratio as a BB indicator. As shown in Figure 8, MAE_{550} is positively correlated with the K^+/EC ratio, which exhibits a clear seasonal pattern that is higher in the rainy season and lower in the dry season (Figure S17a). Southeast Asia has the highest fire emission density globally due to the high biofuel consumption along with frequent fire activity in this region (Aouizerats et al., 2015), making Southeast Asia a large contributor to BC emissions (Jason Blake, 2014). During the rainy season when oceanic wind prevails, BC from BB emission in Southeast Asia can reach PRD through long range transport (LRT), resulting in an elevated K^+/EC ratio and MAE_{550}. The Deming regression intercept (11.89) in Figure 8 represents the MAE without the BB effect. This non-BB MAE_{550} (11.89 $m^2 g^{-1}$) is only slightly lower than $MAE_{p,550}$ (13 $m^2 g^{-1}$) obtained in section 4.3, implying that a large fraction of $MAE_{p,550}$ could not be explained by the BB source. Additional evidence was obtained through examining regression relationships of $MAE_{p,550}$ with K^+/EC month-by-month (Figure S17b). Correlation of monthly $MAE_{p,550}$ vs. K^+/EC ratio yield a R^2 of 0.23 (Figure S17c). In contrast, a much higher correlation (R^2=0.58) was observed (Figure S17d) between $MAE_{p,550}$ and non-BB MAE_{550} (i.e., K^+/EC intercepts from Figure S17b). These results imply that BB is one of the contributors to the $MAE_{p,550}$ variations, but unlikely the dominating one.

Many studies have found that BB influenced samples exhibit elevated AAE due to the presence of wavelength dependent light absorbing substances like BrC and HUmic-LIke Substances (HULIS) (Kirchstetter et al., 2004; Hoffer et al., 2006; Sandradewi et al., 2008; Herich et al., 2011; Pokhrel et al., 2017). It is of interest to investigate whether elevated AAE observed in the PRD during the dry

season is associated with BB influence. As shown in Figure S18, $AAE_{370-470}$ and $AAE_{470-660}$ did not correlate with the BB indicator, K^+/EC ratio. These results suggest that the elevated AAE observed in the PRD wintertime is unlikely to be dominated by the BB effect. Beside the independency between $AAE_{470-660}$ and K^+/EC ratio, the measured $AAE_{470-660}$ range also implies that BB is not the major driving force of $AAE_{470-660}$ variations. The limited light absorption contribution from BrC in RPD region is observed in a recent study (Yuan et al., 2016) , which suggest an upper limit of BrC contribution of 10% at 405 nm in the winter time using the AAE approach. As discussed in our Mie simulation (section 3.1) and a previous study (Lack and Cappa, 2010), coating of non-absorbing materials onto soot particles can increase AAE up to 2. Since the monthly average $AAE_{470-660}$ in wintertime did not exceed 1.2 (Table S3), the variations of $AAE_{470-660}$ in the PRD are more likely associated with coatings rather than the contribution of BrC. The results also imply that attempts on BrC absorption attribution for the PRD dataset presented in this study could be risky, considering that elevation of AAE is actually dominated by coating (Lack and Langridge, 2013).

4.5 The effect of relative humidity (RH) on optical properties

Soot particles are relatively hydrophobic when freshly emitted, but tend to gain hygroscopicity during atmospheric aging. Hygroscopic growth of coated laboratory generated model BC was reported by McMeeking et al. (2011). Growth of ambient BC particle size by a factor of 1.4-1.6 under high RH has been observed in a UK study (Liu et al., 2013). Located in the subtropical zone, RH plays an important role on aerosol optical properties in the PRD region. The yearlong measurements at the NC site provide a unique opportunity to investigate the effect of RH on aerosol optical properties, since most existing ad hoc studies in the PRD only last for months. Liquid water content (LWC) was calculated using the E-AIM (model 2) thermodynamic model (Clegg et al., 1998). As shown in Figure S19, LWC on average accounted for a significant fraction (44%) of non-EC $PM_{2.5}$ mass, making it an important component of $PM_{2.5}$ mass and due to high RH in the PRD. Previously, hygroscopic growth was only considered for particle scattering in the IMPROVE formula for chemically resolved light extinction budget studies. In this study f(RH) of MAE was obtained from yearlong measurements as shown in Figure 9a for RH = 30 ~100% and color coded for LWC. It clearly shows that MAE_{550}

measured in NC is positively correlated with RH and the enhancement can be fitted by a polynomial equation. When RH is close to 100%, the LWC can account for 70% of $PM_{2.5}$ mass. The maximum f(RH) can reach 1.3, which is higher than the value found in Beijing (1.2) (Wu et al., 2016b), but lower than a numerical study (1.35) (Nessler et al., 2005). These results reveal that a large contribution of E_{abs} is coming from high LWC under high RH in the PRD region. Because RH has a clear diurnal pattern, it can affect the diurnal pattern of E_{abs} in the PRD. Since the RH effect on E_{abs} is rarely considered in existing climate models, the inclusion of RH effect can reduce the uncertainty for assessing BC's climate effect.

The $AAE_{470\text{-}660}$ dependency on RH is shown in Figure 9b. When RH is low (e.g. 30%), the $AAE_{470\text{-}660}$ is around 1.25 and decreases to 1.10 as RH increases to 50%. $AAE_{470\text{-}660}$ remains around 1.12 when RH is 50-70%. Then $AAE_{470\text{-}660}$ decreases again when RH is higher than 70% and can reach 1 when RH is close to 100%. Since a higher RH results in hygroscopic growth and larger particle diameters, the negative correlation between $AAE_{470\text{-}660}$ and RH provides a clue on soot particles' primary diameter and mixing state. As shown in the Mie simulation in Figure 2b, for a particle with D_{core} of 130 nm and D_{shell}/D_{core} of 2 to 4, $AAE_{470\text{-}660}$ decreases as the coating increases, and the decrease tapers off when $D_{shell}/D_{core} = 3$. The D_{core} obtained here (130nm) is comparable with D_{core} obtained from SP2 measurements (110nm) in the PRD (Huang et al., 2011a).

4.6 Implications for mixing state

Quantitative direct measurements of BC mixing state and coating thickness are still challenging. SP2 can estimate the coating thickness using a lag-time approach or a Mie calculation approach can be employed, but both methods have a limited range in coating thickness and uncertainties arise from the assumptions made during the retrieval. For example, recent studies found that the mass equivalent diameter of soot core measured by SP2 could be underestimated due to density assumptions (Zhang et al., 2016b). Although size distribution measurement is not available in this study, clues of mixing state still can be derived from bulk measurements of optical properties. As discussed in section 4.4.1, elevated E_{abs550} observed in the rainy season is associated with aged air masses from a marine origin. To probe the possible mixing state difference between dry and rainy season, E_{abs550} , SSA_{525} and

$AAE_{470\text{-}660}$ are used to narrow down the possible core-shell size range as shown in Figure S20. Monthly averages with one standard deviation of $AAE_{470\text{-}660}$, SSA_{525} and E_{abs550} are used as constraints to extract the intersecting core-shell size range from Figure 2a, Figure S4 and Figure 3a. January and August data are used to represent two different scenarios: elevated $AAE_{470\text{-}660}$ (1.19±0.11) with lower E_{abs550} (1.31±0.32) in dry season and low $AAE_{470\text{-}660}$ (1.04±0.09) with elevated E_{abs550} (1.97±0.71) in rainy season. The results show that January and August have a very different core-shell size range: in January, the core and shell range are 100 ~ 160 nm and 120 ~ 250 nm, respectively; in August, the core and shell range are 120 ~ 165 nm and 170 ~ 430 nm, respectively. This confirms again that the soot particles in the rainy season are likely to have a thicker coating than in the dry season.

5 Caveats of the MRS method in its applications to ambient data

The data in this study is dominated by BC absorption that did not show much influence from BrC. However, extra care should be taken if the samples exhibit substantial BrC signature (e.g. AAE>2). Such situations are equivalent to the two-source scenarios discussed in our previous paper on the MRS method (Wu and Yu, 2016) and the major findings are described below. Two types of two-source scenarios are considered: two correlated primary sources (scenario A) and two independent primary sources (scenario B). In scenario A in which both BC and primary BrC are dominated by BB, using BC as a solo tracer to calculate the primary ratio (MAE_p) still works. In scenario B in which BC and primary BrC are independent, using BC alone to determine a single primary MAE_p could lead to a considerable bias in E_{abs} estimation. Alternatively, if a reliable primary BrC tracer is available, the corresponding $MAE_{p,BrC}$ can be determined by MRS. With the knowledge of $MAE_{p,BrC}$ and $MAE_{p,BC}$, light absorption by BC and BrC can be calculated separately and the E_{abs} can be determined using Eq. (11) :

$$E_{abs} = \frac{\sigma_{abs,t}}{\sigma_{abs,p,BC}+\sigma_{abs,p,BrC}} = \frac{\sigma_{abs,t}}{MAE_{p,BC}\times EC+MAE_{p,BrC}\times BrC} \quad (11)$$

However, the implementation of Eq.11 is challenging due to the complexity in the chemical composition of BrC. For example, a recent study found that the 20 most absorbing BrC chromophores account for ~50% BrC light absorption and there is not a single compound contributing more than 10% (Lin et al., 2016), making it difficult to choose a single compound as the BrC tracer. In addition, time

resolved measurement of BrC chromophores has yet to emerge. As a result, for scenario B (sample AAE>2 & primary BrC variations independent of BC), estimation of E_{abs} by MRS is not practical at this stage due to the lack of required input data. Using BC alone to determine a single primary MAE_p could lead to a considerable bias and should be avoided.

6 Conclusions

In this study, a novel statistical approach is proposed and its application on ambient data is demonstrated using one-year hourly OC and EC data coupled with Aethalometer measurements. Unlike conventional E_{abs} determination approaches that require expensive instrumentation (e.g. TD-PAS, VTDMA, SP2), this new approach employs widely deployed instruments (field carbon analyzer and Aethalometer). The key of this new approach involves calculating MAE_p by the Minimum R Squared (MRS) method (Wu and Yu, 2016). It is found that E_{abs} estimation by MRS is insensitive to systematic biases in EC and σ_{abs} measurements. The annual average $MAE_{p,550}$ estimated by MRS is 13 $m^2 g^{-1}$ and annual average MAE_{550} is 18.75±6.16 $m^2 g^{-1}$, suggesting an annual average enhancement factor (E_{abs550}) of 1.50±0.48. This value is within the upper limit of E_{abs} (~2) by core-shell Mie simulations considering the typical soot size distribution and coating thickness in the PRD.

Both $MAE_{p,550}$ and E_{abs} show distinct seasonal variations, implying the complexity of soot particle mixing state variations in this region. The elevated summertime E_{abs550} in the PRD is found to be associated with the domination of aged air masses from the South China Sea, along with the long-range transport of biomass burning influenced air masses from Southeast Asia. Hygroscopic growth with elevated RH contributes to E_{abs} as well, which could be as high as 1.3. A negative correlation is found between $AAE_{470\text{-}660}$ and RH, suggesting a dominant particle size with a D_{core} of 130 nm and D_{shell}/D_{core} range of 2 to 4. Core-shell size ranges narrowed down by E_{abs550} and $AAE_{470\text{-}660}$ constraints suggest that soot particles in the rainy season are likely to have thicker coatings than in the dry season.

Data availability

OC, EC, inorganic ions and σ_{abs} data used in this study are available from corresponding authors upon request.

Acknowledgements

This work is supported by the National Natural Science Foundation of China (41605002, 41475004). We gratefully acknowledge the Fok Ying Tung Foundation for funding to the Atmospheric Research Center at HKUST Fok Ying Tung Graduate School. The authors thank Jingxiang Huang of Fok Ying Tung Graduate School for the assistance in OCEC analyzer maintenance. The authors are also grateful to Dr. Stephen M Griffith and Dr. Yongjie Li for the helpful comments. The authors gratefully acknowledge the NOAA Air Resources Laboratory (ARL) for the provision of the HYSPLIT transport and dispersion model used in this publication.

References

Adler, G., Riziq, A. A., Erlick, C., and Rudich, Y.: Effect of intrinsic organic carbon on the optical properties of fresh diesel soot, Proceedings of the National Academy of Sciences, 107, 6699-6704, doi: 10.1073/pnas.0903311106, 2010.

Ajtai, T., Filep, Á., Utry, N., Schnaiter, M., Linke, C., Bozóki, Z., Szabó, G., and Leisner, T.: Inter-comparison of optical absorption coefficients of atmospheric aerosols determined by a multi-wavelength photoacoustic spectrometer and an Aethalometer under sub-urban wintry conditions, J. Aerosol. Sci., 42, 859-866, doi: 10.1016/j.jaerosci.2011.07.008, 2011.

Alexander, D. T. L., Crozier, P. A., and Anderson, J. R.: Brown carbon spheres in East Asian outflow and their optical properties, Science, 321, 833-836, 2008.

Andreae, M. O., Schmid, O., Yang, H., Chand, D., Yu, J. Z., Zeng, L. M., and Zhang, Y. H.: Optical properties and chemical composition of the atmospheric aerosol in urban Guangzhou, China, Atmos. Environ., 42, 6335-6350, doi: 10.1016/j.atmosenv.2008.01.030, 2008.

Aouizerats, B., van der Werf, G. R., Balasubramanian, R., and Betha, R.: Importance of transboundary transport of biomass burning emissions to regional air quality in Southeast Asia during a high fire event, Atmos. Chem. Phys., 15, 363-373, doi: 10.5194/acp-15-363-2015, 2015.

Arnott, W. P., Moosmuller, H., Sheridan, P. J., Ogren, J. A., Raspet, R., Slaton, W. V., Hand, J. L., Kreidenweis, S. M., and Collett, J. L.: Photoacoustic and filter-based ambient aerosol light absorption measurements: Instrument comparisons and the role of relative humidity, J. Geophys. Res., 108, 2003.

Arnott, W. P., Hamasha, K., Moosmuller, H., Sheridan, P. J., and Ogren, J. A.: Towards aerosol light-absorption measurements with a 7-wavelength Aethalometer: Evaluation with a photoacoustic instrument and 3-wavelength nephelometer, Aerosol. Sci. Technol., 39, 17-29, doi: Doi 10.1080/027868290901972, 2005.

Bauer, J. J., Yu, X.-Y., Cary, R., Laulainen, N., and Berkowitz, C.: Characterization of the sunset semi-continuous carbon aerosol analyzer, J. Air Waste Manage. Assoc., 59, 826-833, doi: 10.3155/1047-3289.59.7.826, 2009.

Bohren, C. F. and Huffman, D. R.: Absorption and scattering of light by small particles, Wiley, New York, xiv, 530 p. pp., 1983.

Bond, T. C.: Spectral dependence of visible light absorption by carbonaceous particles emitted from coal combustion, Geophys. Res. Lett., 28, 4075-4078, doi: Doi 10.1029/2001gl013652, 2001.

Bond, T. C. and Bergstrom, R. W.: Light absorption by carbonaceous particles: An investigative review, Aerosol. Sci. Technol., 40, 27-67, doi: Doi 10.1080/02786820500421521, 2006.

Bond, T. C., Habib, G., and Bergstrom, R. W.: Limitations in the enhancement of visible light absorption due to mixing state, J. Geophys. Res., 111, -, 2006.

Bond, T. C., Zarzycki, C., Flanner, M. G., and Koch, D. M.: Quantifying immediate radiative forcing by black carbon and organic matter with the Specific Forcing Pulse, Atmos. Chem. Phys., 11, 1505-1525, doi: 10.5194/acp-11-1505-2011, 2011.

Cappa, C. D., Lack, D. A., Burkholder, J. B., and Ravishankara, A. R.: Bias in Filter-Based Aerosol Light Absorption Measurements Due to Organic Aerosol Loading: Evidence from Laboratory Measurements, Aerosol. Sci. Technol., 42, 1022-1032, doi: 10.1080/02786820802389285, 2008.

671 Cappa, C. D., Onasch, T. B., Massoli, P., Worsnop, D. R., Bates, T. S., Cross, E. S., Davidovits, P.,
672 Hakala, J., Hayden, K. L., Jobson, B. T., Kolesar, K. R., Lack, D. A., Lerner, B. M., Li, S.-M., Mellon,
673 D., Nuaaman, I., Olfert, J. S., Petäjä, T., Quinn, P. K., Song, C., Subramanian, R., Williams, E. J., and
674 Zaveri, R. A.: Radiative Absorption Enhancements Due to the Mixing State of Atmospheric Black
675 Carbon, Science, 337, 1078-1081, doi: 10.1126/science.1223447, 2012.
676 Chan, T. W., Brook, J. R., Smallwood, G. J., and Lu, G.: Time-resolved measurements of black carbon
677 light absorption enhancement in urban and near-urban locations of southern Ontario, Canada, Atmos.
678 Chem. Phys., 11, 10407-10432, 2011.
679 Chen, B., Bai, Z., Cui, X., Chen, J., Andersson, A., and Gustafsson, Ö.: Light absorption enhancement
680 of black carbon from urban haze in Northern China winter, Environ Pollut, 221, 418-426, doi:
681 10.1016/j.envpol.2016.12.004, 2017.
682 Cheng, Y., Engling, G., Moosmüller, H., Arnott, W. P., Chen, L. W. A., Wold, C. E., Hao, W. M., and
683 He, K.-b.: Light absorption by biomass burning source emissions, Atmos. Environ., 127, 347-354, doi:
684 10.1016/j.atmosenv.2015.12.045, 2016.
685 China, S., Mazzoleni, C., Gorkowski, K., Aiken, A. C., and Dubey, M. K.: Morphology and mixing
686 state of individual freshly emitted wildfire carbonaceous particles, Nat Commun, 4, doi:
687 10.1038/ncomms3122, 2013.
688 Chow, J. C., Watson, J. G., Doraiswamy, P., Chen, L. W. A., Sodeman, D. A., Lowenthal, D. H., Park,
689 K., Arnott, W. P., and Motallebi, N.: Aerosol light absorption, black carbon, and elemental carbon at
690 the Fresno Supersite, California, Atmos Res, 93, 874-887, doi: DOI 10.1016/j.atmosres.2009.04.010,
691 2009.
692 Clegg, S. L., Brimblecombe, P., and Wexler, A. S.: Thermodynamic Model of the System
693 H+−NH4+−SO42-−NO3-−H2O at Tropospheric Temperatures, The Journal of Physical Chemistry A,
694 102, 2137-2154, doi: 10.1021/jp973042r, 1998.
695 Coen, M. C., Weingartner, E., Apituley, A., Ceburnis, D., Fierz-Schmidhauser, R., Flentje, H.,
696 Henzing, J. S., Jennings, S. G., Moerman, M., Petzold, A., Schmid, O., and Baltensperger, U.:
697 Minimizing light absorption measurement artifacts of the Aethalometer: evaluation of five correction
698 algorithms, Atmos. Meas. Tech., 3, 457-474, doi: 10.5194/amt-3-457-2010, 2010.
699 Cui, F., Chen, M., Ma, Y., Zheng, J., Zhou, Y., Li, S., Qi, L., and Wang, L.: An intensive study on
700 aerosol optical properties and affecting factors in Nanjing, China, Journal of Environmental Sciences,
701 40, 35-43, doi: 10.1016/j.jes.2015.08.017, 2016a.
702 Cui, X., Wang, X., Yang, L., Chen, B., Chen, J., Andersson, A., and Gustafsson, Ö.: Radiative
703 absorption enhancement from coatings on black carbon aerosols, Sci.Total.Environ., 551, 51-56, doi:
704 10.1016/j.scitotenv.2016.02.026, 2016b.
705 Dastanpour, R., Momenimovahed, A., Thomson, K., Olfert, J., and Rogak, S.: Variation of the optical
706 properties of soot as a function of particle mass, Carbon, 124, 201-211, doi:
707 10.1016/j.carbon.2017.07.005, 2017.
708 Ding, A. J., Huang, X., Nie, W., Sun, J. N., Kerminen, V. M., Petäjä, T., Su, H., Cheng, Y. F., Yang,
709 X. Q., Wang, M. H., Chi, X. G., Wang, J. P., Virkkula, A., Guo, W. D., Yuan, J., Wang, S. Y., Zhang,
710 R. J., Wu, Y. F., Song, Y., Zhu, T., Zilitinkevich, S., Kulmala, M., and Fu, C. B.: Enhanced haze
711 pollution by black carbon in megacities in China, Geophys. Res. Lett., 43, 2873-2879, doi:
712 10.1002/2016GL067745, 2016.

713 Doran, J. C., Barnard, J. C., Arnott, W. P., Cary, R., Coulter, R., Fast, J. D., Kassianov, E. I., Kleinman,
714 L., Laulainen, N. S., Martin, T., Paredes-Miranda, G., Pekour, M. S., Shaw, W. J., Smith, D. F.,
715 Springston, S. R., and Yu, X. Y.: The T1-T2 study: evolution of aerosol properties downwind of
716 Mexico City, Atmos. Chem. Phys., 7, 1585-1598, doi: 10.5194/acp-7-1585-2007, 2007.
717 Draxier, R. R. and Hess, G. D.: An overview of the HYSPLIT_4 modelling system for trajectories,
718 dispersion and deposition, Aust Meteorol Mag, 47, 295-308, 1998.
719 Drinovec, L., Gregorič, A., Zotter, P., Wolf, R., Bruns, E. A., Prévôt, A. S. H., Petit, J. E., Favez, O.,
720 Sciare, J., Arnold, I. J., Chakrabarty, R. K., Moosmüller, H., Filep, A., and Močnik, G.: The filter-
721 loading effect by ambient aerosols in filter absorption photometers depends on the coating of the
722 sampled particles, Atmos. Meas. Tech., 10, 1043-1059, doi: 10.5194/amt-10-1043-2017, 2017.
723 Fuller, K. A., Malm, W. C., and Kreidenweis, S. M.: Effects of mixing on extinction by carbonaceous
724 particles, J. Geophys. Res., 104, 15941-15954, 1999.
725 Gong, X., Zhang, C., Chen, H., Nizkorodov, S. A., Chen, J., and Yang, X.: Size distribution and mixing
726 state of black carbon particles during a heavy air pollution episode in Shanghai, Atmos. Chem. Phys.,
727 16, 5399-5411, doi: 10.5194/acp-16-5399-2016, 2016.
728 Guo, S., Hu, M., Lin, Y., Gomez-Hernandez, M., Zamora, M. L., Peng, J., Collins, D. R., and Zhang,
729 R.: OH-Initiated Oxidation of m-Xylene on Black Carbon Aging, Environ. Sci. Technol., doi:
730 10.1021/acs.est.6b01272, 2016.
731 Guyon, P., Graham, B., Roberts, G. C., Mayol-Bracero, O. L., Maenhaut, W., Artaxo, P., and Andreae,
732 M. O.: Sources of optically active aerosol particles over the Amazon forest, Atmos. Environ., 38, 1039-
733 1051, doi: 10.1016/j.atmosenv.2003.10.051, 2004.
734 Hansen, A. D. A.: The Aethalometer Manual, Berkeley, California,USA, Magee Scientific, 2005.
735 Hansen, J. and Nazarenko, L.: Soot climate forcing via snow and ice albedos, P Natl Acad Sci USA,
736 101, 423-428, doi: DOI 10.1073/pnas.2237157100, 2004.
737 Herich, H., Hueglin, C., and Buchmann, B.: A 2.5 year's source apportionment study of black carbon
738 from wood burning and fossil fuel combustion at urban and rural sites in Switzerland, Atmos. Meas.
739 Tech., 4, 1409-1420, doi: DOI 10.5194/amt-4-1409-2011, 2011.
740 Hoffer, A., Gelencser, A., Guyon, P., Kiss, G., Schmid, O., Frank, G. P., Artaxo, P., and Andreae, M.
741 O.: Optical properties of humic-like substances (HULIS) in biomass-burning aerosols, Atmos. Chem.
742 Phys., 6, 3563-3570, 2006.
743 Huang, X. F., Gao, R. S., Schwarz, J. P., He, L. Y., Fahey, D. W., Watts, L. A., McComiskey, A.,
744 Cooper, O. R., Sun, T. L., Zeng, L. W., Hu, M., and Zhang, Y. H.: Black carbon measurements in the
745 Pearl River Delta region of China, J. Geophys. Res., 116, D12208, doi: 10.1029/2010jd014933, 2011a.
746 Huang, X. F., He, L. Y., Hu, M., Canagaratna, M. R., Kroll, J. H., Ng, N. L., Zhang, Y. H., Lin, Y.,
747 Xue, L., Sun, T. L., Liu, X. G., Shao, M., Jayne, J. T., and Worsnop, D. R.: Characterization of
748 submicron aerosols at a rural site in Pearl River Delta of China using an Aerodyne High-Resolution
749 Aerosol Mass Spectrometer, Atmos. Chem. Phys., 11, 1865-1877, doi: 10.5194/acp-11-1865-2011,
750 2011b.
751 IPCC: Climate change 2013 : the physical science basis : Working Group I contribution to the Fifth
752 Assessment Report of the Intergovernmental Panel on Climate Change, xi, 1535 pages. pp., 2013.
753 Jacobson, M. Z.: Effects of externally-through-internally-mixed soot inclusions within clouds and
754 precipitation on global climate, J Phys Chem A, 110, 6860-6873, 2006.

Jason Blake, C.: Quantifying the occurrence and magnitude of the Southeast Asian fire climatology, Environmental Research Letters, 9, 114018, 2014.
Jung, J., Lee, H., Kim, Y. J., Liu, X., Zhang, Y., Gu, J., and Fan, S.: Aerosol chemistry and the effect of aerosol water content on visibility impairment and radiative forcing in Guangzhou during the 2006 Pearl River Delta campaign, Journal of Environmental Management, 90, 3231-3244, doi: 10.1016/j.jenvman.2009.04.021, 2009.
Khalizov, A. F., Xue, H. X., Wang, L., Zheng, J., and Zhang, R. Y.: Enhanced Light Absorption and Scattering by Carbon Soot Aerosol Internally Mixed with Sulfuric Acid, J Phys Chem A, 113, 1066-1074, 2009.
Kirchstetter, T. W., Novakov, T., and Hobbs, P. V.: Evidence that the spectral dependence of light absorption by aerosols is affected by organic carbon, J. Geophys. Res., 109, D21208, doi: 10.1029/2004jd004999, 2004.
Knox, A., Evans, G. J., Brook, J. R., Yao, X., Jeong, C. H., Godri, K. J., Sabaliauskas, K., and Slowik, J. G.: Mass Absorption Cross-Section of Ambient Black Carbon Aerosol in Relation to Chemical Age, Aerosol. Sci. Technol., 43, 522-532, doi: Doi 10.1080/02786820902777207, 2009.
Koch, D. and Del Genio, A.: Black carbon semi-direct effects on cloud cover: review and synthesis, Atmos. Chem. Phys., 10, 7685-7696, 2010.
Kozlov, V. S., Panchenko, M. V., Tikhomirov, A. B., Tikhomirov, B. A., and Shmargunov, V. P.: Effect of relative air humidity on photoacoustic aerosol absorption measurements in the near-ground atmospheric layer, Atmospheric and Oceanic Optics, 24, 487, doi: 10.1134/s1024856011050101, 2011.
Laborde, M., Mertes, P., Zieger, P., Dommen, J., Baltensperger, U., and Gysel, M.: Sensitivity of the Single Particle Soot Photometer to different black carbon types, Atmos. Meas. Tech., 5, 1031-1043, 2012.
Lack, D. A. and Cappa, C. D.: Impact of brown and clear carbon on light absorption enhancement, single scatter albedo and absorption wavelength dependence of black carbon, Atmos. Chem. Phys., 10, 4207-4220, doi: DOI 10.5194/acp-10-4207-2010, 2010.
Lack, D. A., Langridge, J. M., Bahreini, R., Cappa, C. D., Middlebrook, A. M., and Schwarz, J. P.: Brown carbon and internal mixing in biomass burning particles, P Natl Acad Sci USA, 109, 14802-14807, doi: 10.1073/pnas.1206575109, 2012a.
Lack, D. A., Richardson, M. S., Law, D., Langridge, J. M., Cappa, C. D., McLaughlin, R. J., and Murphy, D. M.: Aircraft instrument for comprehensive characterization of aerosol optical properties, Part 2: black and brown carbon absorption and absorption enhancement measured with photo acoustic spectroscopy, Aerosol. Sci. Technol., 46, 555-568, 2012b.
Lack, D. A. and Langridge, J. M.: On the attribution of black and brown carbon light absorption using the Ångström exponent, Atmos. Chem. Phys., 13, 10535-10543, doi: 10.5194/acp-13-10535-2013, 2013.
Lan, Z.-J., Huang, X.-F., Yu, K.-Y., Sun, T.-L., Zeng, L.-W., and Hu, M.: Light absorption of black carbon aerosol and its enhancement by mixing state in an urban atmosphere in South China, Atmos. Environ., 69, 118-123, doi: 10.1016/j.atmosenv.2012.12.009, 2013.
Langridge, J. M., Richardson, M. S., Lack, D. A., Brock, C. A., and Murphy, D. M.: Limitations of the Photoacoustic Technique for Aerosol Absorption Measurement at High Relative Humidity, Aerosol. Sci. Technol., 47, 1163-1173, doi: 10.1080/02786826.2013.827324, 2013.

797 Leung, K. K., Schnitzler, E. G., Jäger, W., and Olfert, J. S.: Relative Humidity Dependence of Soot
798 Aggregate Restructuring Induced by Secondary Organic Aerosol: Effects of Water on Coating
799 Viscosity and Surface Tension, Environmental Science & Technology Letters, doi:
800 10.1021/acs.estlett.7b00298, 2017.
801 Lewis, K. A., Arnott, W. P., Moosmuller, H., Chakrabarty, R. K., Carrico, C. M., Kreidenweis, S. M.,
802 Day, D. E., Malm, W. C., Laskin, A., Jimenez, J. L., Ulbrich, I. M., Huffman, J. A., Onasch, T. B.,
803 Trimborn, A., Liu, L., and Mishchenko, M. I.: Reduction in biomass burning aerosol light absorption
804 upon humidification: roles of inorganically-induced hygroscopicity, particle collapse, and
805 photoacoustic heat and mass transfer, Atmos. Chem. Phys., 9, 8949-8966, 2009a.
806 Lewis, K. A., Arnott, W. P., Moosmüller, H., Chakrabarty, R. K., Carrico, C. M., Kreidenweis, S. M.,
807 Day, D. E., Malm, W. C., Laskin, A., Jimenez, J. L., Ulbrich, I. M., Huffman, J. A., Onasch, T. B.,
808 Trimborn, A., Liu, L., and Mishchenko, M. I.: Reduction in biomass burning aerosol light absorption
809 upon humidification: roles of inorganically-induced hygroscopicity, particle collapse, and
810 photoacoustic heat and mass transfer, Atmos. Chem. Phys., 9, 8949-8966, doi: 10.5194/acp-9-8949-
811 2009, 2009b.
812 Lin, P., Aiona, P. K., Li, Y., Shiraiwa, M., Laskin, J., Nizkorodov, S. A., and Laskin, A.: Molecular
813 Characterization of Brown Carbon in Biomass Burning Aerosol Particles, Environ. Sci. Technol., 50,
814 11815-11824, doi: 10.1021/acs.est.6b03024, 2016.
815 Liu, D., Allan, J., Whitehead, J., Young, D., Flynn, M., Coe, H., McFiggans, G., Fleming, Z. L., and
816 Bandy, B.: Ambient black carbon particle hygroscopic properties controlled by mixing state and
817 composition, Atmos. Chem. Phys., 13, 2015-2029, doi: 10.5194/acp-13-2015-2013, 2013.
818 Liu, D., Whitehead, J., Alfarra, M. R., Reyes-Villegas, E., Spracklen, D. V., Reddington, C. L., Kong,
819 S., Williams, P. I., Ting, Y.-C., Haslett, S., Taylor, J. W., Flynn, M. J., Morgan, W. T., McFiggans, G.,
820 Coe, H., and Allan, J. D.: Black-carbon absorption enhancement in the atmosphere determined by
821 particle mixing state, Nature Geosci, 10, 184-188, doi: 10.1038/ngeo2901, 2017.
822 Liu, F., Yon, J., and Bescond, A.: On the radiative properties of soot aggregates – Part 2: Effects of
823 coating, Journal of Quantitative Spectroscopy and Radiative Transfer, 172, 134-145, doi:
824 10.1016/j.jqsrt.2015.08.005, 2016a.
825 Liu, J., Lin, P., Laskin, A., Laskin, J., Kathmann, S. M., Wise, M., Caylor, R., Imholt, F., Selimovic,
826 V., and Shilling, J. E.: Optical properties and aging of light-absorbing secondary organic aerosol,
827 Atmos. Chem. Phys., 16, 12815-12827, doi: 10.5194/acp-16-12815-2016, 2016b.
828 Liu, S., Aiken, A. C., Gorkowski, K., Dubey, M. K., Cappa, C. D., Williams, L. R., Herndon, S. C.,
829 Massoli, P., Fortner, E. C., Chhabra, P. S., Brooks, W. A., Onasch, T. B., Jayne, J. T., Worsnop, D. R.,
830 China, S., Sharma, N., Mazzoleni, C., Xu, L., Ng, N. L., Liu, D., Allan, J. D., Lee, J. D., Fleming, Z.
831 L., Mohr, C., Zotter, P., Szidat, S., and Prevot, A. S. H.: Enhanced light absorption by mixed source
832 black and brown carbon particles in UK winter, Nat Commun, 6, doi: 10.1038/ncomms9435, 2015.
833 Ma, N., Zhao, C. S., Muller, T., Cheng, Y. F., Liu, P. F., Deng, Z. Z., Xu, W. Y., Ran, L., Nekat, B.,
834 van Pinxteren, D., Gnauk, T., Mueller, K., Herrmann, H., Yan, P., Zhou, X. J., and Wiedensohler, A.:
835 A new method to determine the mixing state of light absorbing carbonaceous using the measured
836 aerosol optical properties and number size distributions, Atmos. Chem. Phys., 12, 2381-2397, doi:
837 DOI 10.5194/acp-12-2381-2012, 2012.

Replacement Filter Tape for the Magee Scientific Model AE33 Aethalometer®: http://www.mageesci.com/images/stories/docs/Magee_Scientific_Filter_Aethalometer_AE_Tape_Replacement_discussion.pdf, 2017.
Matsui, H., Koike, M., Kondo, Y., Moteki, N., Fast, J. D., and Zaveri, R. A.: Development and validation of a black carbon mixing state resolved three-dimensional model: Aging processes and radiative impact, J. Geophys. Res., 118, 2304-2326, doi: 10.1029/2012JD018446, 2013.
McMeeking, G. R., Good, N., Petters, M. D., McFiggans, G., and Coe, H.: Influences on the fraction of hydrophobic and hydrophilic black carbon in the atmosphere, Atmos. Chem. Phys., 11, 5099-5112, doi: 10.5194/acp-11-5099-2011, 2011.
McMeeking, G. R., Fortner, E., Onasch, T. B., Taylor, J. W., Flynn, M., Coe, H., and Kreidenweis, S. M.: Impacts of nonrefractory material on light absorption by aerosols emitted from biomass burning, J. Geophys. Res., 119, 12,272-212,286, doi: 10.1002/2014JD021750, 2014.
Moffet, R. C., O'Brien, R. E., Alpert, P. A., Kelly, S. T., Pham, D. Q., Gilles, M. K., Knopf, D. A., and Laskin, A.: Morphology and mixing of black carbon particles collected in central California during the CARES field study, Atmos. Chem. Phys., 16, 14515-14525, doi: 10.5194/acp-16-14515-2016, 2016.
Moosmuller, H., Chakrabarty, R. K., Ehlers, K. M., and Arnott, W. P.: Absorption Angstrom coefficient, brown carbon, and aerosols: basic concepts, bulk matter, and spherical particles, Atmos. Chem. Phys., 11, 1217-1225, doi: DOI 10.5194/acp-11-1217-2011, 2011.
Moteki, N., Kondo, Y., and Adachi, K.: Identification by single-particle soot photometer of black carbon particles attached to other particles: Laboratory experiments and ground observations in Tokyo, J. Geophys. Res., 119, 2013JD020655, doi: 10.1002/2013jd020655, 2014.
Nakayama, T., Ikeda, Y., Sawada, Y., Setoguchi, Y., Ogawa, S., Kawana, K., Mochida, M., Ikemori, F., Matsumoto, K., and Matsumi, Y.: Properties of light-absorbing aerosols in the Nagoya urban area, Japan, in August 2011 and January 2012: Contributions of brown carbon and lensing effect, J. Geophys. Res., 119, 2014JD021744, doi: 10.1002/2014JD021744, 2014.
Naoe, H., Hasegawa, S., Heintzenberg, J., Okada, K., Uchiyama, A., Zaizen, Y., Kobayashi, E., and Yamazaki, A.: State of mixture of atmospheric submicrometer black carbon particles and its effect on particulate light absorption, Atmos. Environ., 43, 1296-1301, doi: 10.1016/j.atmosenv.2008.11.031, 2009.
Nessler, R., Weingartner, E., and Baltensperger, U.: Effect of humidity on aerosol light absorption and its implications for extinction and the single scattering albedo illustrated for a site in the lower free troposphere, J. Aerosol. Sci., 36, 958-972, doi: 10.1016/j.jaerosci.2004.11.012, 2005.
Nordmann, S., Cheng, Y. F., Carmichael, G. R., Yu, M., Denier van der Gon, H. A. C., Zhang, Q., Saide, P. E., Pöschl, U., Su, H., Birmili, W., and Wiedensohler, A.: Atmospheric black carbon and warming effects influenced by the source and absorption enhancement in central Europe, Atmos. Chem. Phys., 14, 12683-12699, doi: 10.5194/acp-14-12683-2014, 2014.
Pandey, A., Pervez, S., and Chakrabarty, R. K.: Filter-based measurements of UV–vis mass absorption cross sections of organic carbon aerosol from residential biomass combustion: Preliminary findings and sources of uncertainty, Journal of Quantitative Spectroscopy and Radiative Transfer, 182, 296-304, doi: 10.1016/j.jqsrt.2016.06.023, 2016.
Peng, J., Hu, M., Guo, S., Du, Z., Zheng, J., Shang, D., Levy Zamora, M., Zeng, L., Shao, M., Wu, Y.-S., Zheng, J., Wang, Y., Glen, C. R., Collins, D. R., Molina, M. J., and Zhang, R.: Markedly enhanced

absorption and direct radiative forcing of black carbon under polluted urban environments, Proceedings of the National Academy of Sciences, 113, 4266-4271, doi: 10.1073/pnas.1602310113, 2016.
Pokhrel, R. P., Beamesderfer, E. R., Wagner, N. L., Langridge, J. M., Lack, D. A., Jayarathne, T., Stone, E. A., Stockwell, C. E., Yokelson, R. J., and Murphy, S. M.: Relative importance of black carbon, brown carbon, and absorption enhancement from clear coatings in biomass burning emissions, Atmos. Chem. Phys., 17, 5063-5078, doi: 10.5194/acp-17-5063-2017, 2017.
Ramanathan, V. and Carmichael, G.: Global and regional climate changes due to black carbon, Nat Geosci, 1, 221-227, doi: Doi 10.1038/Ngeo156, 2008.
Raspet, R., Slaton, W. V., Arnott, W. P., and Moosmüller, H.: Evaporation–Condensation Effects on Resonant Photoacoustics of Volatile Aerosols, Journal of Atmospheric and Oceanic Technology, 20, 685-695, doi: 10.1175/1520-0426(2003)20<685:eceorp>2.0.co;2, 2003.
Reid, J. S., Eck, T. F., Christopher, S. A., Koppmann, R., Dubovik, O., Eleuterio, D. P., Holben, B. N., Reid, E. A., and Zhang, J.: A review of biomass burning emissions part III: intensive optical properties of biomass burning particles, Atmos. Chem. Phys., 5, 827-849, doi: 10.5194/acp-5-827-2005, 2005.
Roden, C. A., Bond, T. C., Conway, S., and Pinel, A. B. O.: Emission factors and real-time optical properties of particles emitted from traditional wood burning cookstoves, Environ. Sci. Technol., 40, 6750-6757, doi: 10.1021/es052080i, 2006.
Rose, D., Wehner, B., Ketzel, M., Engler, C., Voigtländer, J., Tuch, T., and Wiedensohler, A.: Atmospheric number size distributions of soot particles and estimation of emission factors, Atmos. Chem. Phys., 6, 1021-1031, doi: 10.5194/acp-6-1021-2006, 2006.
Saathoff, H., Naumann, K. H., Schnaiter, M., Schöck, W., Möhler, O., Schurath, U., Weingartner, E., Gysel, M., and Baltensperger, U.: Coating of soot and (NH4)2SO4 particles by ozonolysis products of α-pinene, J. Aerosol. Sci., 34, 1297-1321, doi: 10.1016/S0021-8502(03)00364-1, 2003.
Sandradewi, J., Prévôt, A. S. H., Weingartner, E., Schmidhauser, R., Gysel, M., and Baltensperger, U.: A study of wood burning and traffic aerosols in an Alpine valley using a multi-wavelength Aethalometer, Atmos. Environ., 42, 101-112, doi: 10.1016/j.atmosenv.2007.09.034, 2008.
Saturno, J., Pöhlker, C., Massabò, D., Brito, J., Carbone, S., Cheng, Y., Chi, X., Ditas, F., Hrabě de Angelis, I., Morán-Zuloaga, D., Pöhlker, M. L., Rizzo, L. V., Walter, D., Wang, Q., Artaxo, P., Prati, P., and Andreae, M. O.: Comparison of different Aethalometer correction schemes and a reference multi-wavelength absorption technique for ambient aerosol data, Atmos. Meas. Tech., 10, 2837-2850, doi: 10.5194/amt-10-2837-2017, 2017.
Schmid, O., Artaxo, P., Arnott, W. P., Chand, D., Gatti, L. V., Frank, G. P., Hoffer, A., Schnaiter, M., and Andreae, M. O.: Spectral light absorption by ambient aerosols influenced by biomass burning in the Amazon Basin. I: Comparison and field calibration of absorption measurement techniques, Atmos. Chem. Phys., 6, 3443-3462, 2006.
Schnaiter, M., Linke, C., Mohler, O., Naumann, K. H., Saathoff, H., Wagner, R., Schurath, U., and Wehner, B.: Absorption amplification of black carbon internally mixed with secondary organic aerosol, J. Geophys. Res., 110, -, 2005.
Schwarz, J. P., Spackman, J. R., Fahey, D. W., Gao, R. S., Lohmann, U., Stier, P., Watts, L. A., Thomson, D. S., Lack, D. A., Pfister, L., Mahoney, M. J., Baumgardner, D., Wilson, J. C., and Reeves,

J. M.: Coatings and their enhancement of black carbon light absorption in the tropical atmosphere, J. Geophys. Res., 113, -, 2008.
Sedlacek, A. J., Lewis, E. R., Kleinman, L., Xu, J. Z., and Zhang, Q.: Determination of and evidence for non-core-shell structure of particles containing black carbon using the Single-Particle Soot Photometer (SP2), Geophys. Res. Lett., 39, 2012.
Shen, G., Chen, Y., Wei, S., Fu, X., Zhu, Y., and Tao, S.: Mass absorption efficiency of elemental carbon for source samples from residential biomass and coal combustions, Atmos. Environ., 79, 79-84, doi: 10.1016/j.atmosenv.2013.05.082, 2013.
Shiraiwa, M., Kondo, Y., Iwamoto, T., and Kita, K.: Amplification of Light Absorption of Black Carbon by Organic Coating, Aerosol. Sci. Technol., 44, 46-54, 2010.
Suglia, S. F., Gryparis, A., Wright, R. O., Schwartz, J., and Wright, R. J.: Association of Black Carbon with Cognition among Children in a Prospective Birth Cohort Study, American Journal of Epidemiology, 167, 280-286, doi: 10.1093/aje/kwm308, 2008.
Tan, H., Liu, L., Fan, S., Li, F., Yin, Y., Cai, M., and Chan, P. W.: Aerosol optical properties and mixing state of black carbon in the Pearl River Delta, China, Atmos. Environ., 131, 196-208, doi: 10.1016/j.atmosenv.2016.02.003, 2016.
Tao, W. K., Chen, J. P., Li, Z. Q., Wang, C., and Zhang, C. D.: Impact of Aerosols on Convective Clouds and Precipitation, Rev Geophys, 50, Rg2001, doi: Doi 10.1029/2011rg000369, 2012.
Tavakoli, F. and Olfert, J. S.: Determination of particle mass, effective density, mass–mobility exponent, and dynamic shape factor using an aerodynamic aerosol classifier and a differential mobility analyzer in tandem, J. Aerosol. Sci., 75, 35-42, doi: 10.1016/j.jaerosci.2014.04.010, 2014.
ten Brink, H., Otjes, R., Jongejan, P., and Slanina, S.: An instrument for semi-continuous monitoring of the size-distribution of nitrate, ammonium, sulphate and chloride in aerosol, Atmos. Environ., 41, 2768-2779, doi: 10.1016/j.atmosenv.2006.11.041, 2007.
Turpin, B. J. and Huntzicker, J. J.: Secondary Formation of Organic Aerosol in the Los-Angeles Basin - a Descriptive Analysis of Organic and Elemental Carbon Concentrations, Atmos. Environ., 25, 207-215, 1991.
Ueda, S., Nakayama, T., Taketani, F., Adachi, K., Matsuki, A., Iwamoto, Y., Sadanaga, Y., and Matsumi, Y.: Light absorption and morphological properties of soot-containing aerosols observed at an East Asian outflow site, Noto Peninsula, Japan, Atmos. Chem. Phys., 16, 2525-2541, doi: 10.5194/acp-16-2525-2016, 2016.
Virkkula, A., Makela, T., Hillamo, R., Yli-Tuomi, T., Hirsikko, A., Hameri, K., and Koponen, I. K.: A simple procedure for correcting loading effects of aethalometer data, J. Air Waste Manage. Assoc., 57, 1214-1222, 2007.
Wang, Q., Huang, R., Zhao, Z., Cao, J., Ni, H., Tie, X., Zhu, C., Shen, Z., Wang, M., and Dai, W.: Effects of photochemical oxidation on the mixing state and light absorption of black carbon in the urban atmosphere of China, Environmental Research Letters, 12, 044012, 2017.
Wang, Q. Y., Huang, R. J., Cao, J. J., Han, Y. M., Wang, G. H., Li, G. H., Wang, Y. C., Dai, W. T., Zhang, R. J., and Zhou, Y. Q.: Mixing State of Black Carbon Aerosol in a Heavily Polluted Urban Area of China: Implications for Light Absorption Enhancement, Aerosol. Sci. Technol., 48, 689-697, doi: 10.1080/02786826.2014.917758, 2014.

962 Wang, Y. Q.: MeteoInfo: GIS software for meteorological data visualization and analysis,
963 Meteorological Applications, 21, 360-368, doi: 10.1002/met.1345, 2014.
964 Weingartner, E., Saathoff, H., Schnaiter, M., Streit, N., Bitnar, B., and Baltensperger, U.: Absorption
965 of light by soot particles: determination of the absorption coefficient by means of aethalometers, J.
966 Aerosol. Sci., 34, 1445-1463, doi: 10.1016/S0021-8502(03)00359-8, 2003.
967 Weyant, C. L., Shepson, P. B., Subramanian, R., Cambaliza, M. O. L., Heimburger, A., McCabe, D.,
968 Baum, E., Stirm, B. H., and Bond, T. C.: Black Carbon Emissions from Associated Natural Gas Flaring,
969 Environ. Sci. Technol., 50, 2075-2081, doi: 10.1021/acs.est.5b04712, 2016.
970 Wild, M.: Enlightening Global Dimming and Brightening, B Am Meteorol Soc, 93, 27-37, doi:
971 10.1175/bams-d-11-00074.1, 2011.
972 Wu, C., Ng, W. M., Huang, J., Wu, D., and Yu, J. Z.: Determination of Elemental and Organic Carbon
973 in PM2.5 in the Pearl River Delta Region: Inter-Instrument (Sunset vs. DRI Model 2001
974 Thermal/Optical Carbon Analyzer) and Inter-Protocol Comparisons (IMPROVE vs. ACE-Asia
975 Protocol), Aerosol. Sci. Technol., 46, 610-621, doi: 10.1080/02786826.2011.649313, 2012.
976 Wu, C., Huang, X. H. H., Ng, W. M., Griffith, S. M., and Yu, J. Z.: Inter-comparison of NIOSH and
977 IMPROVE protocols for OC and EC determination: implications for inter-protocol data conversion,
978 Atmos. Meas. Tech., 9, 4547-4560, doi: 10.5194/amt-9-4547-2016, 2016a.
979 Wu, C. and Yu, J. Z.: Determination of primary combustion source organic carbon-to-elemental carbon
980 (OC/EC) ratio using ambient OC and EC measurements: secondary OC-EC correlation minimization
981 method, Atmos. Chem. Phys., 16, 5453-5465, doi: 10.5194/acp-16-5453-2016, 2016.
982 Wu, D., Mao, J. T., Deng, X. J., Tie, X. X., Zhang, Y. H., Zeng, L. M., Li, F., Tan, H. B., Bi, X. Y.,
983 Huang, X. Y., Chen, J., and Deng, T.: Black carbon aerosols and their radiative properties in the Pearl
984 River Delta region, Sci China Ser D, 52, 1152-1163, doi: 10.1007/s11430-009-0115-y, 2009.
985 Wu, D., Wu, C., Liao, B., Chen, H., Wu, M., Li, F., Tan, H., Deng, T., Li, H., Jiang, D., and Yu, J. Z.:
986 Black carbon over the South China Sea and in various continental locations in South China, Atmos.
987 Chem. Phys., 13, 12257-12270, doi: 10.5194/acp-13-12257-2013, 2013.
988 Wu, Y., Zhang, R., Tian, P., Tao, J., Hsu, S. C., Yan, P., Wang, Q., Cao, J., Zhang, X., and Xia, X.:
989 Effect of ambient humidity on the light absorption amplification of black carbon in Beijing during
990 January 2013, Atmos. Environ., 124, Part B, 217-223, doi: 10.1016/j.atmosenv.2015.04.041, 2016b.
991 Yang, M., Howell, S. G., Zhuang, J., and Huebert, B. J.: Attribution of aerosol light absorption to black
992 carbon, brown carbon, and dust in China - interpretations of atmospheric measurements during EAST-
993 AIRE, Atmos. Chem. Phys., 9, 2035-2050, 2009.
994 Yu, H., Wu, C., Wu, D., and Yu, J. Z.: Size distributions of elemental carbon and its contribution to
995 light extinction in urban and rural locations in the pearl river delta region, China, Atmos. Chem. Phys.,
996 10, 5107-5119, doi: 10.5194/acp-10-5107-2010, 2010.
997 Yuan, J. F., Huang, X. F., Cao, L. M., Cui, J., Zhu, Q., Huang, C. N., Lan, Z. J., and He, L. Y.: Light
998 absorption of brown carbon aerosol in the PRD region of China, Atmos. Chem. Phys., 16, 1433-1443,
999 doi: 10.5194/acp-16-1433-2016, 2016.
1000 Zhang, G., Bi, X., Qiu, N., Han, B., Lin, Q., Peng, L., Chen, D., Wang, X., Peng, P., Sheng, G., and
1001 Zhou, Z.: The real part of the refractive indices and effective densities for chemically segregated
1002 ambient aerosols in Guangzhou measured by a single-particle aerosol mass spectrometer, Atmos.
1003 Chem. Phys., 16, 2631-2640, doi: 10.5194/acp-16-2631-2016, 2016a.

Zhang, R. Y., Khalizov, A. F., Pagels, J., Zhang, D., Xue, H. X., and McMurry, P. H.: Variability in morphology, hygroscopicity, and optical properties of soot aerosols during atmospheric processing, P Natl Acad Sci USA, 105, 10291-10296, 2008.

Zhang, Y., Zhang, Q., Cheng, Y., Su, H., Kecorius, S., Wang, Z., Wu, Z., Hu, M., Zhu, T., Wiedensohler, A., and He, K.: Measuring the morphology and density of internally mixed black carbon with SP2 and VTDMA: new insight into the absorption enhancement of black carbon in the atmosphere, Atmos. Meas. Tech., 9, 1833-1843, doi: 10.5194/amt-9-1833-2016, 2016b.

1013 Table 1. Abbreviations.

1014

Abbreviation	Definition
$AAE_{470\text{-}660}$	Absorption Angstrom Exponent between 470 and 660 nm
BB	Biomass burning
BrC	Brown Carbon
D_{core}, D_{shell}	Particle diameter of core/shell
E_{abs550}	Light absorption enhancement factor at 550 nm
σ_{abs550}	Light absorption coefficient at 550 nm
$\sigma_{abs,t}$	Total light absorption coefficient of a coated particle
$\sigma_{abs,p}$	Primary light absorption coefficient attributed to the soot core alone of a coated particle
$\sigma_{abs,c}$	Extra light absorption coefficient due to the lensing effect of coating on the soot core
LII	Laser induced incandescence technique for soot measurement
LWC	Liquid water content
MAE_{550}	Mass absorption efficiency at 550 nm, also known as mass absorption cross-section (MAC)
$MAE_{p,550}$	Primary MAE of freshly emitted soot particles at 550 nm
MAAP	Multi Angle Absorption Photometer
MOUDI	Micro Orifice Uniform Deposit Impactor
MRS	Minimum R squared method
PAS	Photo acoustic spectrometer
PRD	Pearl River Delta region, China
SP2	Single particle soot photometer
SSA	Single scattering albedo
TD	Thermal denuder
TOA	Thermal optical analysis
TSV	Total spatial variance in backward trajectories cluster analysis

1015

1016 Table 2. Comparison of MRS application on $(OC/EC)_p$ (for SOC estimation) and MAE_p (for E_{abs} estimation).

1017

	MRS in EC tracer method for SOC estimation (Wu and Yu, 2016)	**MRS in EC tracer method for E_{abs} estimation (this study)**
Key parameter of fresh EC particles to be determined	$(\frac{OC}{EC})_p = \frac{POC}{EC}$	$MAE_p = \frac{O\sigma_{abs,p}}{EC}$
Input quantities for MRS from measurements	OC, EC (tracer)	$\sigma_{abs,t}$, EC (tracer)
Variable to be decoupled by the tracer	OC=POC+SOC $=(\frac{OC}{EC})_p \times EC + SOC$	$\sigma_{abs,t} = \sigma_{abs,p} + \sigma_{abs,c}$ $=(\frac{O\sigma_{abs,tC}}{EC})_p \times EC + \sigma_{abs,c}$
Ambient measurement at its closest to fresh emissions	Minimum R^2 (SOC, EC) $SOC = OC - (\frac{OC}{EC})_p \times EC$	Minimum R^2 ($\sigma_{abs,c}$, EC) $\sigma_{abs,c} = \sigma_{abs,t} - MAE_p \times EC$
Graph	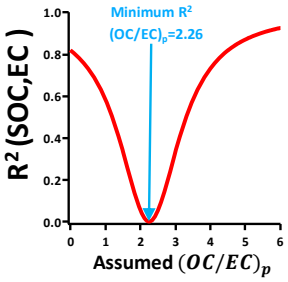	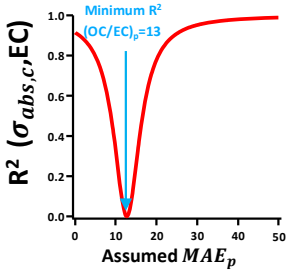

1018

1019 Table 3. Comparison of E_{abs} between various studies.

1020

Location	Type	Sampling Duration	λ (nm)	Instrument	E_{abs}	Method	Reference
Guangzhou, China	Suburban	2012.2-2013.1	550	AE+OCEC	1.50±0.48	MAE	This study
Xi'an, China	Urban	2012.12-2013.1	870	PAS	1.8	MAE	(Wang et al., 2014)
Shenzhen, China	Urban	2011.8-9	532	PAS	1.3	MAE	(Lan et al., 2013)
Jinan, China	Urban	2014.2	678	OCEC	2.07 ± 0.72	AFD	(Chen et al., 2017)
Nanjing, China	Suburban	2012.11	532	PAS	1.6	MAE	(Cui et al., 2016a)
Boulder, USA	Forest fire	2010.9	532	PAS	1.38	TD 200°C	(Lack et al., 2012a)
London, UK	Rural	2012.2	781	PAS	1.4	TD 250°C	(Liu et al., 2015)
California, USA	Rural	2010.6	532	PAS	1.06	TD 250°C	(Cappa et al., 2012)
Noto Peninsula, Japan	Rural	2013.4-5	781	PAS	1.22	TD 300°C	(Ueda et al., 2016)
Yuncheng, China	Rural	2014.6-7	678	OCEC	2.25 ± 0.55	AFD	(Cui et al., 2016b)
San Jose, Costa Rica	Rural	2006 winter	1064	SP2	1.3	Mie+SP2	(Schwarz et al., 2008)

1021 AE: Aethalometer ; OCEC: OCEC analyzer; PAS: photo acoustic spectrometer; SP2: Single particle soot photometer; TD: Thermal
1022 denuder AFD: filter filtration-dissolution

1023

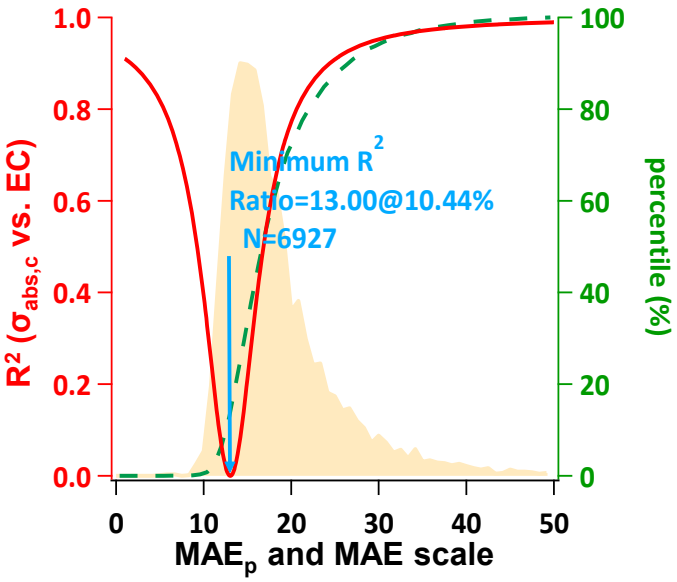

Figure 1. Minimum R squared (MRS) plot for calculating MAE_p at 550 nm. The red curve is the correlation result between $\sigma_{abs,c}$ ($\sigma_{abs,t}$ – EC * MAE_p) and EC mass. The shaded area in light tan represents the frequency distribution of observed MAE. The dashed green line is the cumulative distribution of observed MAE.

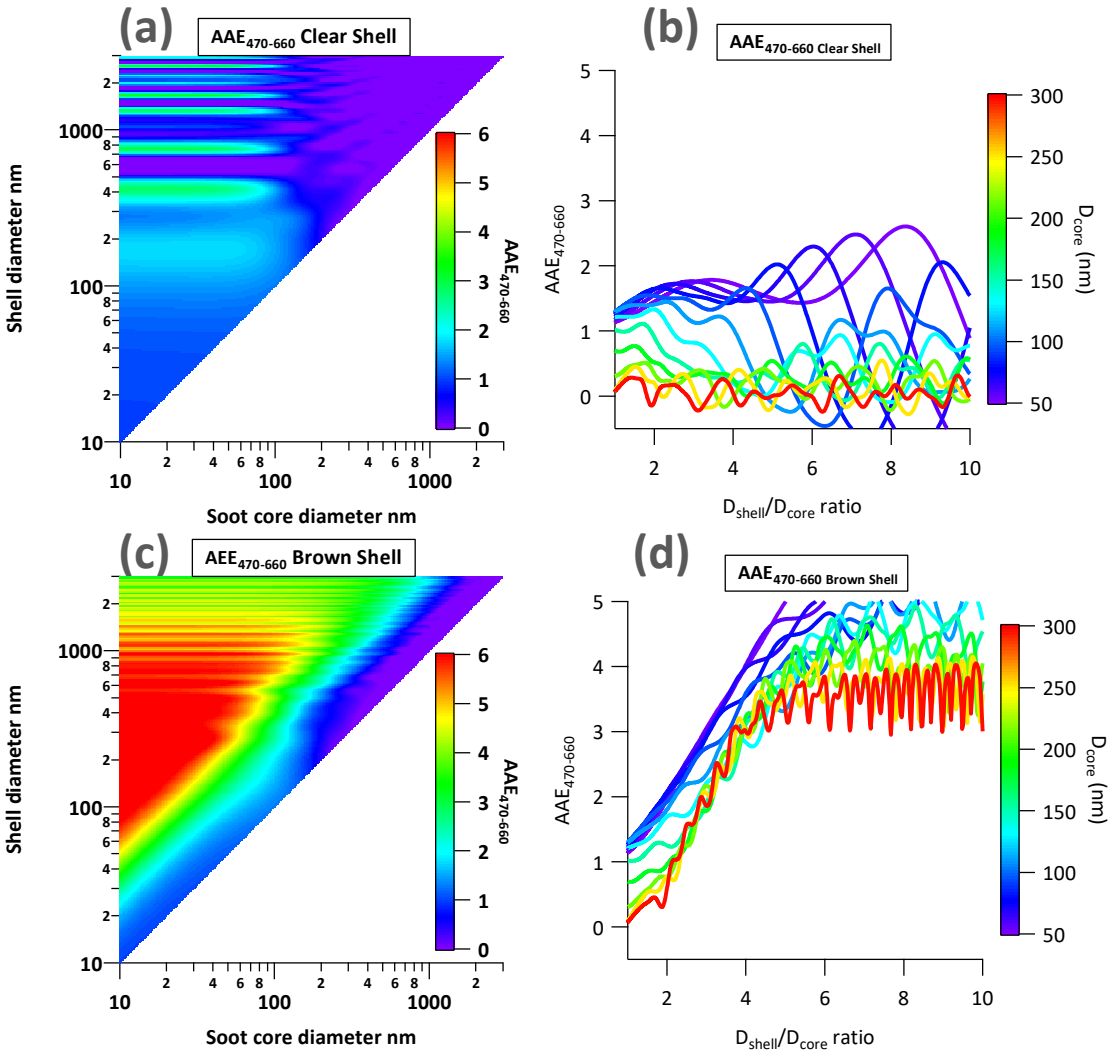

Figure 2. Mie simulated size dependency of soot particles $AAE_{470\text{-}660}$. (a) Combination of different clear shell (y axis) and core diameters (x axis). The color coding represents the $AAE_{470\text{-}660}$ of a particle with specific core and clear shell size; (b) Cross-sections views of (a). The color coding represents different D_{core} in the range of 50 ~ 300 nm. (c)&(d) Similar to (a)&(b) but from the brown shell scenario.

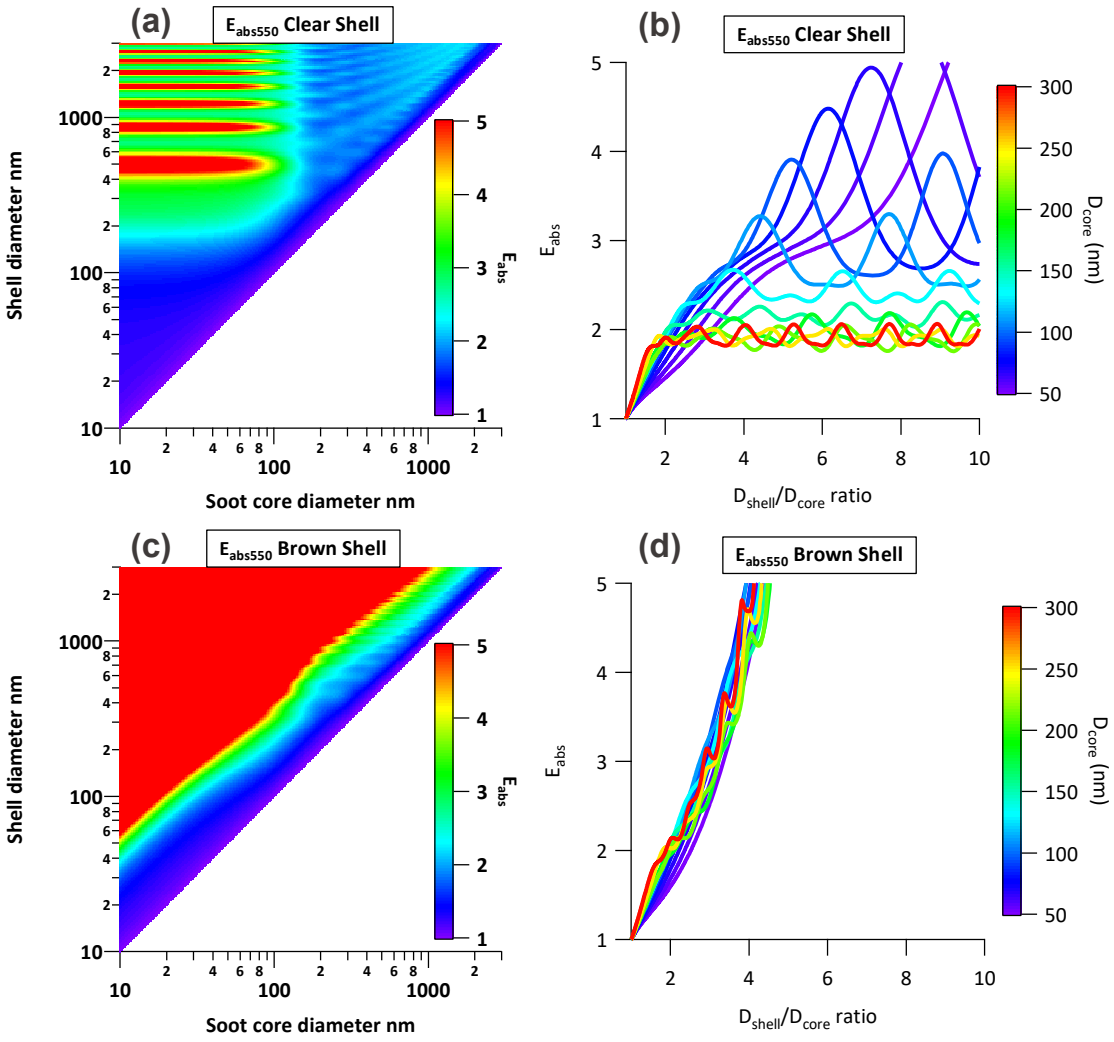

Figure 3. Mie simulated size dependency of soot particles E_{abs} at wavelength 550 nm. (a) Combination of different clear shell (y axis) and core diameters (x axis). The color coding represents the E_{abs} of a particle with specific core and clear shell size; (b) Cross-sections views of (a). The color coding represents different D_{core} in the range of 50 – 300 nm. (c)&(d) Similar to (a)&(b) but from the brown shell scenario.

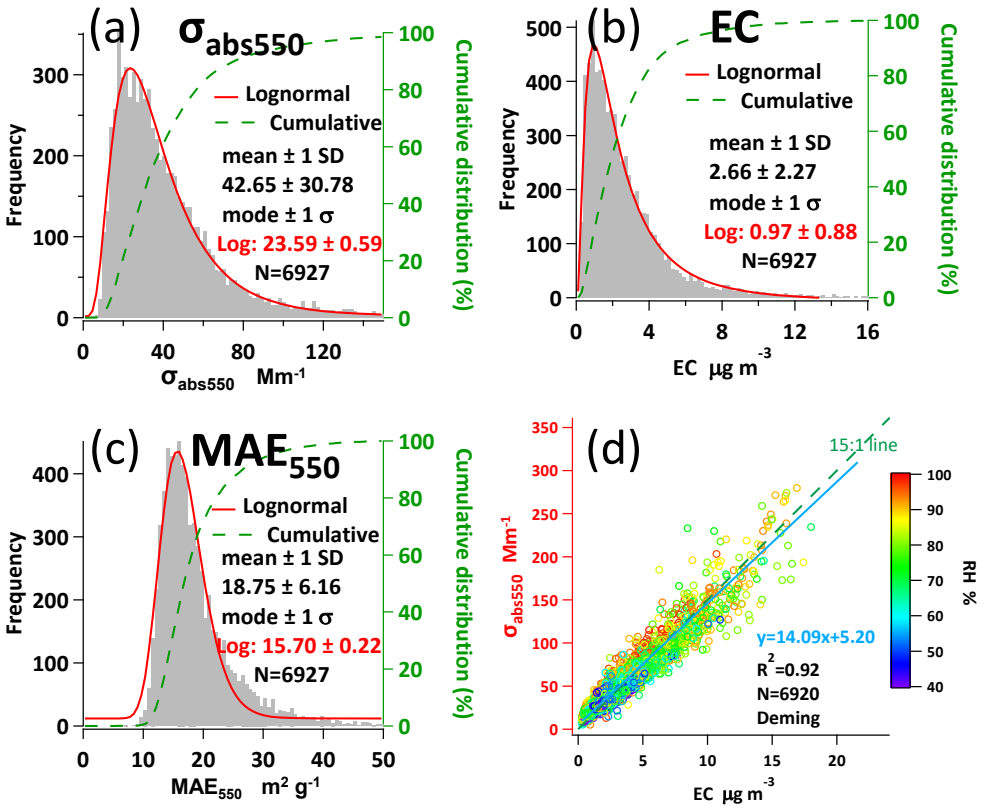

Figure 4. Measured annual statistics of σ_{abs550} , EC and MAE_{550}. (a) Annual frequency distribution of light absorption at 550 nm. The red curve represents the fitting line for a log-normal distribution. (b) Annual frequency distribution of EC mass concentration (c) Frequency distribution of Mass absorption efficiency (MAE) at 550 nm. (d) Scatter plot of light absorption (550 nm) and EC mass. The slope represents MAE_{550}. The blue regression line is by Deming regression. The color coding represents RH.

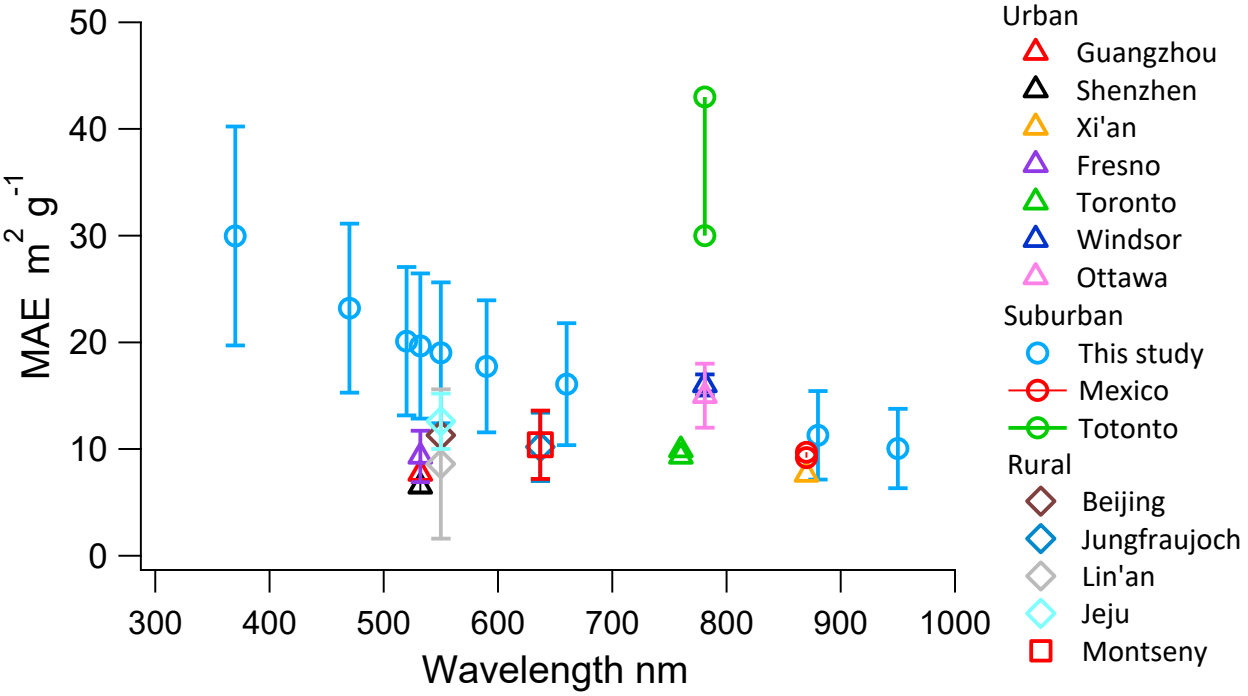

1051

1052 Figure 5. Comparison of spectral MAE measurements from this study with previous studies. Triangle, circle and rhombus
1053 represent urban, suburban and rural respectively. Details and reference can be found in Table S1. The whiskers represent
1054 one standard deviation.

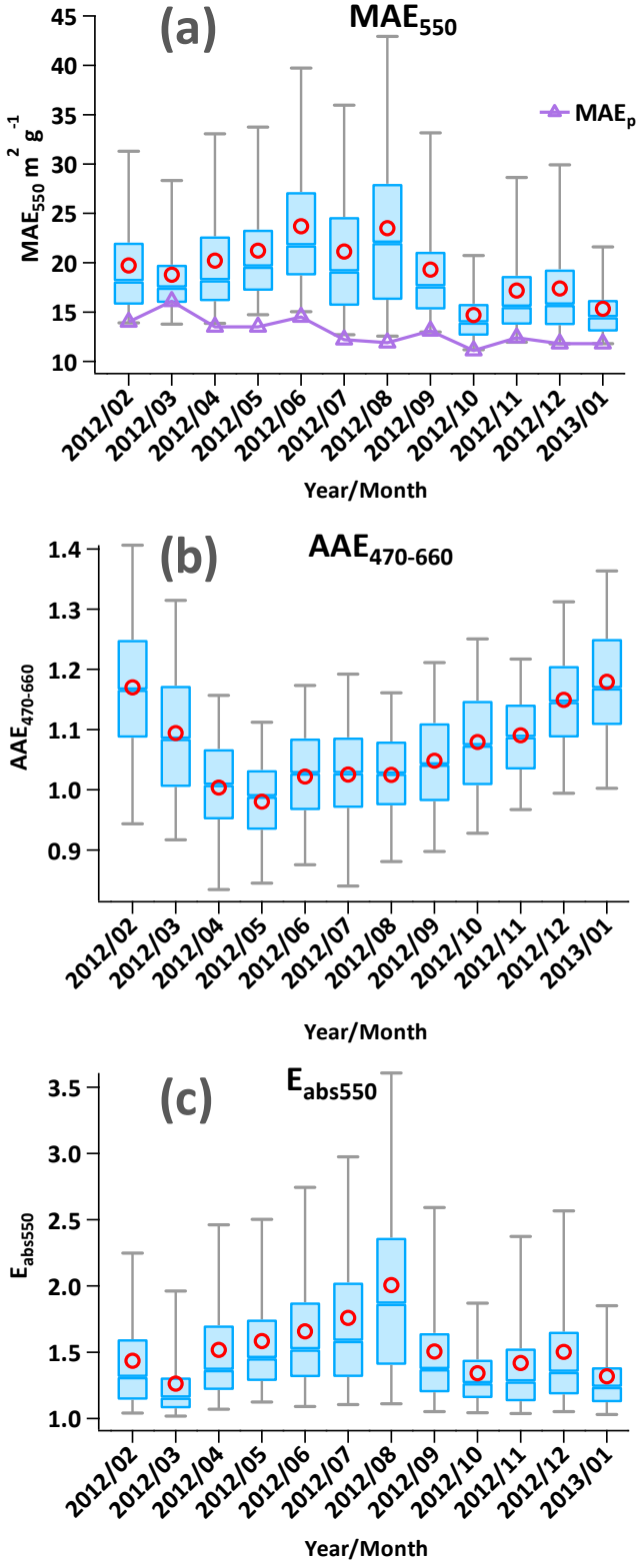

Figure 6. Measured monthly variations of (a) MAE_{550}, the purple line represents MAE_p estimated by MRS (b) $AAE_{470\text{-}660}$ and (c) E_{abs550}. Red circles represent the monthly average. The line inside the box indicates the monthly median. Upper and lower boundaries of the box represent the 75th and the 25th percentiles; the whiskers above and below each box represent the 95th and 5th percentiles.

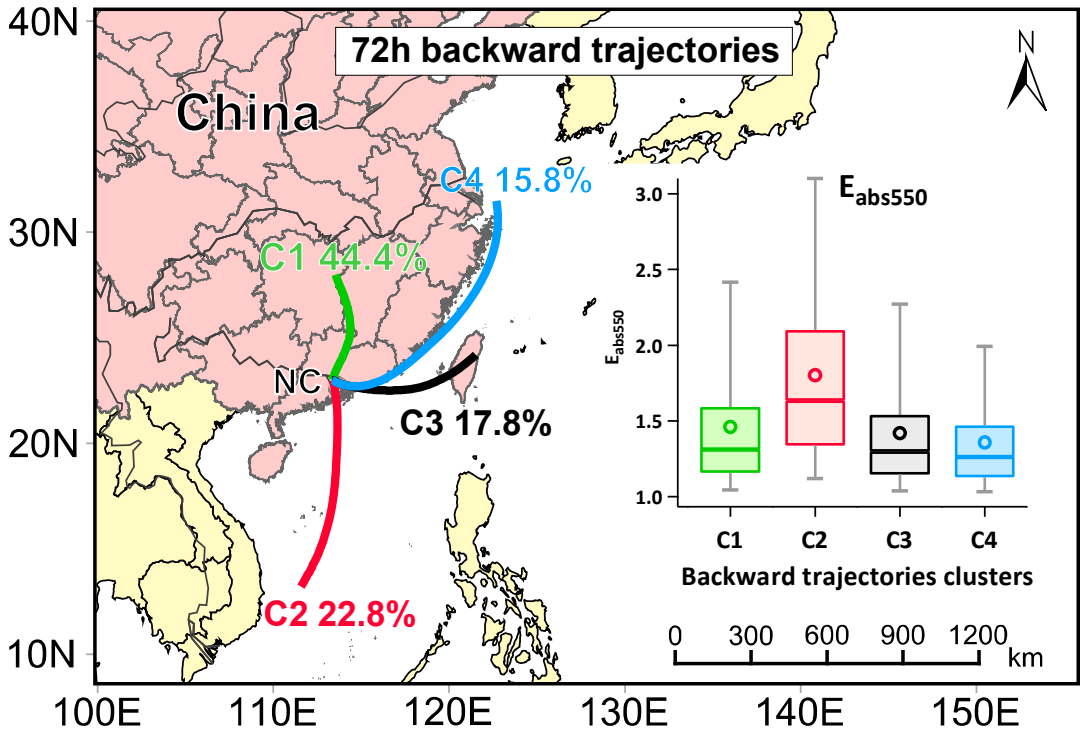

Figure 7. Average backward trajectories arriving at 100 m at NC site for four clusters (2012 Feb - 2013 Jan). E_{abs550} by different clusters are shown in the box plot.

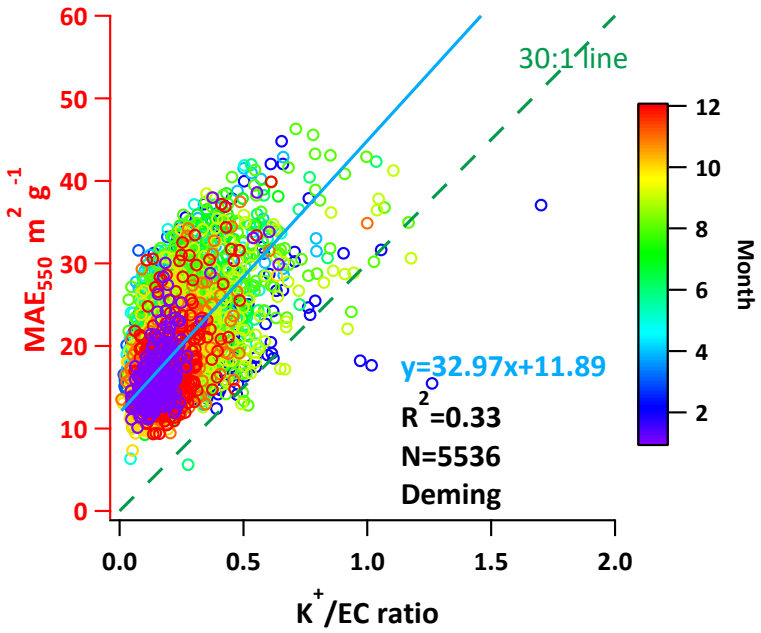

Figure 8. MAE_{550} dependency on biomass burning indicator K^+/EC ratio. The color coding represents months. The intercept represents MAE without biomass burning effect. The 30:1 line serves as a reference line with an integer slope that is close to the regressed slope through the origin.

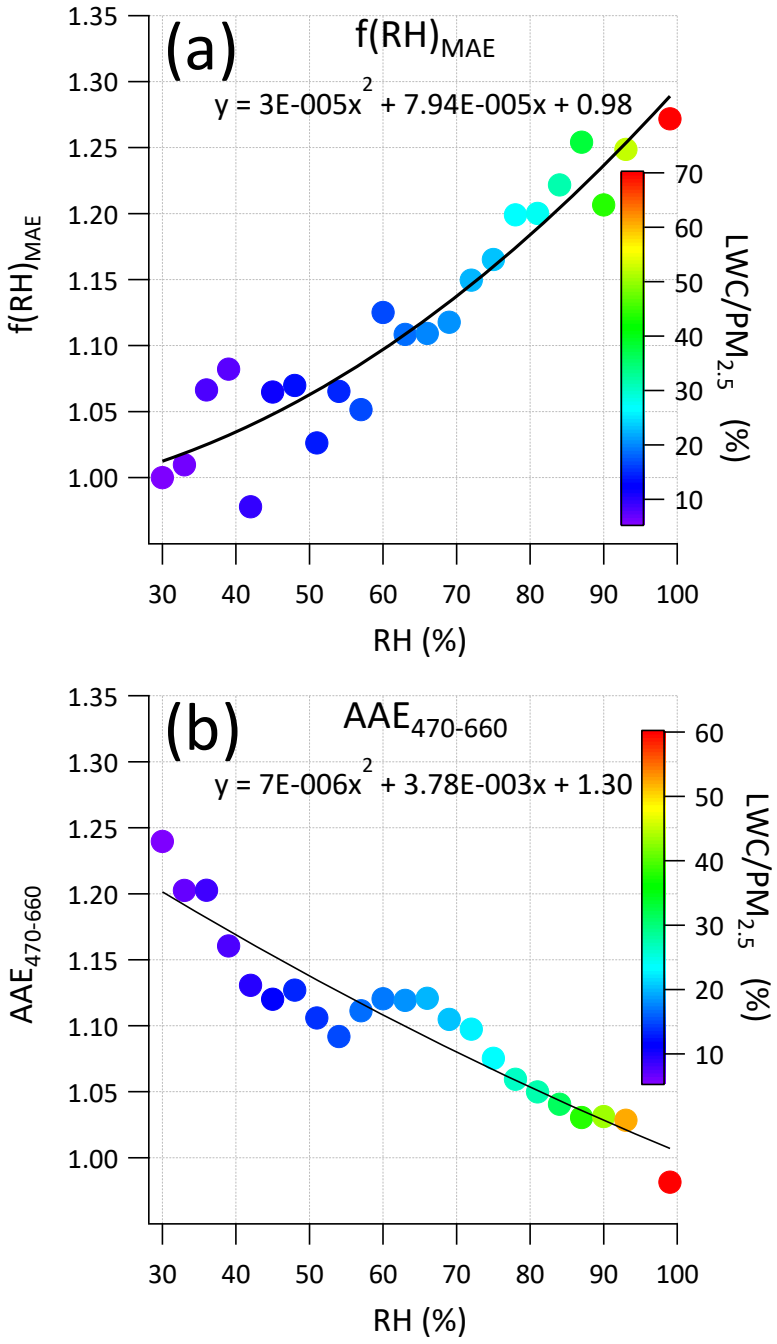

Figure 9. Optical properties dependency on RH determined from one year's sampling data at NC site. (a) Hygroscopic growth factor (f(RH)) of EC MAE_{550} (b) $AAE_{470\text{-}660}$ as a function of RH.

Supplement of

Quantifying black carbon light absorption enhancement by a novel statistical approach

Cheng Wu[1,2], Dui Wu[1,2,3], Jian Zhen Yu[4,5,6]

[1] Institute of Mass Spectrometer and Atmospheric Environment, Jinan University, Guangzhou 510632, China
[2] Guangdong Provincial Engineering Research Center for on-line source apportionment system of air pollution, Guangzhou 510632, China
[3] Institute of Tropical and Marine Meteorology, China Meteorological Administration, Guangzhou 510080, China
[4] Division of Environment, Hong Kong University of Science and Technology, Clear Water Bay, Hong Kong, China
[5] Atmospheric Research Centre, Fok Ying Tung Graduate School, Hong Kong University of Science and Technology, Nansha, China
[6] Department of Chemistry, Hong Kong University of Science and Technology, Clear Water Bay, Hong Kong, China

Corresponding to: Cheng Wu (wucheng.vip@foxmail.com) and Jian Zhen Yu (jian.yu@ust.hk)

This SI contains five tables and twenty-five figures.

Uncertainty of E_{abs} estimation

The uncertainty of E_{abs} estimation depends on uncertainty propagation from MAE uncertainty, which can be calculated from (Harris, 2010):

$$MAE_{Unc} = MAE \times \sqrt{\left(\frac{\sigma_{abs,Unc}}{\sigma_{abs}}\right)^2 + \left(\frac{EC_{Unc}}{EC}\right)^2} \quad \text{S1}$$

$$E_{abs,Unc} = E_{abs} \times \sqrt{\left(\frac{MAE_{Unc}}{MAE}\right)^2 + \left(\frac{MAE_{p,Unc}}{MAE_p}\right)^2} \quad \text{S2}$$

Descriptions of customized programs used in this study for data analysis and visualization

Several computer programs were developed to meet specific research purpose in this study. All the programs are based on Igor Pro (www.wavemetrics.com) that provides a friendly GUI. Brief descriptions are given below.

MRS program (Igor Pro based)

The program (Figure S21) is written in Igro Pro (WaveMetrics, Inc. Lake Oswego, OR, USA) to feasible MRS calculation via a user-friendly GUI. The MRS application is not limited in SOC estimation, but can also be extended to other applications (e.g. E_{abs} estimation) as long as a reliable tracer is available.

MRS calculation can be done by different temporal cycles (batch calculation): by year, by year&season, by season, by year&month, by month, by year&month&hour. Data filter is also available to calculate MRS on a specific subset of data.

The program is available from https://sites.google.com/site/wuchengust.

Mie program and source code written in Igor Pro

A computer program (Figure S22) written in Igro Pro (WaveMetrics, Inc. Lake Oswego, OR, USA) for Mie scattering calculation. Both BHMIE and BHCOAT (coated particles) algorithms(Bohren and Huffman, 1983) are included. The program is also capable of batch calculation for both algorithms. Available from https://sites.google.com/site/wuchengust.

Aethalometer data processing program (Igor Pro based)

This handy tool (Figure S23) can perform different corrections (e.g. Weingartner, Virkkula) on Aethalometer data. Raw Aethalometer data suffers from several artifacts including filter matrix effect (multiple scattering), loading effect (shadowing) and scattering effect. Careful corrections are needed for reporting light absorption coefficient from attenuation measurement. This Igor based program can directly import Aethalometer raw data and perform corrections (algorithm can be selected by user). Results can be exported to .csv files. Extra information including statistics of sensor voltage from each channel, sampling flow rate, etc are plotted for a quick QA/QC check. Available from https://sites.google.com/site/wuchengust.

Histbox program (Igor Pro based)

A handy tool (Figure S24) to generate histogram and box plots with many powerful features. Data can be sorted by different time scale and batch plotting is available. Available from https://sites.google.com/site/wuchengust.

Scatter plot program

Scatter plot (Figure S25) is a handy tool to maximize the efficiency of data visualization in atmospheric science. The program includes Deming, WODR and York algorithm for linear regression, which consider uncertainties in both X and Y, that is more realistic for atmospheric applications. It is Igor based, and packed with lots of useful features for data analysis and graph plotting, including batch plotting, data masking via GUI, color coding in Z axis, data filtering and grouping. Available from https://sites.google.com/site/wuchengust.

Reference

Andreae, M. O., Schmid, O., Yang, H., Chand, D., Yu, J. Z., Zeng, L. M., and Zhang, Y. H.: Optical properties and chemical composition of the atmospheric aerosol in urban Guangzhou, China, Atmos. Environ., 42, 6335-6350, doi: 10.1016/j.atmosenv.2008.01.030, 2008.

Bohren, C. F. and Huffman, D. R.: Absorption and scattering of light by small particles, Wiley, New York, xiv, 530 p. pp., 1983.

Chan, T. W., Brook, J. R., Smallwood, G. J., and Lu, G.: Time-resolved measurements of black carbon light absorption enhancement in urban and near-urban locations of southern Ontario, Canada, Atmos. Chem. Phys., 11, 10407-10432, 2011.

Chow, J. C., Watson, J. G., Doraiswamy, P., Chen, L. W. A., Sodeman, D. A., Lowenthal, D. H., Park, K., Arnott, W. P., and Motallebi, N.: Aerosol light absorption, black carbon, and elemental carbon at the Fresno Supersite, California, Atmos Res, 93, 874-887, doi: DOI 10.1016/j.atmosres.2009.04.010, 2009.

Chuang, P. Y., Duvall, R. M., Bae, M. S., Jefferson, A., Schauer, J. J., Yang, H., Yu, J. Z., and Kim, J.: Observations of elemental carbon and absorption during ACE-Asia and implications for aerosol radiative properties and climate forcing, J. Geophys. Res., 108, 8634, doi: Doi 10.1029/2002jd003254, 2003.

Doran, J. C., Barnard, J. C., Arnott, W. P., Cary, R., Coulter, R., Fast, J. D., Kassianov, E. I., Kleinman, L., Laulainen, N. S., Martin, T., Paredes-Miranda, G., Pekour, M. S., Shaw, W. J., Smith, D. F., Springston, S. R., and Yu, X. Y.: The T1-T2 study: evolution of aerosol properties downwind of Mexico City, Atmos. Chem. Phys., 7, 1585-1598, doi: 10.5194/acp-7-1585-2007, 2007.

Harris, D. C.: Quantitative chemical analysis, 8th ed., W.H. Freeman and Co., New York, 2010.

Knox, A., Evans, G. J., Brook, J. R., Yao, X., Jeong, C. H., Godri, K. J., Sabaliauskas, K., and Slowik, J. G.: Mass Absorption Cross-Section of Ambient Black Carbon Aerosol in Relation to Chemical Age, Aerosol. Sci. Technol., 43, 522-532, doi: Doi 10.1080/02786820902777207, 2009.

Lack, D. A. and Cappa, C. D.: Impact of brown and clear carbon on light absorption enhancement, single scatter albedo and absorption wavelength dependence of black carbon, Atmos. Chem. Phys., 10, 4207-4220, doi: DOI 10.5194/acp-10-4207-2010, 2010.

Lan, Z.-J., Huang, X.-F., Yu, K.-Y., Sun, T.-L., Zeng, L.-W., and Hu, M.: Light absorption of black carbon aerosol and its enhancement by mixing state in an urban atmosphere in South China, Atmos. Environ., 69, 118-123, doi: http://dx.doi.org/10.1016/j.atmosenv.2012.12.009, 2013.

Liu, D., Flynn, M., Gysel, M., Targino, A., Crawford, I., Bower, K., Choularton, T., Jurányi, Z., Steinbacher, M., Hüglin, C., Curtius, J., Kampus, M., Petzold, A., Weingartner, E., Baltensperger, U., and Coe, H.: Single particle characterization of black carbon aerosols at a tropospheric alpine site in Switzerland, Atmos. Chem. Phys., 10, 7389-7407, doi: 10.5194/acp-10-7389-2010, 2010.

Mayol-Bracero, O. L., Gabriel, R., Andreae, M. O., Kirchstetter, T. W., Novakov, T., Ogren, J., Sheridan, P., and Streets, D. G.: Carbonaceous aerosols over the Indian Ocean during the Indian Ocean Experiment (INDOEX): Chemical characterization, optical properties, and probable sources, J. Geophys. Res., 107, 8030, doi: Doi 10.1029/2000jd000039, 2002.

Moosmuller, H., Chakrabarty, R. K., Ehlers, K. M., and Arnott, W. P.: Absorption Angstrom coefficient, brown carbon, and aerosols: basic concepts, bulk matter, and spherical particles, Atmos. Chem. Phys., 11, 1217-1225, doi: DOI 10.5194/acp-11-1217-2011, 2011.

Naoe, H., Hasegawa, S., Heintzenberg, J., Okada, K., Uchiyama, A., Zaizen, Y., Kobayashi, E., and Yamazaki, A.: State of mixture of atmospheric submicrometer black carbon particles and

its effect on particulate light absorption, Atmos. Environ., 43, 1296-1301, doi: https://doi.org/10.1016/j.atmosenv.2008.11.031, 2009.
Pandolfi, M., Cusack, M., Alastuey, A., and Querol, X.: Variability of aerosol optical properties in the Western Mediterranean Basin, Atmos. Chem. Phys., 11, 8189-8203, doi: DOI 10.5194/acp-11-8189-2011, 2011.
Thompson, J. E., Hayes, P. L., Jimenez, K. A. J. L., Zhang, X., Liu, J., Weber, R. J., and Buseck, P. R.: Aerosol Optical Properties at Pasadena, CA During CalNex 2010, Atmos Environ, doi: 10.1016/j.atmosenv.2012.03.011, 2012.
Wang, Q., Huang, R., Zhao, Z., Cao, J., Ni, H., Tie, X., Zhu, C., Shen, Z., Wang, M., and Dai, W.: Effects of photochemical oxidation on the mixing state and light absorption of black carbon in the urban atmosphere of China, Environmental Research Letters, 12, 044012, 2017.
Wang, Q. Y., Huang, R. J., Cao, J. J., Han, Y. M., Wang, G. H., Li, G. H., Wang, Y. C., Dai, W. T., Zhang, R. J., and Zhou, Y. Q.: Mixing State of Black Carbon Aerosol in a Heavily Polluted Urban Area of China: Implications for Light Absorption Enhancement, Aerosol. Sci. Technol., 48, 689-697, doi: 10.1080/02786826.2014.917758, 2014.
Xu, J., Bergin, M. H., Yu, X., Liu, G., Zhao, J., Carrico, C. M., and Baumann, K.: Measurement of aerosol chemical, physical and radiative properties in the Yangtze delta region of China, Atmos. Environ., 36, 161-173, 2002.
Yang, M., Howell, S. G., Zhuang, J., and Huebert, B. J.: Attribution of aerosol light absorption to black carbon, brown carbon, and dust in China - interpretations of atmospheric measurements during EAST-AIRE, Atmos. Chem. Phys., 9, 2035-2050, 2009.

Table S1. Comparison of Mass absorption efficiency (MAE) at various locations. For literature MAE values at different wavelengths rather than 550 nm, an estimated MAE_{550} is given in the brackets following equations given by Moosmuller et al. (2011) assuming AAE of 1.

Location	Type	Sampling Duration	Inlet	λ (nm)	σ_{abs} Instrument	EC determination protocol	σ_{abs} ±1 S.D. (Mm^{-1})	EC mass ($\mu g\ m^{-3}$)	estimated MAE_p* ($m^2\ g^{-1}$)	observed MAE ($m^2\ g^{-1}$) arithmetic mean ±1 S.D.	observed MAE ($m^2\ g^{-1}$) Gaussian fit	Reference
Guangzhou, China	Suburban	2012.2-2013.1	$PM_{2.5}$	550	AE	NIOSH_TOT	42.65±29.41	2.66±2.27	13*	18.75±6.16	16.16	This study
Shenzhen, China	Urban	2011.8-9	$PM_{2.5}$	532	PAS	LII	25.4±19.0	4.0±3.1	/	6.5±0.5[6.29±0.48]	/	(Lan et al., 2013)
Xi'an, China	Urban	2012.12-2013.1	$PM_{2.5}$	870	PAS	LII	/	8.8±7.3	7.17[11.34]	/	7.62[12.05]	(Wang et al., 2014)
Xi'an, China	Urban	2013.2	$PM_{2.5}$	532	PAS	LII				14.6±5.6	12.7	(Wang et al., 2017)
Guangzhou, China	Urban	2004.10	$PM_{2.5}$	532	PAS	NIOSH_TOT	91±60	7.1	7.7[7.44]	/	/	(Andreae et al., 2008)
Fresno, USA	Urban	2005.8-9	$PM_{2.5}$	532	PAS	IMPROVE_A_TOR	5.06	1.01	/	6.1±2.5[5.9±2.42]	/	(Chow et al., 2009)
						NIOSH_TOT		0.58	/	9.3±2.4[8.99±2.32]	/	
T1,Mexico city, Mexico	Suburban	2006.3	$PM_{2.5}$	870	PAS	NIOSH_TOT	/	/	/	9.2~9.7***[14.55~15.34]	/	(Doran et al., 2007)
Tokyo, Japan	Suburban	2005.8	$PM_{2.5}$	565	PSAP	IMPROVE_A_TOR	30.43±20.41	2.9±2.13	11±1	/	/	(Naoe et al., 2009)
Pasadena, USA	Urban	2010.5-6	$PM_{2.5}$	532	AM	NIOSH_TOT	3.8±3.4	0.6~0.7	5.7[5.51]	/	/	(Thompson et al., 2012)
Toronto, Canada	Urban	2006.12-2007.1	$PM_{2.5}$	760	PAS	NIOSH_TOT	/	/	6.9~9.1** [9.53~12.57]	9.3~9.9[12.85~13.68]	/	(Knox et al., 2009)
Toronto, Canada	Suburban						3~6	0.10~0.14	/	30~43[42.6~61.06]	/	
Windsor, Canada	Urban	2007.8	$PM_{2.5}$	781	PAS	LII	4.4±2.9	0.27±0.23	/	16±1[22.72±1.42]	/	(Chan et al., 2011)
Ottawa, Canada	Urban						26±17	1.7±0.9	/	15±3[21.3±4.26]	/	
Beijing, China	Rural	2005.3	/	550	AE	NIOSH_TOT	/	/	9.5	11.3	/	(Yang et al., 2009)
Montseny, Spin	Rural (Mediterranean)	2009.11-2010.10	PM_{10}	637	MAAP	NIOSH_TOT	2.8±2.2	0.271±0.215	/	10.4[12.04]	/	(Pandolfi et al., 2011)
Jungfraujoch, Switzerland	Rural (high alpine)	2007.2-3	/	637	MAAP	LII	/	/	/	10.2±3.2[11.81±3.71]	/	(Liu et al., 2010)
Lin'an, China	Rural	1999.11	$PM_{2.5}$	550	PSAP	NIOSH_TOT	23±14	3.4±1.7	/	8.6±7.0	/	(Xu et al., 2002)
Jeju Island, Korea	Coastal Rural, (East China Sea)	2001.4	PM_{10}	550	PSAP	NIOSH_TOT	/	/	/	12.6±2.6	/	(Chuang et al., 2003)
Maldives	Oceanic rural	1999.2-3	PM_3	550	PSAP	EGA	62±34	2.5±1.4	6.6	8.1	/	(Mayol-Bracero et al., 2002)

*Determined by Minimium R Squared method; ** Median values;

AE:Aethalometer ; PAS photo acoustic spectrometer; MAAP: Multi Angle Absorption Photometer; PSAP: particle soot absorption photometer; AM: albedo meter; LII: Laser induced incandescence

Table S2. Statistics of monthly MAE_{550}.

Month	95th	75th	50th	25th	5th	Mean	Max	Min	S.D.	N
Feb-2012	31.24	22.00	18.12	15.74	13.92	19.66	47.73	11.74	5.66	529
Mar-2012	26.51	19.63	17.45	15.91	13.71	18.46	45.56	10.98	4.30	651
Apr-2012	33.06	22.66	18.24	16.11	13.85	20.21	48.29	6.01	6.23	595
May-2012	33.24	23.25	19.59	17.16	14.82	21.07	46.66	6.33	5.62	528
Jun-2012	35.52	25.86	21.28	18.57	14.99	22.95	49.07	5.62	6.66	315
Jul-2012	33.93	23.77	18.81	15.58	12.71	20.51	49.22	9.23	6.79	587
Aug-2012	40.75	27.72	21.85	16.14	12.51	23.09	49.95	9.75	8.56	545
Sep-2012	30.75	20.86	17.52	15.24	12.97	18.99	46.44	10.39	5.63	674
Oct-2012	20.72	15.84	13.95	12.60	11.18	14.70	34.09	7.34	3.21	715
Nov-2012	26.45	18.10	15.43	13.70	11.89	16.75	39.32	8.34	4.72	495
Dec-2012	28.57	19.04	15.73	13.66	11.78	17.18	47.39	9.33	5.47	585
Jan-2013	21.53	16.24	14.47	13.03	11.80	15.29	43.19	7.16	3.77	708

Table S3. Statistics of monthly $AAE_{470\text{-}660}$.

Month	95th	75th	50th	25th	5th	Mean	Max	Min	S.D.	N
Feb-2012	1.42	1.26	1.18	1.11	0.96	1.19	1.72	0.86	0.14	529
Mar-2012	1.33	1.18	1.10	1.02	0.93	1.10	1.50	0.65	0.12	651
Apr-2012	1.19	1.08	1.02	0.95	0.78	1.01	1.76	0.15	0.14	595
May-2012	1.13	1.05	1.00	0.94	0.84	0.99	1.24	0.39	0.10	528
Jun-2012	1.18	1.10	1.04	0.97	0.90	1.04	1.29	0.78	0.09	315
Jul-2012	1.22	1.11	1.04	0.98	0.83	1.04	1.43	0.20	0.13	587
Aug-2012	1.18	1.10	1.04	0.99	0.90	1.04	1.31	0.69	0.09	545
Sep-2012	1.23	1.13	1.06	1.00	0.91	1.07	1.40	0.64	0.11	674
Oct-2012	1.27	1.16	1.09	1.02	0.93	1.09	1.40	0.85	0.10	715
Nov-2012	1.24	1.16	1.11	1.05	0.97	1.11	1.52	0.79	0.08	495
Dec-2012	1.33	1.22	1.16	1.10	1.01	1.16	1.42	0.77	0.09	585
Jan-2013	1.38	1.27	1.18	1.12	1.01	1.19	1.66	0.93	0.11	708

Table S4. Statistics of monthly SSA_{525}.

Month	95th	75th	50th	25th	5th	Mean	Max	Min	S.D.	N
Feb-2012	0.91	0.89	0.87	0.84	0.79	0.86	0.94	0.65	0.04	526
Mar-2012	0.91	0.89	0.86	0.83	0.77	0.85	0.95	0.42	0.05	648
Apr-2012	0.92	0.89	0.86	0.83	0.76	0.85	0.94	0.45	0.06	552
May-2012	0.92	0.90	0.87	0.83	0.74	0.85	0.94	0.45	0.06	527
Jun-2012	0.92	0.89	0.86	0.81	0.74	0.84	0.95	0.64	0.06	310
Jul-2012	0.91	0.87	0.83	0.79	0.71	0.83	0.95	0.57	0.06	580
Aug-2012	0.94	0.92	0.89	0.85	0.79	0.88	0.96	0.67	0.05	536
Sep-2012	0.93	0.91	0.88	0.84	0.75	0.87	0.96	0.55	0.06	672
Oct-2012	0.94	0.93	0.91	0.89	0.84	0.90	0.96	0.66	0.03	715
Nov-2012	0.91	0.90	0.87	0.83	0.75	0.86	0.94	0.18	0.06	495
Dec-2012	0.91	0.89	0.86	0.82	0.74	0.85	0.94	0.66	0.05	585
Jan-2013	0.91	0.89	0.87	0.85	0.80	0.86	0.93	0.64	0.04	708

Table S5. Statistics of monthly E_{abs550}.

Month	95th	75th	50th	25th	5th	Mean	Max	Min	S.D.	N
Feb-2012	2.23	1.59	1.31	1.14	1.04	1.43	3.41	1.00	0.40	501
Mar-2012	1.76	1.30	1.15	1.07	1.02	1.24	2.83	1.00	0.26	466
Apr-2012	2.46	1.70	1.37	1.21	1.07	1.52	3.58	1.00	0.45	576
May-2012	2.48	1.73	1.45	1.28	1.12	1.57	3.46	1.02	0.41	520
Jun-2012	2.47	1.80	1.49	1.30	1.09	1.61	3.38	1.01	0.45	305
Jul-2012	2.83	1.97	1.57	1.30	1.10	1.71	4.03	1.01	0.55	568
Aug-2012	3.45	2.34	1.86	1.40	1.11	1.97	4.20	1.00	0.71	528
Sep-2012	2.36	1.62	1.36	1.20	1.05	1.48	3.54	1.00	0.42	636
Oct-2012	1.87	1.44	1.27	1.15	1.04	1.34	3.07	1.00	0.28	683
Nov-2012	2.14	1.51	1.27	1.13	1.04	1.38	3.17	1.00	0.38	461
Dec-2012	2.46	1.64	1.35	1.18	1.05	1.49	4.02	1.00	0.46	555
Jan-2013	1.85	1.39	1.24	1.12	1.03	1.31	3.66	1.00	0.32	672

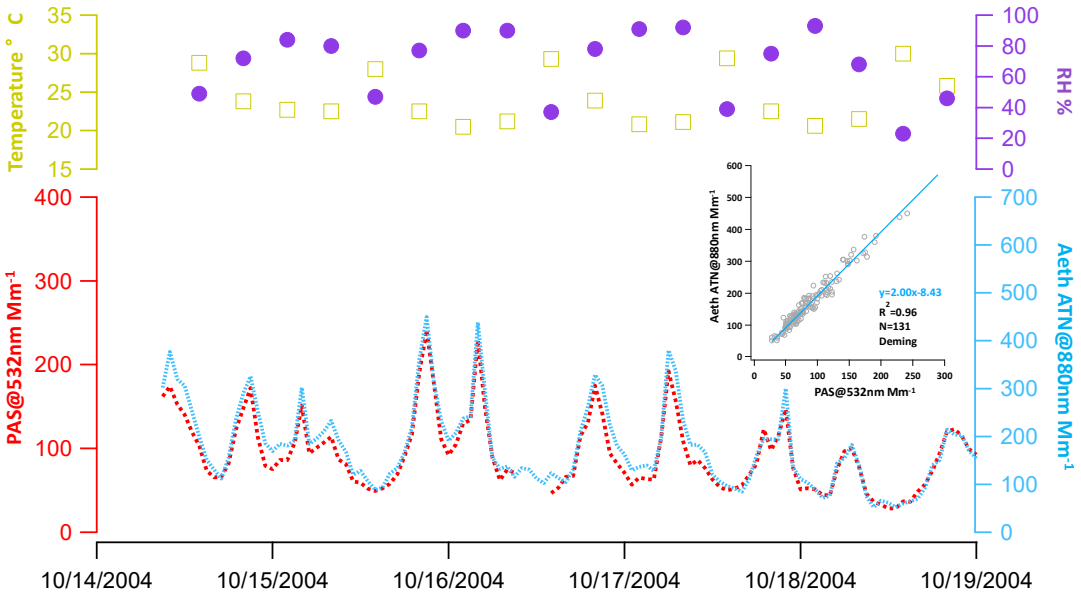

Figure S1. Comparison of collocated Aethalometer and PAS at Guangzhou (Oct 2004). Both PAS and Aethalometer (AE-16) were equipped with $PM_{2.5}$ inlets. RH of the sampled air was controlled to be <45% for PAS. Aethalometer sampling was conducted without RH control.

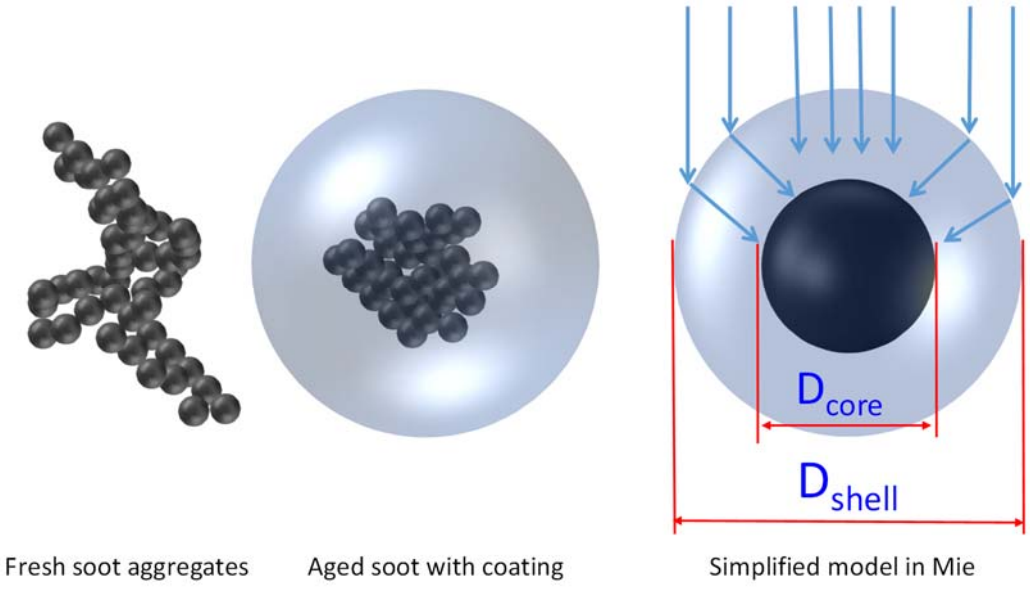

Figure S2. Schematic of the aging effect on light absorption. More light is absorbed by the soot particle core due to the lensing effect of the coating materials.

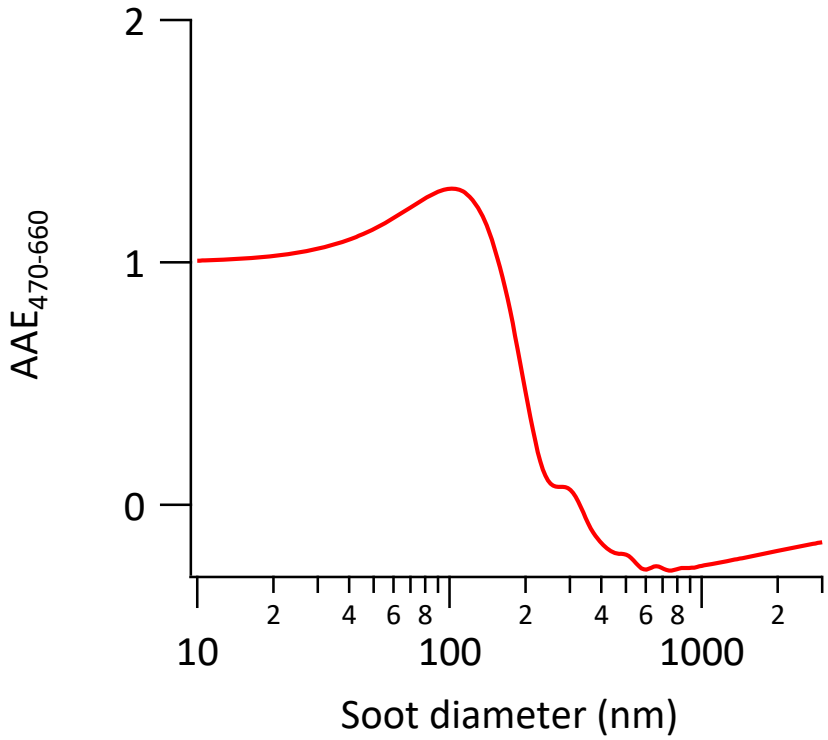

Figure S3. Mie simulated $AAE_{470\text{-}660}$ of a bare soot particle as a function of diameter with a Refractive index of 1.85 – 0.71i.

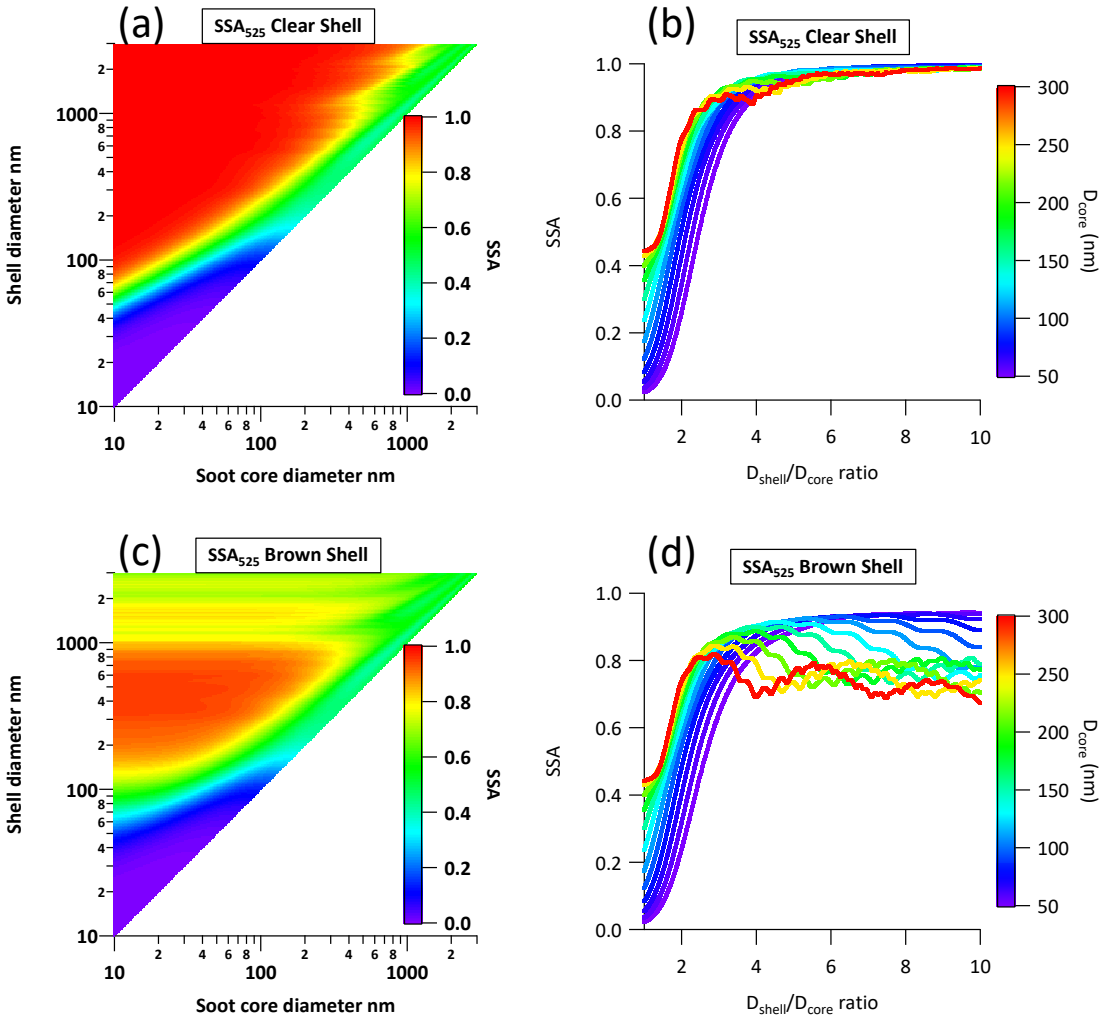

Figure S4. Mie simulated size dependency of soot particles SSA at wavelength 525 nm. (a)Combination of different clear shell (y axis) and core diameters (x axis). The color coding represents the SSA of a particle with specific core and clear shell size; (b) Cross-sections views of (a). The color coding represents different D_{core} in the range of 50 – 300 nm. (c)&(d) Similar to (a)&(b) but from the brown shell scenario.

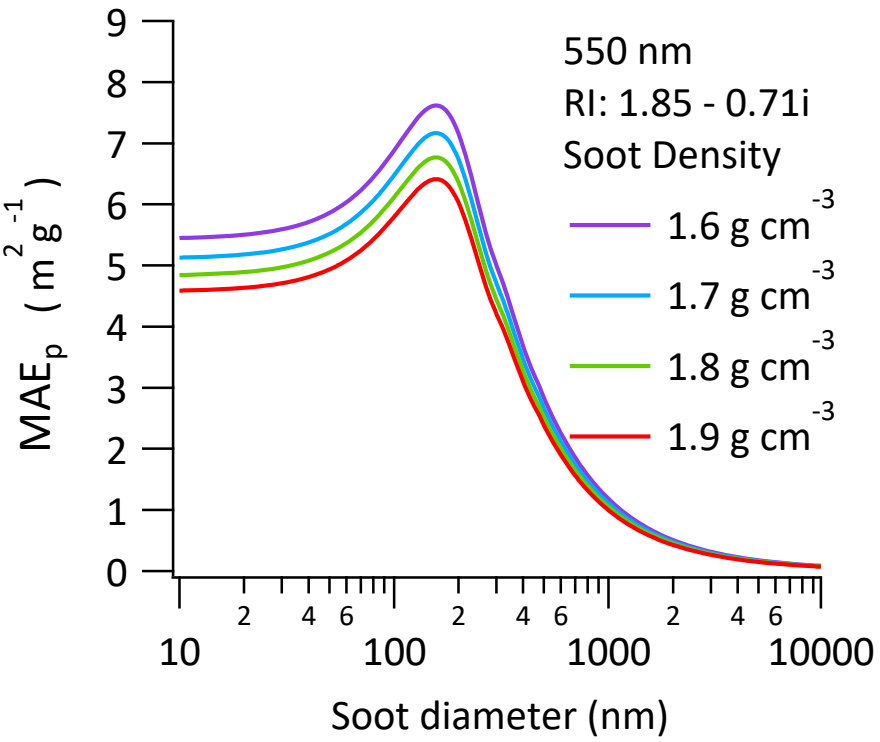

Figure S5. Mie simulated mass absorption efficiency (MAE_p) of a bare soot particle as a function of diameter at a wavelength of 550nm. Refractive index is 1.85 – 0.71i and density varied from 1.6 to 1.9 g cm^{-3}.

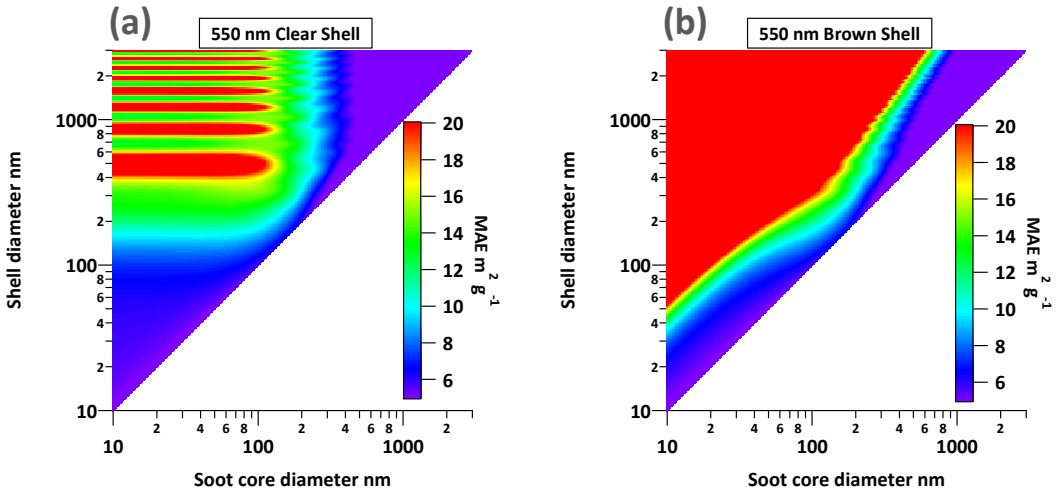

Figure S6. Mie simulated mass absorption efficiency (MAE) of a bare soot particle as a function of diameter at a wavelength of 550nm. Refractive index is 1.85 – 0.71i and density is 1.9 g cm^{-3} for the soot core. Refractive index for clear coating is 1.55. Refractive index for brown coating is wavelength dependent adopted from Lack and Cappa (2010).

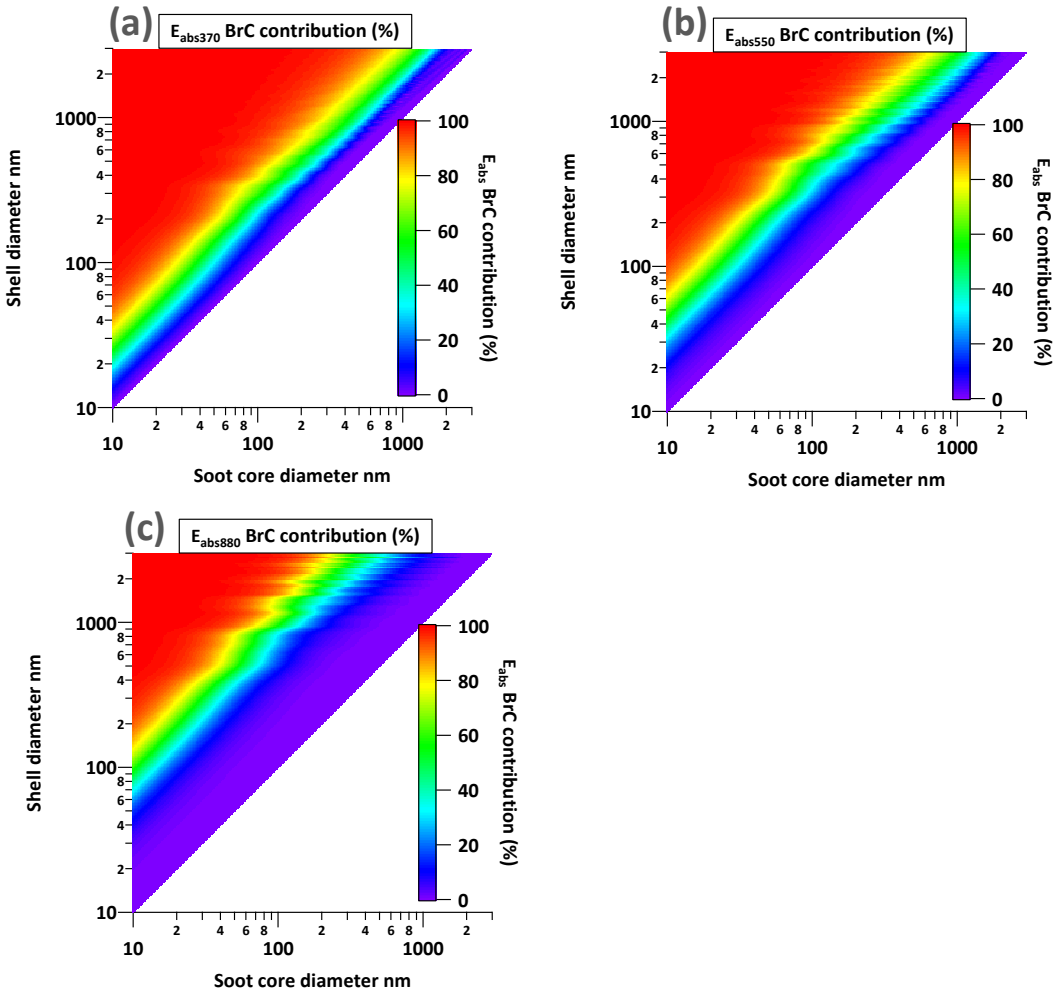

Figure S7. Mie simulated BrC absorption contribution to total E_{abs} (lensing effect + BrC absorption) in the brown shell scenario. (a) 370 nm (b) 550 nm (c) 880 nm.

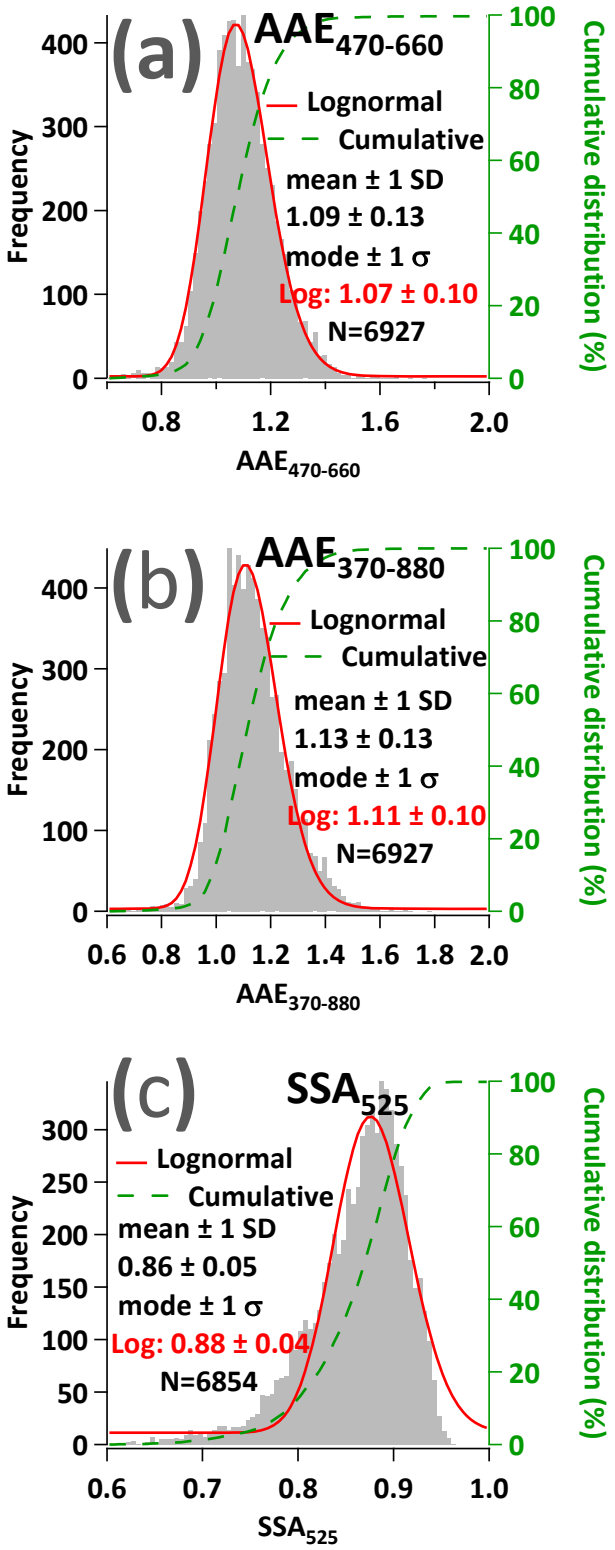

Figure S8. Measured annual statistics of AAE and SSA. (a) Annual frequency distribution of $AAE_{470\text{-}660}$. (b) Annual frequency distribution of $AAE_{370\text{-}880}$. (c) Annual frequency distribution of SSA_{525}. The red line represents lognormal fitting curve.

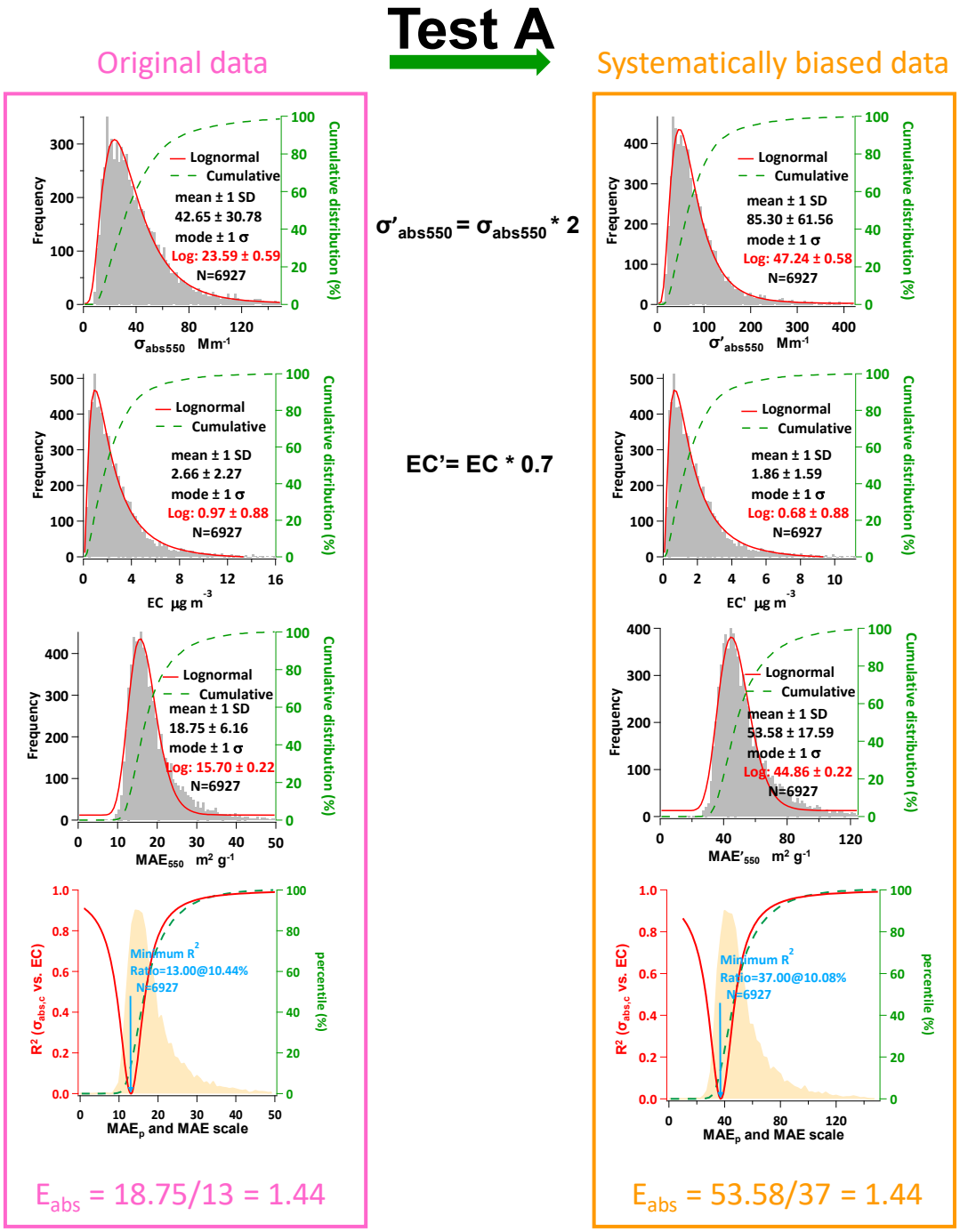

Figure S9. Comparison of E_{abs} from original data and systematically biased data (Test A). It should be noted that the E_{abs} shown here is ratio of averages, which is different form the annual average E_{abs} calculated from average of ratios.

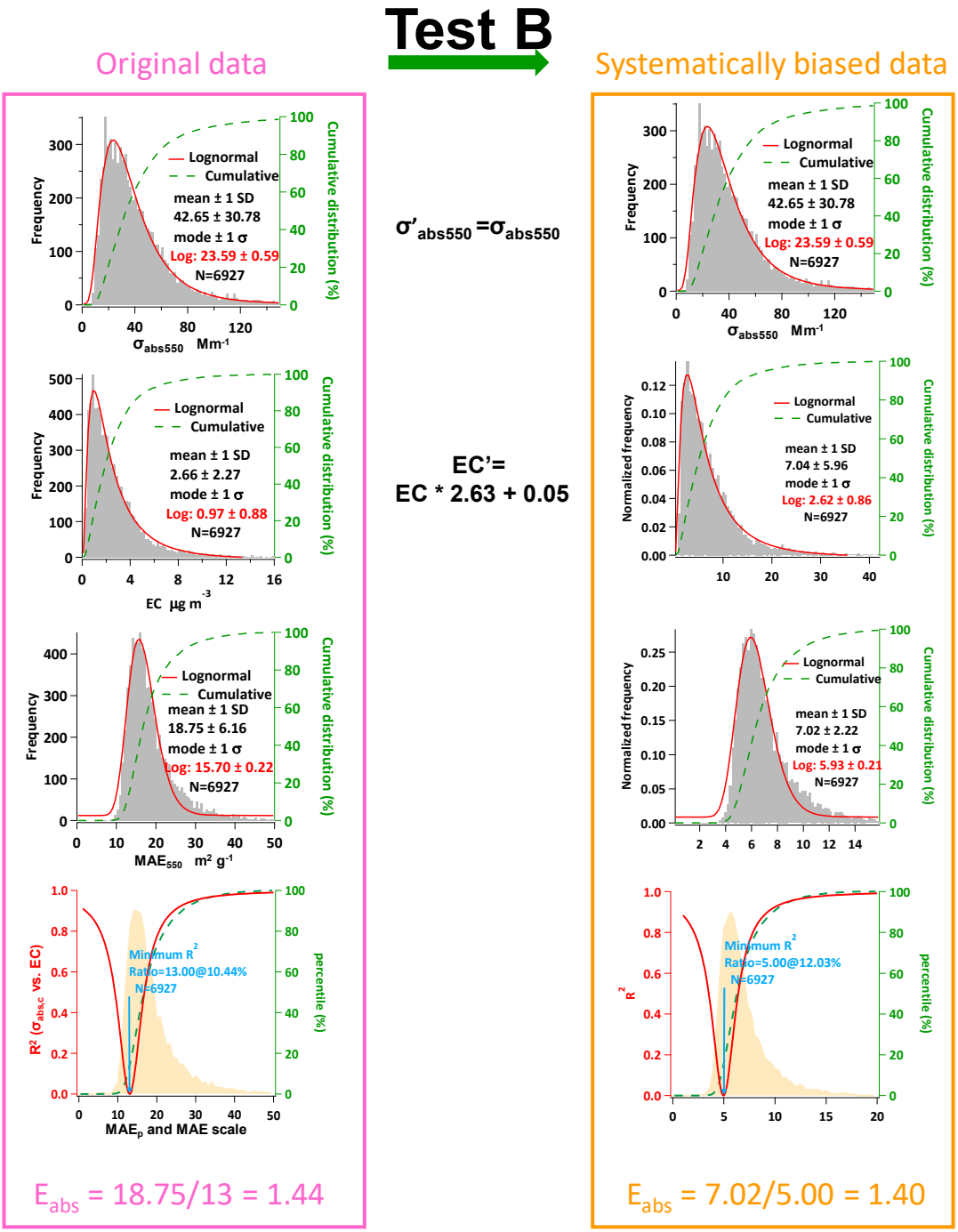

Figure S10. Comparison of E_{abs} from data using NIOSH EC and data using IMPROVE EC (Test B). It should be noted that the E_{abs} shown here is ratio of averages, which is different form the annual average E_{abs} calculated from average of ratios.

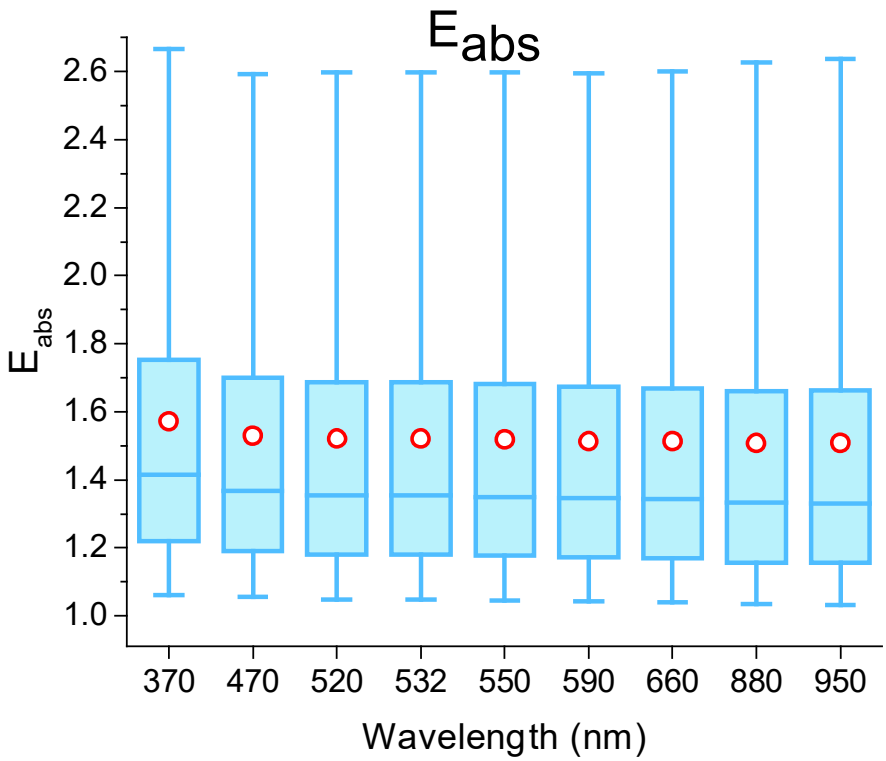

Wavelength (nm)	370	470	520	532	550	590	660	880	950
E_{abs} mean	1.55	1.51	1.50	1.50	1.50	1.49	1.49	1.48	1.49
E_{abs} S.D.	0.48	0.47	0.47	0.47	0.48	0.47	0.48	0.49	0.49

Figure S11. Spectrum annual average E_{abs} from 370 to 950 nm.

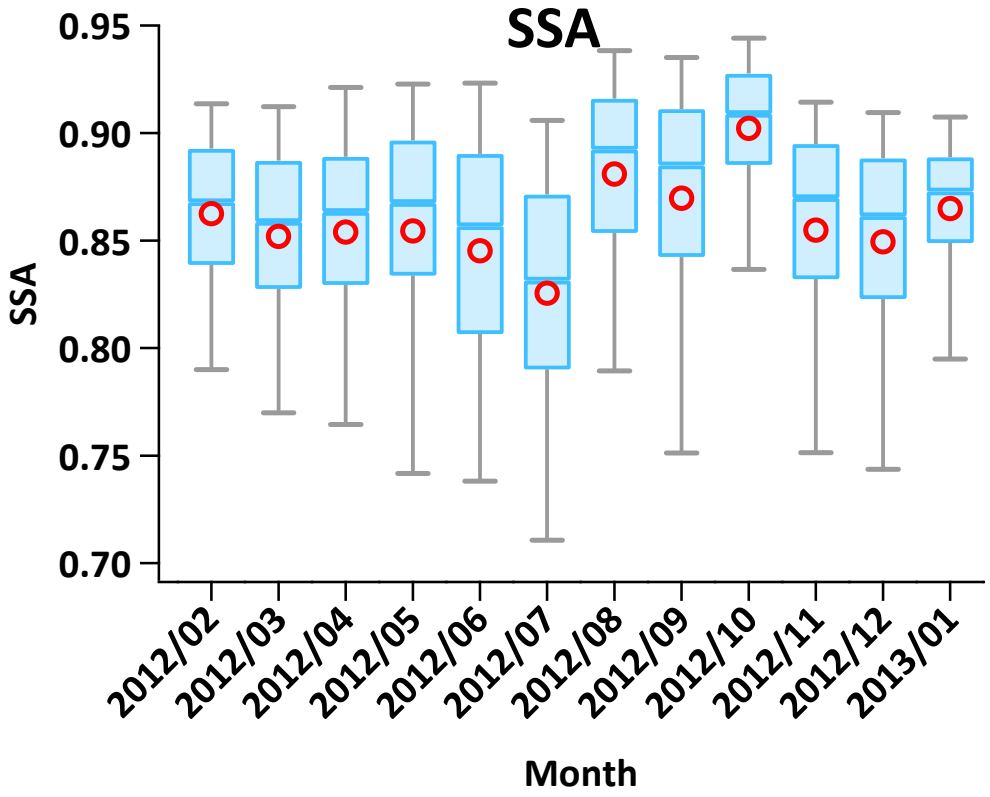

Figure S12. Measured monthly variations of SSA_{525}.

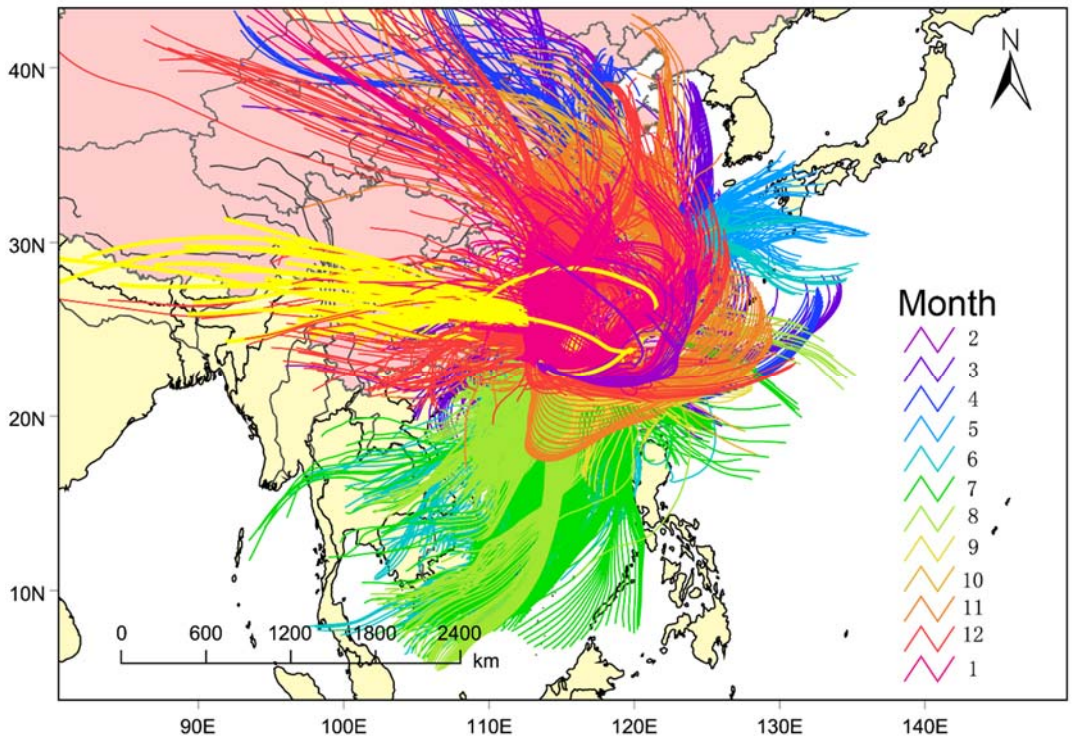

Figure S13. Hourly back trajectories for the past 72 hours calculated using NOAA's HYSPLIT model from Feb 2012 to Jan 2013. The color coding represents different months.

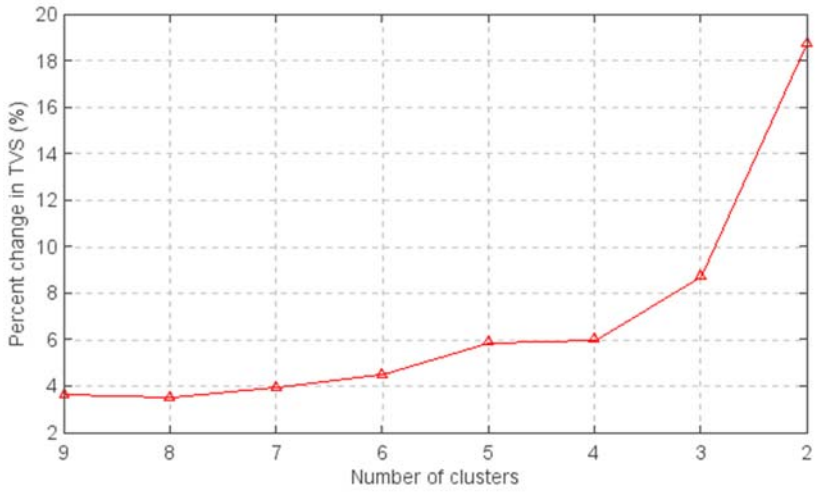

Figure S14. Total spatial variance (TSV) as a function of number of clusters in back trajectories clustering analysis.

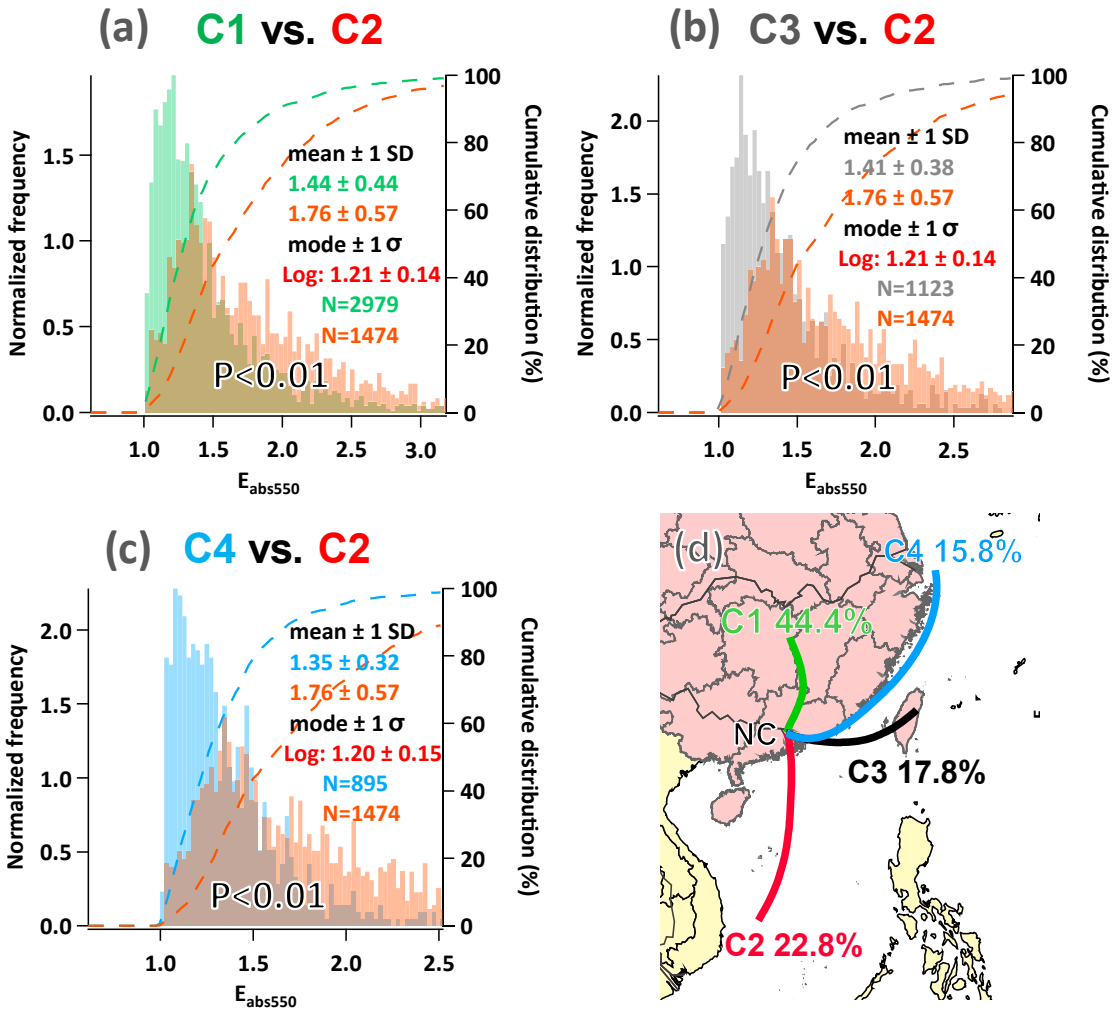

Figure S15. Frequency distributions of E_{abs550} by different air mass clusters. P is calculated by Wilcoxon-Mann-Whitney tests.

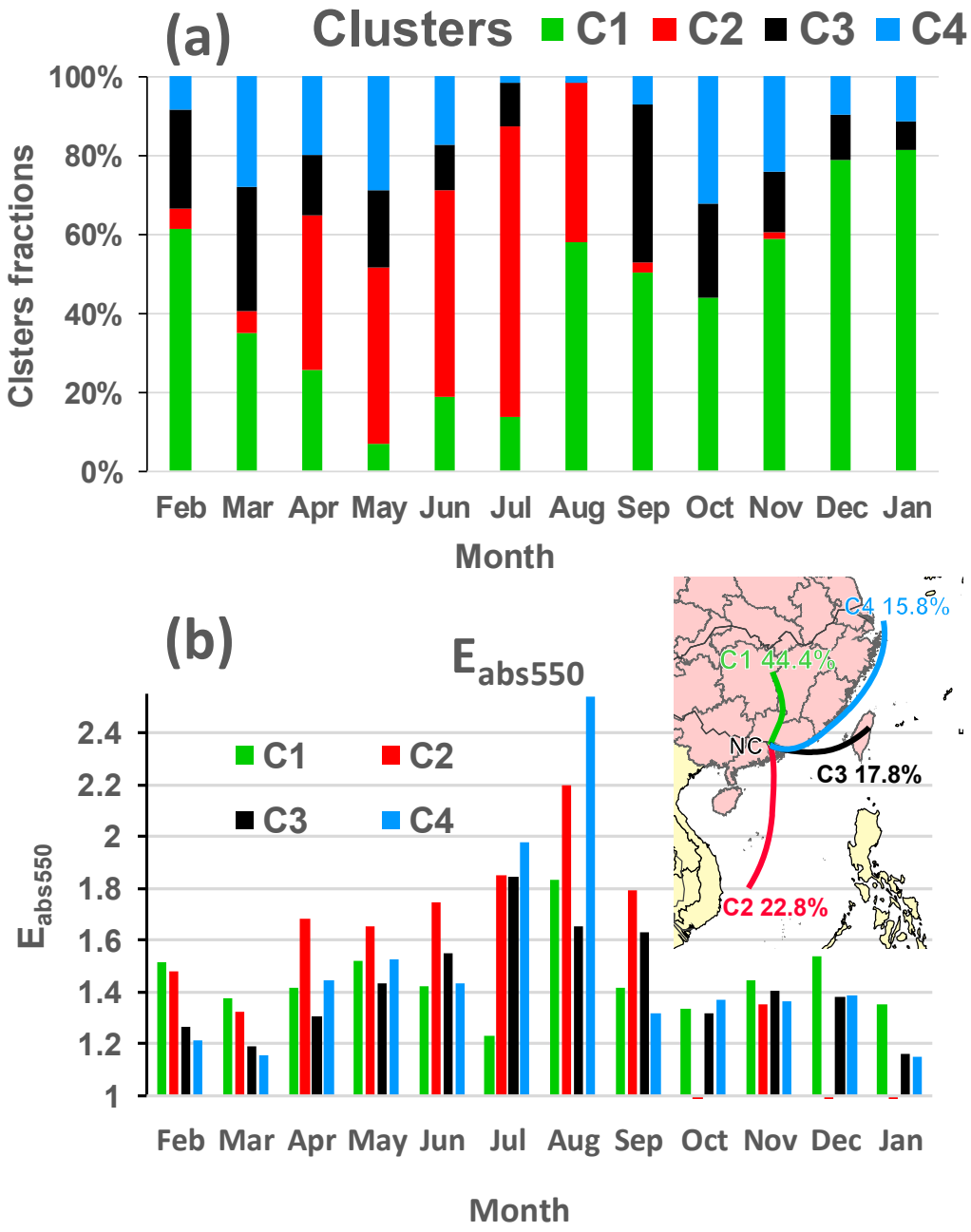

Figure S16. (a) Monthly contribution of each cluster. (b) Monthly E_{abs550} of each cluster.

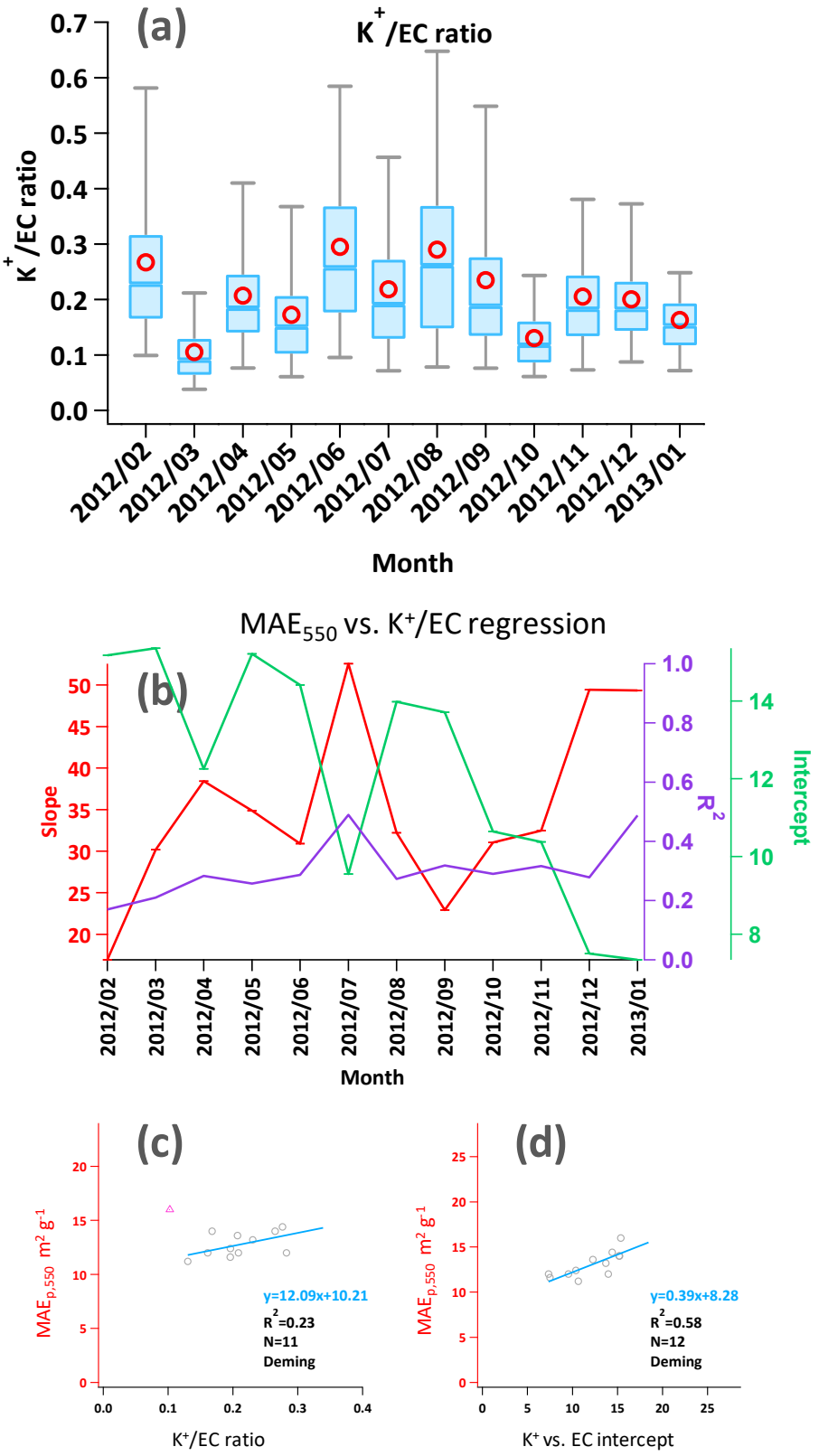

Figure S17. (a) Monthly variations of K^+/EC ratio from 2012 Feb to 2013 Jan at NC site. (b) Monthly regressions between MAE_{550} and K^+/EC with slope in red, intercept in green and R^2 in purple. (c) regressions between monthly $MAE_{p,550}$ and K^+/EC. (d) regression between monthly $MAE_{p,550}$ and intercepts from (b).

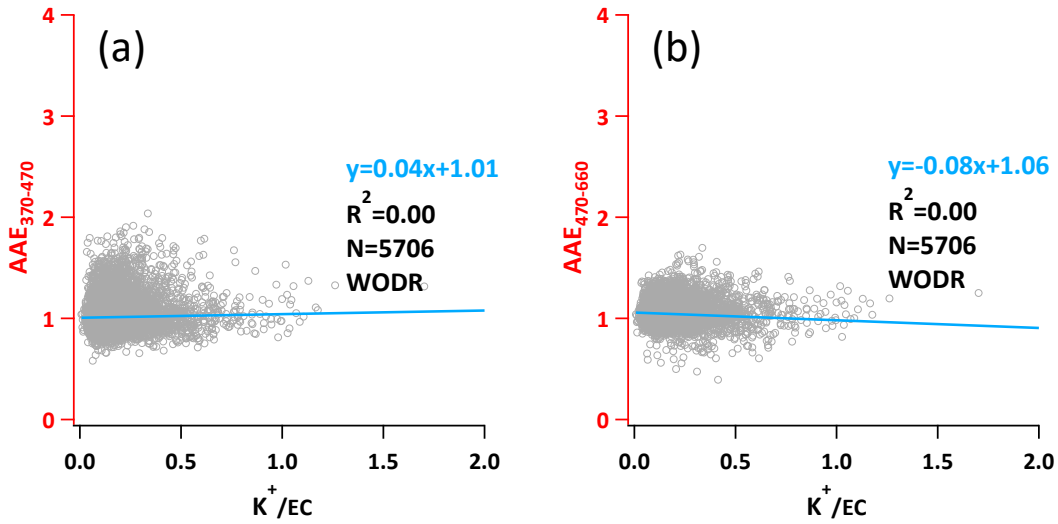

Figure S18. Correlations of AAE with K^+/EC ratio (biomass burning indicator). (a) AAE from 370 – 470 nm. (b) AAE from 470 – 660 nm.

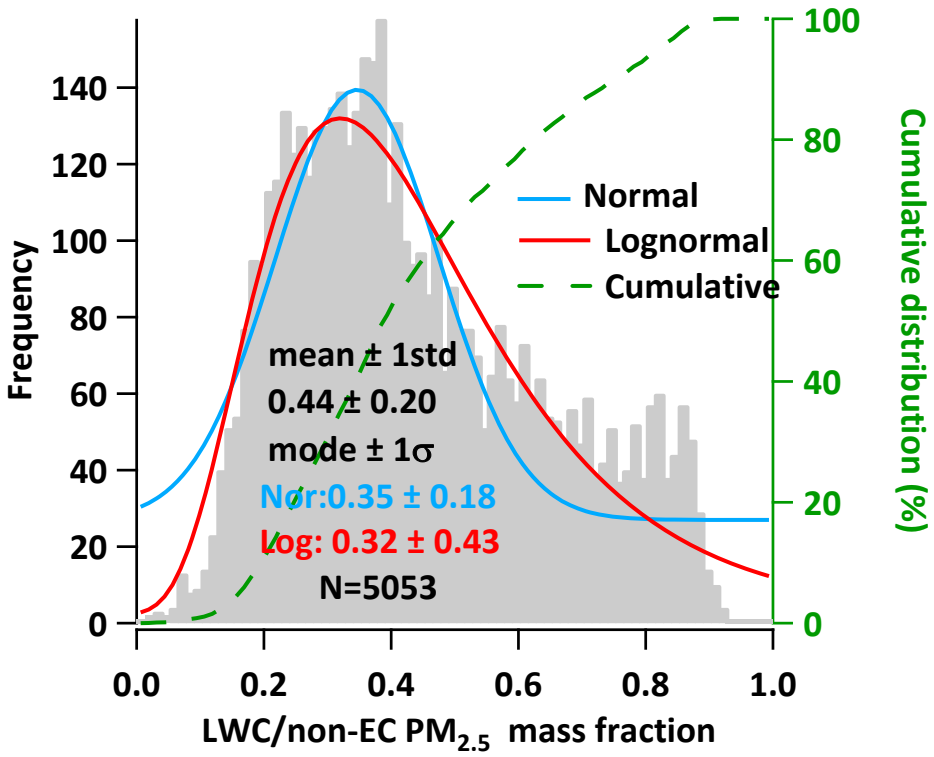

Figure S19. Annual frequency distribution of LWC/non-EC $PM_{2.5}$ mass fraction.

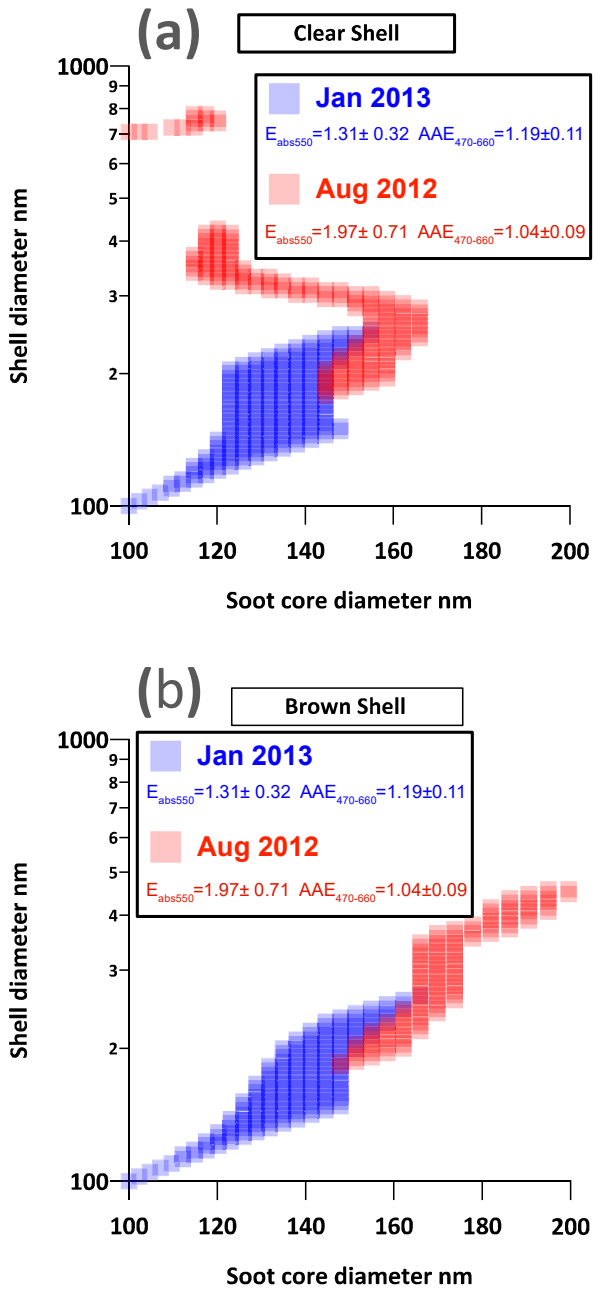

Figure S20. Size range of soot particles constrained by E_{abs}, SSA_{525} and $AAE_{470\text{-}660}$ from measurements. (a) Clear shell scenario; (b) Brown shell scenario

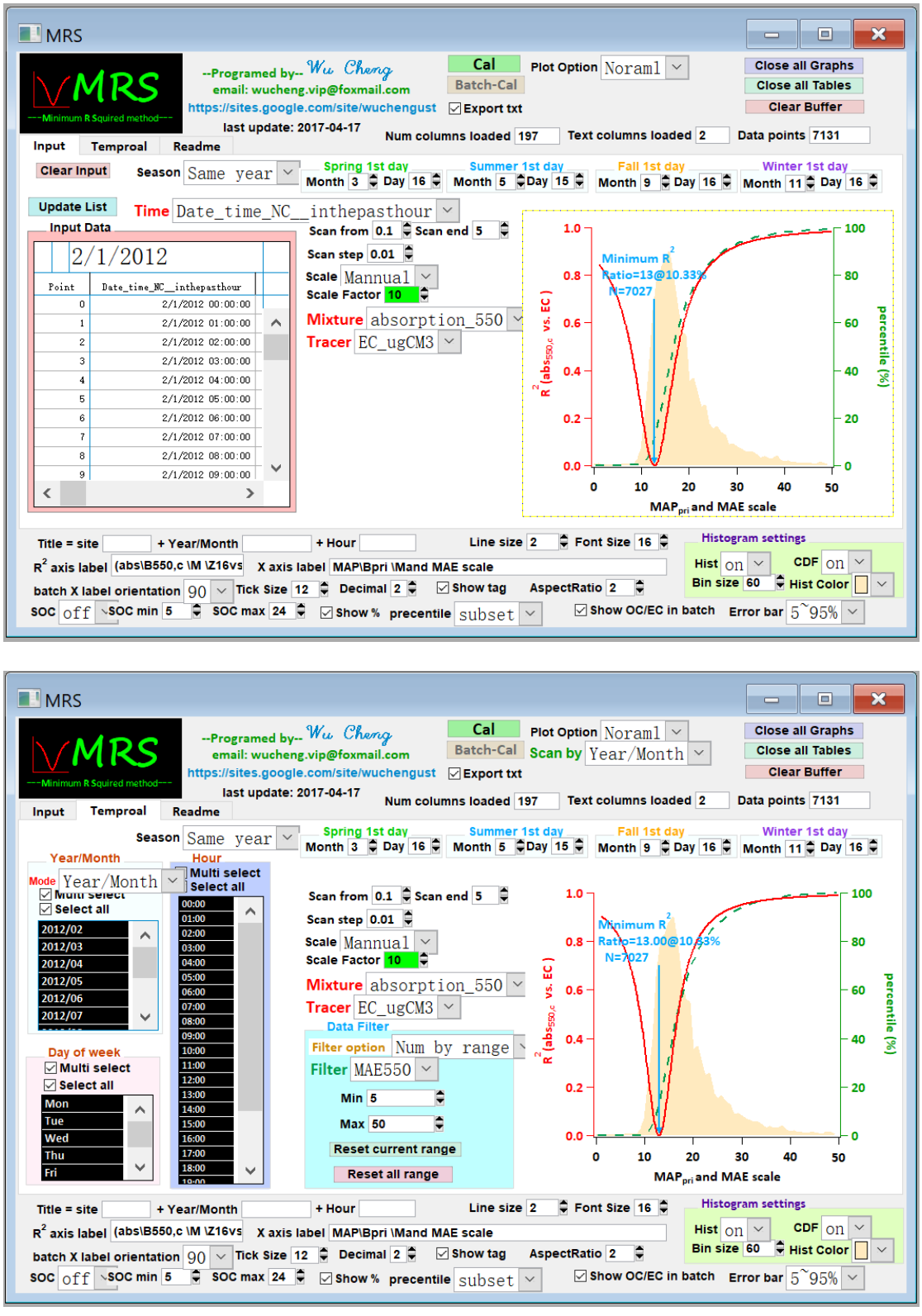

Figure S21. MRS program written in Igro Pro (WaveMetrics, Inc. Lake Oswego, OR, USA). Available from https://sites.google.com/site/wuchengust.

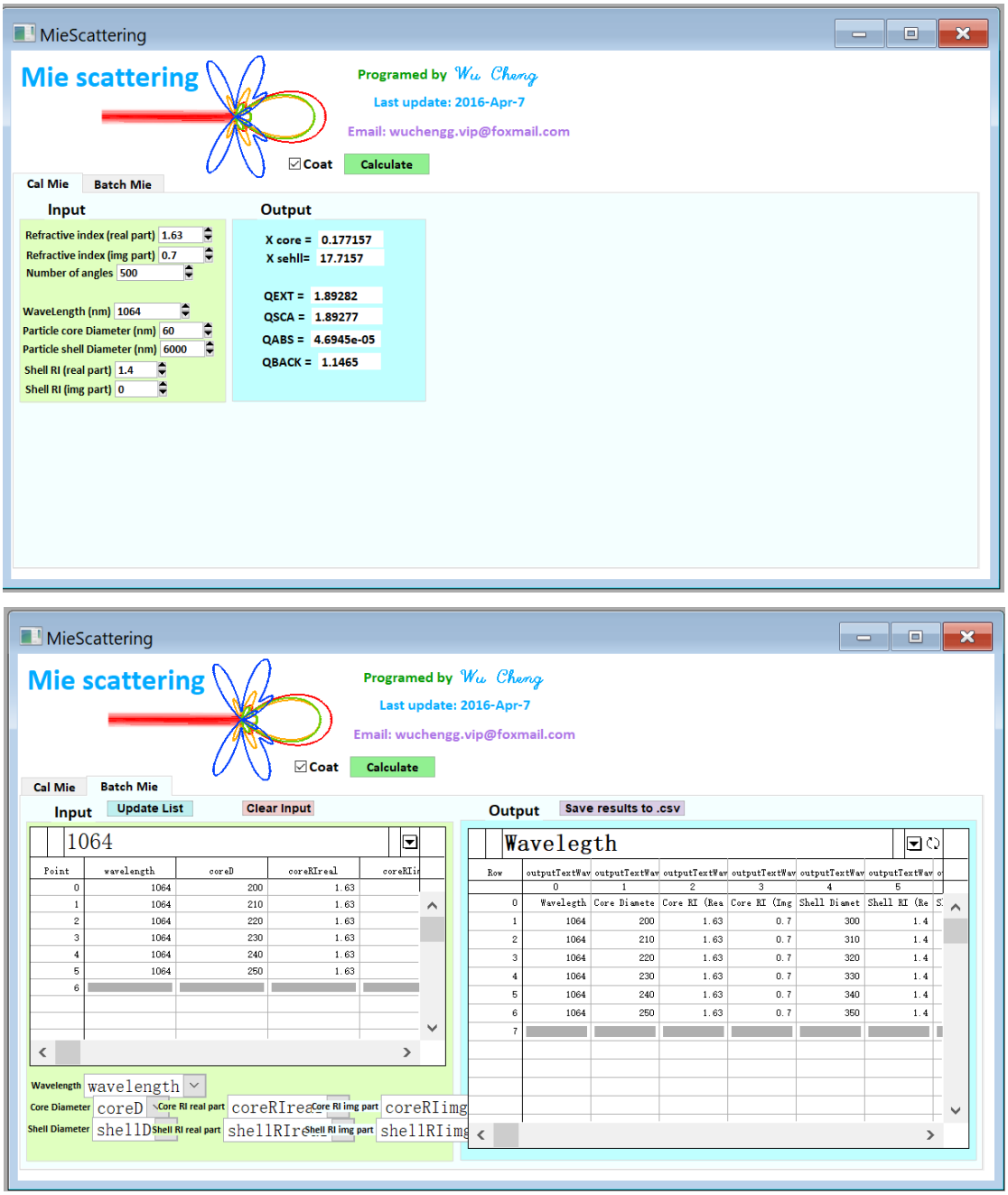

Figure S22. Mie program written in Igro Pro (WaveMetrics, Inc. Lake Oswego, OR, USA). Available from https://sites.google.com/site/wuchengust.

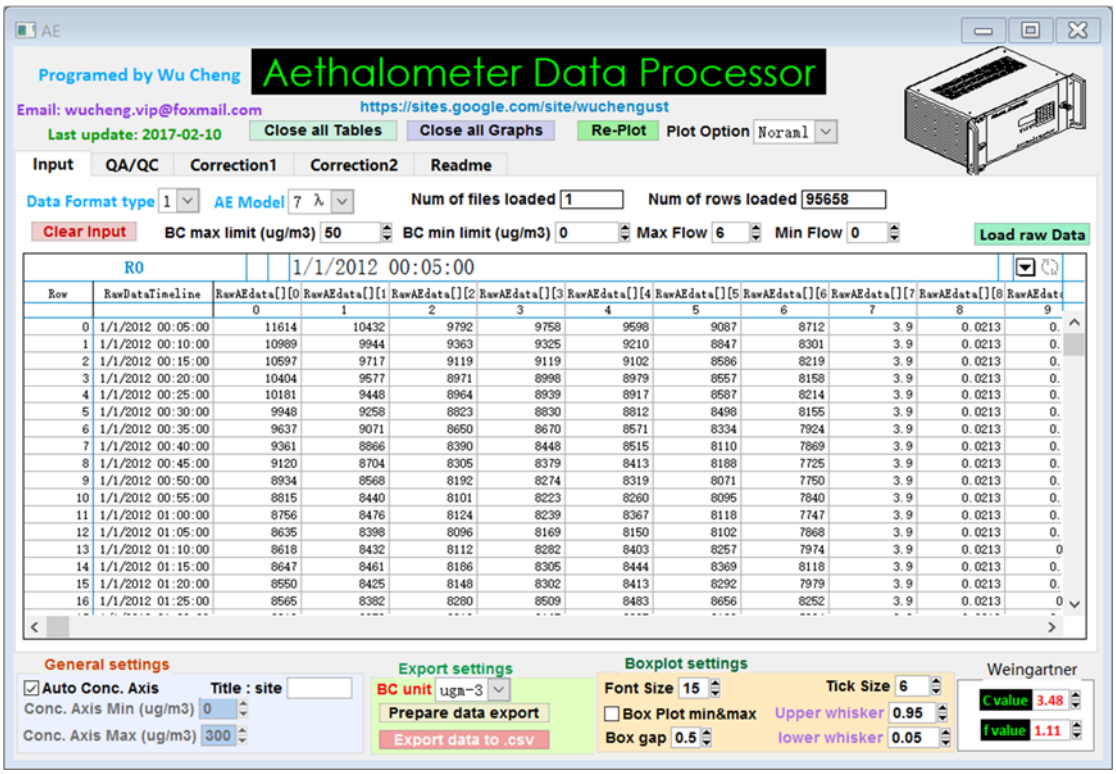

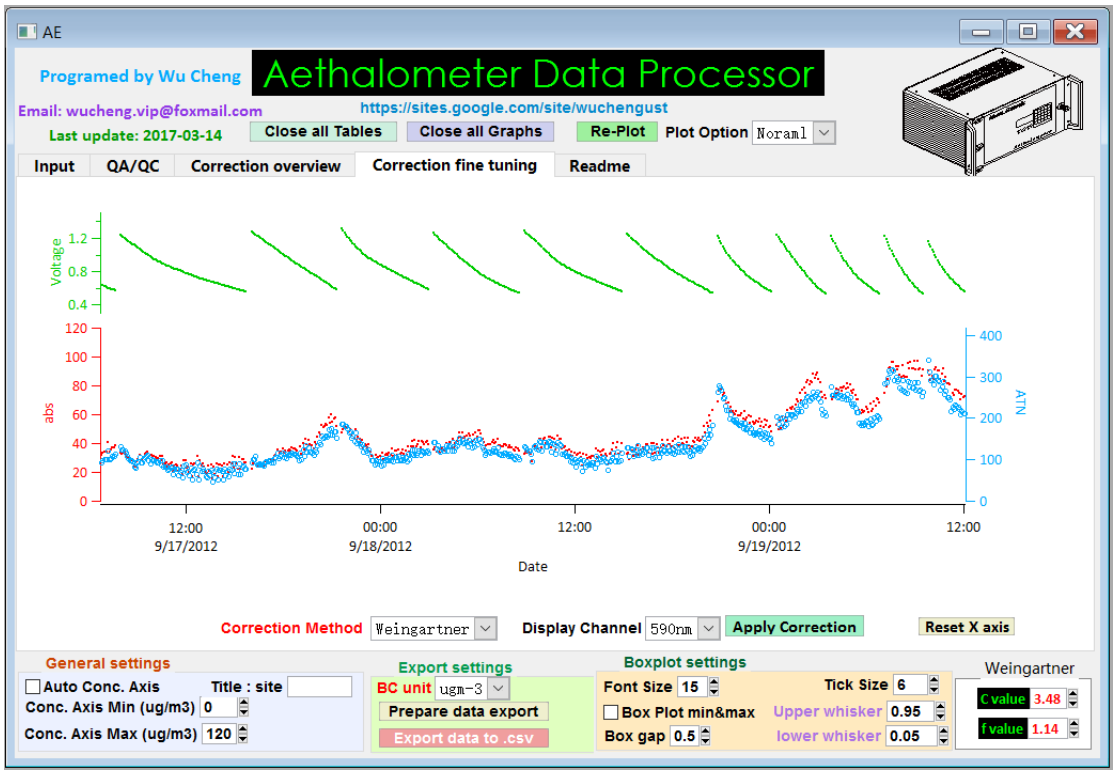

Figure S23. Aethalometer data processing program written in Igro Pro (WaveMetrics, Inc. Lake Oswego, OR, USA). Available from https://sites.google.com/site/wuchengust.

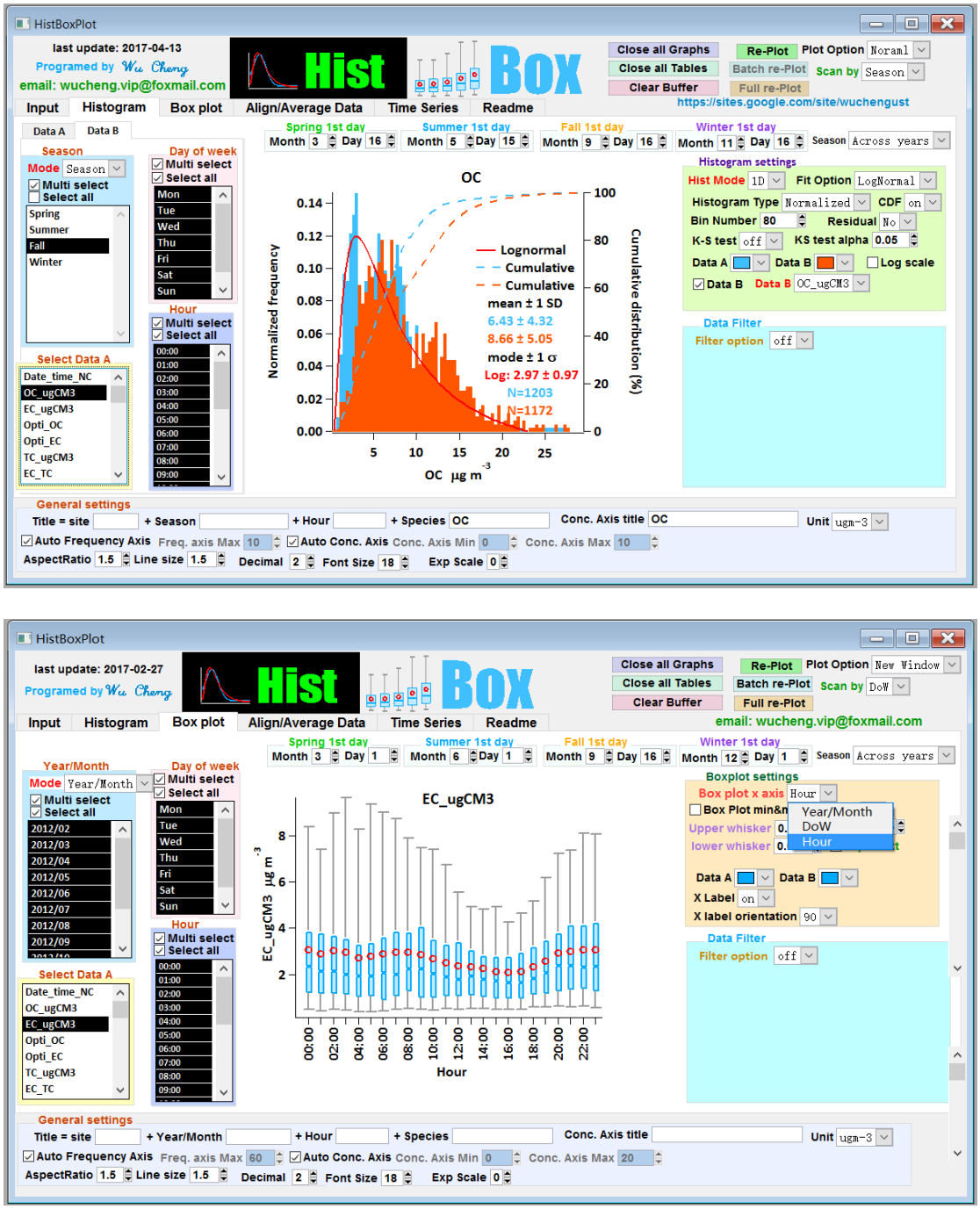

Figure S24. Histbox program written in Igro Pro (WaveMetrics, Inc. Lake Oswego, OR, USA). Available from https://sites.google.com/site/wuchengust.

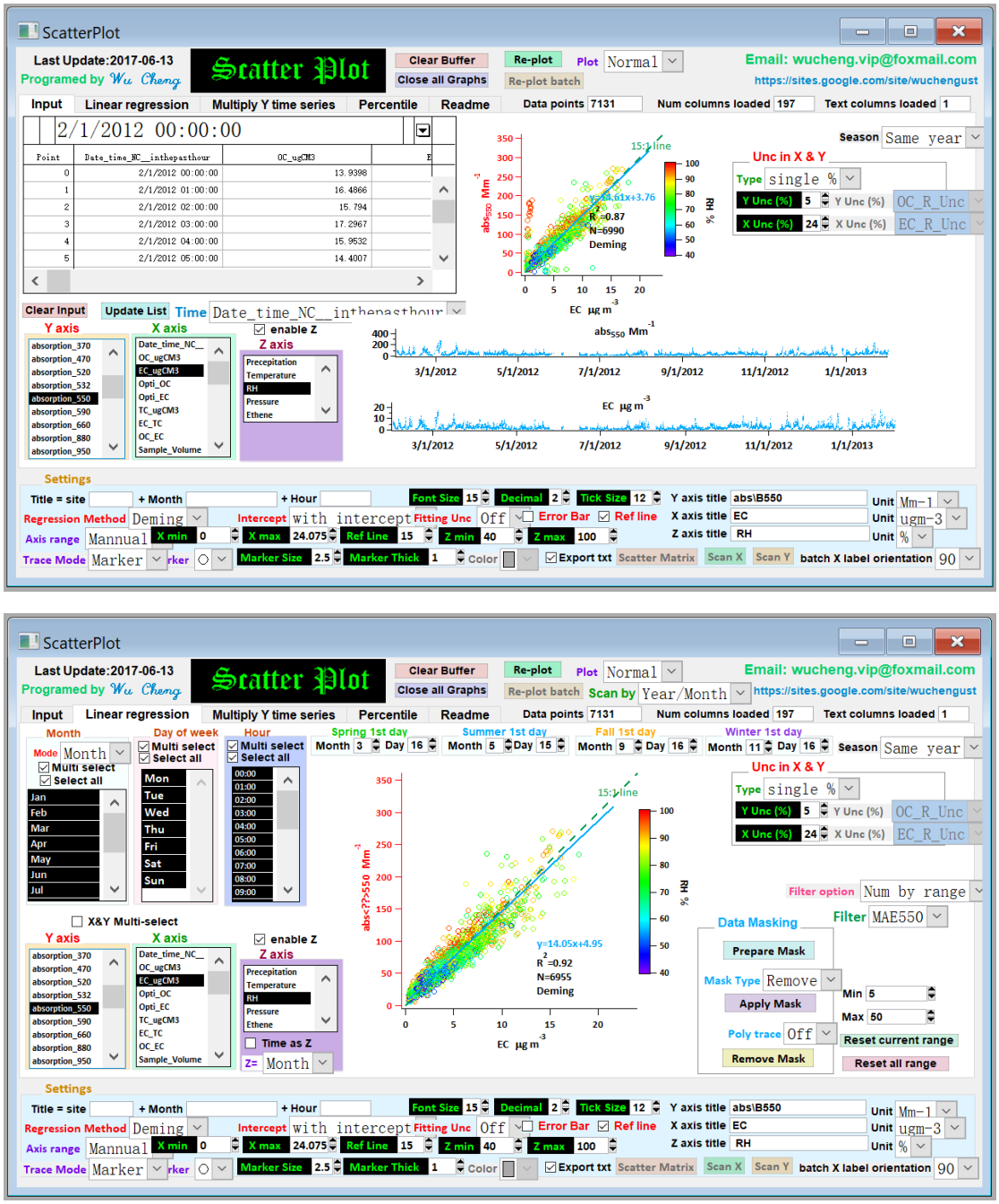

Figure S25. Scatter plot program written in Igro Pro (WaveMetrics, Inc. Lake Oswego, OR, USA). Available from https://sites.google.com/site/wuchengust.